

**An-Najah National University
Faculty of Graduate Studies**

**DYE-MODIFIED NANO-CRYSTALLINE TiO₂ SURFACES IN
LIGHT-DRIVEN WATER PURIFICATION FROM ORGANIC
CONTAMINANTS**

**By
Lamees Zuhair Abdul Razeq Majjad**

**Supervisor
Prof. Hikmat Hilal
Co supervisor
Dr. Nidal Zatar**

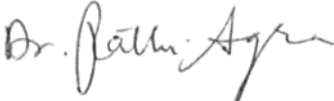
*Submitted in Partial Fulfillment of the Requirements for the Ph.D. of
Science in Chemistry, Faculty of Graduate Studies, at An-Najah National
University, Nablus, Palestine.*

2005

**DYE-MODIFIED NANO-CRYSTALLINE TiO₂ SURFACES IN
LIGHT-DRIVEN WATER PURIFICATION FROM ORGANIC
CONTAMINANTS**

**By
Lamees Zuhair Abdul Razeq Majjad**

This Thesis was successfully defended on 10/12/2005 and approved by:

Committee Members	Signature
1) Prof. Hikmat S. Hilal, <i>Ph.D. (Committee Chairman)</i>	
2) Dr. Nidal Zatar, <i>(Co supervisor)</i>	
3) Dr. Fathi Aqraa, <i>(External Examiner)</i>	
4) Dr. Raqi Shubietah, <i>(Internal Examiner)</i>	

III

TO MY PARENTS AND HUSBAND

WITH LOVE AND REGARDS

Acknowledgements

I would like to thank and express my indebtedness to my supervisors Prof. Hikmat Hilal, Ph.D. and Dr. Nidal Zatar, for their sincere encouragement, helpful guidance and close supervision which have been invaluable for me throughout all stages of the study.

My sincere thanks are also due to members of Chemistry Department especially for Dr. Shukri Khalaf for help in surface area measurement. I also thank the Chemistry technical staff for technical help. Thanks are due to the Chemical, Biological and Drug Analysis Center.

Thanks are due to Palestinian-French University Cooperation program for donation of UV lamp, housing and accessories.

I would like to thank Dr. A'mer El-Hamouz for discussions, and Dr. Mohammad Najeeb for personal help.

I would like to thank Mr. Iyad Saadeddin (ICMCB, France) for his help in TGA measurements.

Finally I wish to express my sincere gratitude and thanks to my family for their endless support and help, with special appreciation and thanks to my brother Mahdi.

Table of Contents

<i>Section</i>	<i>Subject</i>	<i>Page</i>
	Committee decision	II
	Dedication	III
	Acknowledgments	IV
	Table of Contents	V
	List of Tables	VIII
	List of Figures	IX
	Abstract	XVII
1	INTRODUCTION	1
1.1	Semiconductor Electrodes	2
1.1.1	Introduction	2
1.1.2	Fundamentals: Energy and Band Model	3
1.1.2.1	Energy bands in solids	3
1.1.2.2	Charge carrier generation	6
1.1.2.3	The Fermi level	7
1.1.2.4	Photo-effect	7
1.2	Nanocrystals	8
1.2.1	Introduction	8
1.2.2	Manufacturing processes	10
1.2.3	The nanostructured electrode	12
1.2.4	Applications	14
1.3	Titanium Dioxide	15
1.3.1	Introduction	15
1.3.2	TiO ₂ bulk properties	16
1.3.2.1	Crystal phases	16
1.3.2.2	Optical properties	17
1.3.2.3	Electrical properties	18
1.3.3	Applications of TiO ₂	18
1.3.4	Objectives of the present work	27
1.3.5	Hypothesis	28
	References	31
2	EXPERIMENTAL	40
2.1	Reagents	41
2.2	Equipment	41
2.2.1	Reactor	41
2.2.2	Measuring Devices	42
2.2.3	Light Source	43
2.3	MnP preparation and characterization	45
2.4	Surface area measurement	46
2.5	Photolysis experiments	49

Table of contents (contd.)

Section	Subject	Page
2.5.1	Naked TiO ₂ as catalyst	49
2.5.2	Dye as catalyst	49
2.5.3	TiO ₂ /TPPHS catalyst	50
2.5.4	AC/TiO ₂ /TPPHS catalyst	50
2.5.5	Metalloporphyrin (MnP) modified TiO ₂ catalyst	50
2.5.6	Control experiments	51
2.5.7	Reuse experiments	51
2.5.8	Catalyst analysis	51
2.5.8.1	Using FT-IR	51
2.5.8.2	Thermal Gravimetric analysis (TGA)	52
	References	57
3	PHOTO-DEGRADATION OF PHENOL	59
3.1	Introduction	60
3.2	Experimental	62
3.2.1	Chemicals	62
3.2.2	Equipment	63
3.2.3	Photo-degradation experiments	63
3.2.4	Concentration measurements	63
3.3	Results	64
3.3.1	Calibration curve	64
3.3.2	Control experiments	64
3.3.3	Naked TiO ₂ and naked TPPHS dye	64
3.3.4	TiO ₂ /TPPHS catalyst	68
3.3.5	AC supported TiO ₂ /TPPHS catalyst	71
3.3.6	Reuse experiments	76
3.3.7	Metalloporphyrin (MnP) modified TiO ₂ catalyst	76
3.4	Discussion	83
3.4.1	Introduction	83
3.4.2	Effect of TPPHS dye	89
3.4.3	Effect of MnP dye	95
	References	98
4	PHOTO-DEGRADATION OF BENZOIC ACID	101
4.1	Introduction	102
4.2	Experimental	103
4.2.1	Chemicals	103
4.2.2	Equipment	103
4.2.3	Photo-degradation experiments	104
4.2.4	Concentration measurements	104
4.3	Results	104
4.3.1	Calibration curve	104

Table of contents (contd.)

Section	Subject	Page
4.3.2	Control experiments	104
4.3.3	Naked TiO ₂ and naked TPPHS dye	108
4.3.4	TiO ₂ /TPPHS catalyst	108
4.3.5	AC/TiO ₂ /TPPHS catalyst	114
4.3.6	Metalloporphyrin (MnP) modified TiO ₂ catalyst	115
4.4	Discussion	122
4.4.1	Introduction	122
4.4.2	Effect of TPPHS dye	122
4.4.3	Effect of MnP dye	125
	References	127
5	PHOTO-DEGRADATION OF TAMARON	129
5.1	Introduction	130
5.2	Experimental	131
5.2.1	Chemicals	131
5.2.2	Equipment	132
5.2.3	Photo-degradation experiments	132
5.2.4	Concentration measurements	133
5.3	Results	133
5.3.1	Calibration curve	133
5.3.2	Control experiments	133
5.3.3	Naked TiO ₂ and naked TPPHS dye	133
5.3.4	TPPHS sensitized TiO ₂ catalyst	137
5.3.5	AC supported TiO ₂ /TPPHS catalyst	137
5.3.6	Metalloporphyrin (MnP) modified TiO ₂ catalyst	148
5.4	Discussion	152
5.4.1	Introduction	152
5.4.2	Effect of TPPHS dye	152
5.4.3	Effect of MnP dye	155
	References	157
6	CONCLUSIONS AND SUGGESTIONS FOR FURTHER WORK	159
6.1	Conclusions	160
6.1.1	Phenol	160
6.1.2	Benzoic acid	161
6.1.3	Tamaron	161
6.2	Suggestions For Further Work	162
	List of symbols	164
	Appendix	166
	Abstract in Arabic	ب

VIII

List of Tables

<i>Table No.</i>	<i>Table Title</i>	<i>Page</i>
Table (1)	Crystallographic parameters for rutile and anatase TiO ₂	17
Table (2)	Photochemical water purification processes using TiO ₂ catalysts	26
Table (3)	Arc lamp description	43
Table (4)	Surface area of TiO ₂	46
Table (5)	Surface area of activated carbon (AC)	47
Table (6)	Surface area data measured for TiO ₂ and AC based on Langmuir plots	49
Table (7)	Values of turnover number for different catalytic systems in phenol degradation	97
Table (8)	Values of turnover number for different catalytic systems in benzoic acid degradation	126
Table (9)	Physical properties of methamidophos	130
Table (10)	Values of turnover number for different catalytic systems in Tamaron degradation	156

List of Figures

<i>Figure No.</i>	<i>Figure Title</i>	<i>Page</i>
Figure (1.1)	The energy band diagram for a semiconductor in contact with an electrolyte. E_c : conduction band; E_v : valence band; E_{bg} : band gap energy	4
Figure (1.2)	Band positions (top of valence band and bottom of conduction band) of several semiconductors together with some selected redox potentials	5
Figure (1.3)	Mechanisms of charge carrier generation in a semiconductor, A: Thermal generation, B: n-type doping, C: p-type doping, D: Photo excitation	6
Figure (1.4)	photocurrent generation at n-type semiconductor	8
Figure (1.5)	TiO ₂ crystal structures. A: The unit cell for rutile, B: The unit cell for anatase. The small circles are the Ti cations and the large circles are the O anions	16
Figure (2.1)	Schematic photodegradation reactor	41
Figure (2.2)	Spectral irradiance of various Arc Lamps	44
Figure (2.3)	Typical spectral irradiance of 150 W Xe Lamp, showing % of total irradiance in specific UV, VIS and NiR spectral ranges	44
Figure (2.4)	The electronic absorption spectra in the UV/visible region for MnP solution in methanol.	45
Figure (2.5)	A plot of C/N vs. C for TiO ₂ surface	48
Figure (2.6)	A plot of C/N _m vs. C for AC	49
Figure (2.7)	TGA results for a fresh AC/TiO ₂ /TPPHS sample	53
Figure (2.8)	TGA results for a sample of AC/TiO ₂ /TPPHS recovered from phenol photo-degradation reaction	54
Figure (2.9)	TGA results for a fresh TiO ₂ /TPPHS sample	55
Figure (2.10)	TGA results for a sample of AC/TiO ₂ /TPPHS recovered from phenol photo-degradation reaction	56
Figure (3.1)	Plots of remaining phenol concentration (M) vs. time for phenol degradation experiments for the control experiments. (a) AC alone, (b) UV light with no catalyst, (c) catalyst with no light	65
Figure (3.2)	Plots of remaining phenol concentration (M) vs. time for phenol degradation experiments for the control experiments. (a) AC alone, (b) UV light with no catalyst, (c) catalyst with no light	66
Figure (3.3)	Plots of remaining phenol concentration (M) vs. time for phenol degradation experiments. (a)	

List of Figures (contd.)

<i>Figure No.</i>	<i>Figure Title</i>	<i>Page</i>
	Naked dye, (b) Naked TiO ₂	67
Figure (3.4)	Plots of remaining phenol concentration (M) vs. time for phenol degradation experiments for the effect of initial phenol concentration. Different initial phenol concentrations are studied, (a) 0.1, (b) 0.08, (c) 0.06, (d) 0.04, (e) 0.01	69
Figure (3.5)	Plots of remaining phenol concentration (M) vs. time for phenol degradation experiments for the effect of oxygen concentration, TiO ₂ (0.5g), dye (0.003g, 0.738×10^{-5} mol). (a), reactor not closed, (b) reactor closed, (c) bubbles of air. Experiments were conducted in the UV region at room temperature	70
Figure (3.6)	Plots of remaining phenol concentration (M) vs. time for phenol degradation experiments for the effect of dye concentration, TiO ₂ (0.5g), dye (a) 0.005g, 1.23×10^{-5} mol, (b) 0.003g, 0.738×10^{-5} mol, (c) 0.004g, 0.984×10^{-5} mol, (d) 0.01g, 2.46×10^{-5} mol, (e) 0.006g, 1.476×10^{-5} mol, (f) 0.007g, 1.772×10^{-5} mol. All experiments were conducted in the UV region at room temperature	72
Figure (3.7)	Plots of remaining phenol concentration (M) vs. time, in phenol degradation experiments for the effect of radiation, TiO ₂ (0.5g), dye (0.003g, 0.738×10^{-5} mol). (a), UV- light, (b) visible light. All experiments were conducted at room temperature	73
Figure (3.8)	Plots of remaining phenol concentration (M) vs. time, in phenol degradation experiments for the effect of AC, TiO ₂ (0.5g), dye (0.006g, 1.476×10^{-5} mol). (a) with AC (0.1g), (b) no AC. All experiments were conducted in the UV at room temperature	74
Figure (3.9)	Plots of remaining phenol concentration (M) vs. time, in phenol degradation experiments for the effect of AC supported catalyst concentration, TiO ₂ (0.5g), AC (0.1g), dye (a) 0.006g, 1.476×10^{-5} mol, (b) 0.01g, 2.46×10^{-5} mol, (c) 0.012g, 20952×10^{-5} mol, (d) 0.003g, 0.738×10^{-5} mol. All experiments	

List of Figures (contd.)

<i>Figure No.</i>	<i>Figure Title</i>	<i>Page</i>
	were conducted in the UV region at room temperature	75
Figure (3.10)	Plots of remaining phenol concentration (M) vs. time for phenol degradation experiments for the effect of radiation, TiO ₂ (0.5g), dye (0.006g, 1.476×10 ⁻⁵ mol), AC (0.1g). (a) UV-light, (b) visible light. Experiments were conducted at room temperature	78
Figure (3.11)	Plots of remaining phenol concentration (M) vs. time for phenol degradation experiments, for the effect of temperature, TiO ₂ (0.5g), dye (0.006g, 1.476×10 ⁻⁵ mol), AC (0.1g). (a), 20°C, (b) 40°C, (c) 30°C. Experiments were conducted in the UV region	79
Figure (3.12)	Plots of remaining phenol concentration (M) vs. time for phenol degradation experiments, for the effect of catalyst concentration. (a) 1.0g catalyst, (b) 0.6g catalyst, (c) 0.3g catalyst. Experiments were conducted in the UV at room temperature	80
Figure (3.13)	Plots of remaining phenol concentration (M) vs. time for phenol degradation experiments, for the effect speed of stirring, TiO ₂ (0.5g), dye (0.006g, 1.476×10 ⁻⁵ mol), AC (0.1g). (a) Low speed, (b) moderate speed, (c) high speed. Experiments were conducted in the UV at room temperature.	81
Figure (3.14)	Plots of remaining phenol concentration (M) vs. time for phenol degradation experiments, for the reuse experiments, TiO ₂ (0.5g), dye (0.006g, 1.476×10 ⁻⁵ mol), AC (0.1g). (a) First time, (b) second time, third time, (d) fourth time fresh dye (0.006g, 1.476×10 ⁻⁵ mol) sample added. Experiments were conducted in the UV at room temperature	82
Figure (4.1)	A calibration curve showing a plot of absorbance vs. benzoic acid concentration (M). Measurements were conducted in	

List of Figures (contd.)

<i>Figure No.</i>	<i>Figure Title</i>	<i>Page</i>
	aqueous media, at room temperature	106
Figure (4.2)	Plots of remaining benzoic acid concentration (ppm) vs. time for benzoic acid degradation experiments, for the control experiments. (a) UV light with no catalyst, (b) catalyst with no light, (c) AC alone	107
Figure (4.3)	Plots of remaining benzoic acid concentration (M) vs. time for benzoic acid degradation experiments. (a) Naked dye, (b) Naked TiO ₂ . Experiments were conducted in the UV at room temperature	110
Figure (4.4)	Plots of remaining benzoic acid concentration (ppm) vs. time for benzoic acid degradation experiments for the effect of initial benzoic acid concentration. Different initial benzoic acid concentrations. (a) 200, (b) 150, (c) 100, (d) 70, (e) 20 ppm	111
Figure (4.5)	Plots of remaining benzoic acid concentration (M) vs. time for benzoic acid degradation experiments for the effect of oxygen concentration, TiO ₂ (0.5g), dye (0.003g, 0.738×10^{-5} mol). (a) opened reactor, (b) reactor closed, (c) bubbles of air. Experiments were conducted in the UV region at room temperature	112
Figure (4.6)	Plots of remaining benzoic acid concentration (M) vs. time for benzoic acid degradation experiments for the effect of dye concentration, TiO ₂ (0.5g), dye (a) 0.005g, 1.23×10^{-5} mol, (b) 0.004g, 0.984×10^{-5} mol, (c) 0.006g, 1.476×10^{-5} mol, (d) 0.007g, 1.772×10^{-5} mol, (e) 0.003g, 0.738×10^{-5} mol, (f) 0.01g, 2.46×10^{-5} mol. All experiments were conducted in the UV region at room temperature	113
Figure (4.7)	Plots of remaining benzoic acid concentration (M) vs. time for benzoic acid degradation experiments for the effect of radiation, TiO ₂ (0.5g), dye (0.003g,	

Figure No.	Figure Title	Page
	0.738×10 ⁻⁵ mol). (a) UV- light, (b) visible light. All experiments were conducted at room temperature	116
Figure (4.8)	Plots of remaining benzoic acid concentration (M) vs. time for benzoic acid degradation experiments for the effect of AC, TiO ₂ (0.5g), dye (0.006g, 1.476×10 ⁻⁵ mol). (a) With AC (0.1g), (b) no AC. All experiments were conducted in the UV at room temperature	117
Figure (4.9)	Plots of remaining benzoic acid concentration (M) vs. time for benzoic acid degradation experiments for the effect of dye concentration, TiO ₂ (0.5g), AC (0.1g), dye (a) 0.006g, 1.476×10 ⁻⁵ mol, (b) 0.01g, 2.46×10 ⁻⁵ mol, (c) 0.012g, 20952×10 ⁻⁵ mol, (d) 0.003g, 0.738×10 ⁻⁵ mol. All experiments were conducted in the UV region at room temperature	118
Figure (4.10)	Plots of remaining benzoic acid concentration (M) vs. time for benzoic acid degradation experiments for the effect of radiation, TiO ₂ (0.5g), dye (0.006g, 1.476×10 ⁻⁵ mol), AC (0.1g). (a) UV-light, (b) visible light. Experiments were conducted at room temperature	119
Figure (4.11)	Plots of remaining benzoic acid concentration (ppm) vs. time for benzoic acid degradation experiments for the effect of catalyst concentration. (a) 1.0g catalyst, (b) 0.6g catalyst, (c) 0.3g catalyst. Experiments were conducted in the UV at room temperature	120
Figure (4.12)	Plots of remaining benzoic acid concentration (ppm) vs. time for benzoic acid degradation experiments for the effect of temperature, TiO ₂ (0.5g), dye (0.006g, 1.476×10 ⁻⁵ mol), AC (0.1g). (a) 20°C, (b) 30°C, (c) 40°C. Experiments were conducted in the UV region	121

List of Figures (contd.)

Figure No.	Figure Title	Page
Figure (5.1)	A calibration curve showing a plot of absorbance vs. Tamaron concentration (M). Measurements were conducted in aqueous media, at room temperature	134
Figure (5.2)	Plots of remaining Tamaron concentration (M) vs. time for Tamaron degradation experiments for the control experiments. (a) visible light with no catalyst, (b) catalyst with no light, (c) AC alone	135
Figure (5.3)	Plots of remaining Tamaron concentration (M) vs. time for Tamaron degradation experiments, using visible light. (a) Naked dye (b) Naked TiO ₂	136
Figure (5.4)	Plots of remaining Tamaron concentration (M) vs. time for Tamaron degradation experiments for the effect of dye concentration, TiO ₂ (0.5g), dye (a) 0.005g, 1.23×10^{-5} mol, (b) 0.003g, 0.738×10^{-5} mol, (c) 0.01g, 2.46×10^{-5} mol. All experiments were conducted using visible light, at room temperature	139
Figure (5.5)	Plots of remaining Tamaron concentration (M) vs. time for Tamaron degradation experiments for the effect of radiation, TiO ₂ (0.5g), dye (0.003g, 0.738×10^{-5} mol). (a) UV region (b) visible region	140
Figure (5.6)	Plots of remaining Tamaron concentration (M) vs. time for Tamaron degradation experiments for the effect of initial Tamaron concentration. Different initial Tamaron concentrations. (a) 0.01, (b) 0.008, (c) 0.006, (d) 0.004, (e) 0.001M	141
Figure (5.7)	Plots of remaining Tamaron concentration (M) vs. time for Tamaron degradation experiments for the effect of oxygen concentration, TiO ₂ (0.5g), dye (0.006g, 1.476×10^{-5} mol), AC (0.1g). (a) Reactor not closed, (b) reactor closed, (c) bubbles of air. Experiments were conducted in the visible region at room temperature	142

List of Figures (contd.)

Figure No.	Figure Title	Page
Figure (5.8)	Plots of remaining Tamaron concentration (M) vs. time for Tamaron degradation experiments for the effect of dye concentration, TiO ₂ (0.5g), AC (0.1g), dye (a) 0.006g, 1.476×10^{-5} mol, , (b) 0.01g, 2.46×10^{-5} mol, (c) 0.012g, 20952×10^{-5} mol, (d) 0.003g, 0.738×10^{-5} mol. All experiments were conducted using visible light, at room temperature	143
Figure (5.9)	Plots of remaining Tamaron concentration (M) vs. time for Tamaron degradation experiments for the effect of radiation, TiO ₂ (0.5g), dye (0.006g, 1.476×10^{-5} mol), AC (0.1g) (a) UV-light, (b) visible light, at room temperature	144
Figure (5.10)	Plots of remaining Tamaron concentration (M) vs. time for Tamaron degradation experiments for the effect of AC, TiO ₂ (0.5g), dye (0.006g, 1.476×10^{-5} mol), (a) with AC (0.1g), (b) no AC. All experiments were conducted using visible light, at room temperature	145
Figure (5.11)	Plots of remaining Tamaron concentration (M) vs. time for Tamaron degradation experiments for the effect of temperature, TiO ₂ (0.5g), dye (0.006g, 1.476×10^{-5} mol), AC (0.1g), (a) 20°C, (b) 30°C, (c) 40°C. All experiments were conducted using visible light	146
Figure (5.12)	Plots of remaining Tamaron concentration (M) vs. time for Tamaron degradation experiments for the effect of catalyst concentration. (a) 1.0g catalyst, (b) 0.6g catalyst, (c) 0.4g catalyst, (d) 0.3g catalyst, (e) 0.1g catalyst . Experiments were conducted in the visible at room temperature	147
Figure (5.13)	Plots of remaining Tamaron concentration (M) vs. time for Tamaron degradation experiments for the effect of AC, TiO ₂	

List of Figures (contd.)

<i>Figure No.</i>	<i>Figure Title</i>	<i>Page</i>
	(2.0g), MnP (0.06 ml) (a) with AC (0.1g), (b) no AC, (c) naked TiO ₂ . All experiments were conducted using visible light, at room temperature	149
Figure (5.14)	Plots of remaining Tamaron concentration (M) vs. time for Tamaron degradation experiments for the effect of radiation, TiO ₂ (2.0g), MnP (0.06 ml) (a) UV-light (b) visible light, at room temperature	150
Figure (5.15)	Plots of remaining Tamaron concentration (M) vs. time for Tamaron degradation experiments for the effect of radiation, TiO ₂ (2.0g), MnP (0.06 ml), AC (0.1g) (a) UV-light, (b) visible light, at room temperature	151

XVII
**DYE-MODIFIED NANO-CRYSTALLINE TiO₂ SURFACES IN
LIGHT-DRIVEN WATER PURIFICATION FROM ORGANIC
CONTAMINANTS**

By
Lamees Zuhair Abdul Razeq Majjad
Supervisor
Prof. Hikmat Hilal
Co supervisor
Dr. Nidal Zatar

Abstract

Phenol and benzoic acid are examples of water contaminants that are difficult to degrade by conventional chemical and/or biological methods in water. Photo-electrochemical methods have been examined to degrade phenol and benzoic acid, in this work. Naked, and/or modified TiO₂ (anatase) surfaces have been examined for such purposes. There are many researches in this field, but for the first time TiO₂, modified with metalloporphyrins (MnP) and triphenylpyrilium hydrogen sulfate (TPPHS) have been prepared and used, and also for the first time the modified TiO₂ systems were supported onto activated carbon (AC) and used in degradation experiments. UV light was needed for degradation of phenol and benzoic acid, giving CO₂ and H₂O as final products.

Visible light was successfully used to degrade Tamaron insecticide using TiO₂/TPPHS and AC/TiO₂/TPPHS catalytic systems, which are prepared for the first time in this research. Supported and unsupported TiO₂/MnP was also catalytically active in visible light degradation of Tamaron, which are also prepared for the first time in this research.

All photo-degradation processes demanded oxygen but not in high concentrations. It was noticed that the degradation was also temperature, speed of stirring, catalyst concentration, and initial concentration of contaminants independent. Recovered AC/TiO₂/TPPHS catalyst samples

showed lower activity than fresh ones. The activity loss is attributed not to TPPHS degradation but to TiO_2 /TPPHS burial inside AC bulk.

The results indicate the importance of TPPHS or MnP dyes in activating TiO_2 in degradation processes, by behaving either as sensitizers, when using visible light, or as charge transfer catalysts, when using ultra violet light. Considering that, we propose charge transfer catalyst model for the first time.

CHAPTER 1

INTRODUCTION

1.1 SEMICONDUCTOR ELECTRODES

1.1.1 Introduction

Semiconductor electrochemistry is a relatively new but mature branch of electrochemistry. Although, many early reports exist of electrodes that exhibit semiconductor behavior, the first paper on a well-defined semiconductor appeared in 1955 [1]. The behavior of germanium, polarized in aqueous electrolytes was described. In 1960 many workers contribute to the fundamental study of semiconductor electrodes, the bulk of the work focused on silicon and germanium [2]. From these studies the chief attributes of semiconductor electrodes were delineated as:

- (1) The presence of two energy bands separated by a band gap, with charge transfer proceeding by either the two energy bands.
- (2) The low concentration of mobile charge carriers within the semiconductor relative to the electrolyte.
- (3) The photo-excitation of electrons from the valence to the conduction band, leading to enormous photo effects in semiconductor electrochemistry.

In 1971, and 1972 Fujishima and Honda [3] reported that water could be electrolyzed to oxygen and hydrogen in simple cells using platinum and TiO_2 electrodes.

Attention was turned to the regenerative solid liquid junction/ space charge (SLJSC). In this device a reversible redox couple is simultaneously oxidized and reduced at the semiconductor and metal electrodes. Sunlight is converted to electrical current with no net change in SLJSC [4].

1.1.2 Fundamentals: Energy and Band Model

As pointed out earlier, the semiconductor electrochemistry has forced the alliance of solid state physics with electrochemistry. An important result of such alliance is the emergence of a new term, semiconductor/electrolyte interface. The convention is largely based on the energy band diagram of solid state physics [5].

1.1.2.1 Energy bands in solids

Mainly, the semiconductors of interest are network solids; the bond network extends throughout the volume of the crystal. The energy levels that exist for a discrete bond between a pair of atoms split into a very large number of closely spaced energy levels in the macroscopic solid. The ensemble of energy levels is called an energy band. The energy spacing between adjacent energy levels is so small that energy bands are treated as a continuum of energy levels. The continuum has well-defined upper and lower energetic limits. The energy level diagram of a network solid consists of a stacked series of energy bands. The highest filled energy band [valence] and the lowest empty energy band [conduction] are the most important in terms of charge transport and charge transfer, in a semiconductor or an insulator. These bands are separated by a gap devoid of energy levels, Figure (1.1) [6]. In a metal, the two bands overlap, or the valence band is partially filled with electrons.

The band gap energy and the positions of E_v and E_c band edges on an electrochemical potential scale are the primary determinants of the properties and behaviors of semiconductor electrodes. The preferred energy unit for E_{bg} is electron-volts (eV), since this unit translates readily into the electrochemical scale, Figure (1.2) [7].

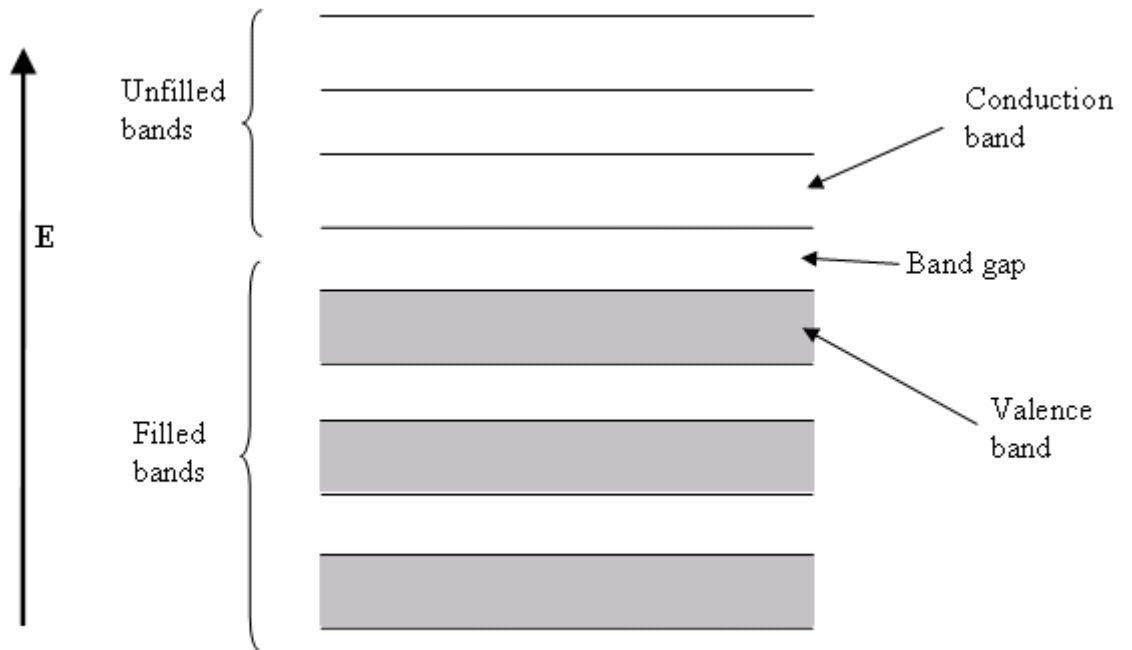


Figure (1.1): The energy band diagram for a semiconductor in contact with an electrolyte. E_c : conduction band; E_v : valence band; E_{bg} : band gap energy.

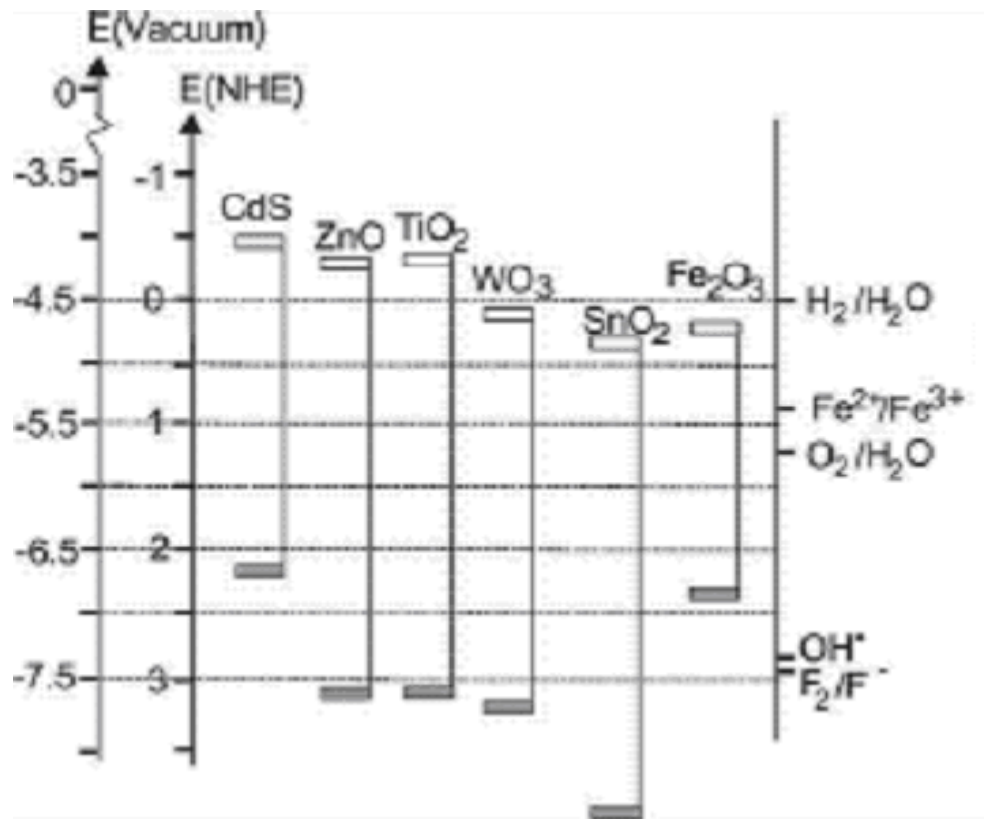


Figure (1.2): Band positions (top of valence band and bottom of conduction band) of several semiconductors together with some selected redox potentials

1.1.2.2 Charge carrier generation

A metal conducts electricity because it has empty energy levels immediately above the occupied ones. Electrons are thermally excited to the empty levels and acquire lateral mobility along the adjacent empty levels. A perfect semiconductor at absolute zero is a non-conductor, because the valence band is completely occupied and the conduction band is totally empty. To impart electrical conduction, charge carriers must be created by at least one of the following mechanisms [8]: Thermal generation, doping, or photo-excitation. Figure (1.3) shows such mechanisms [6].

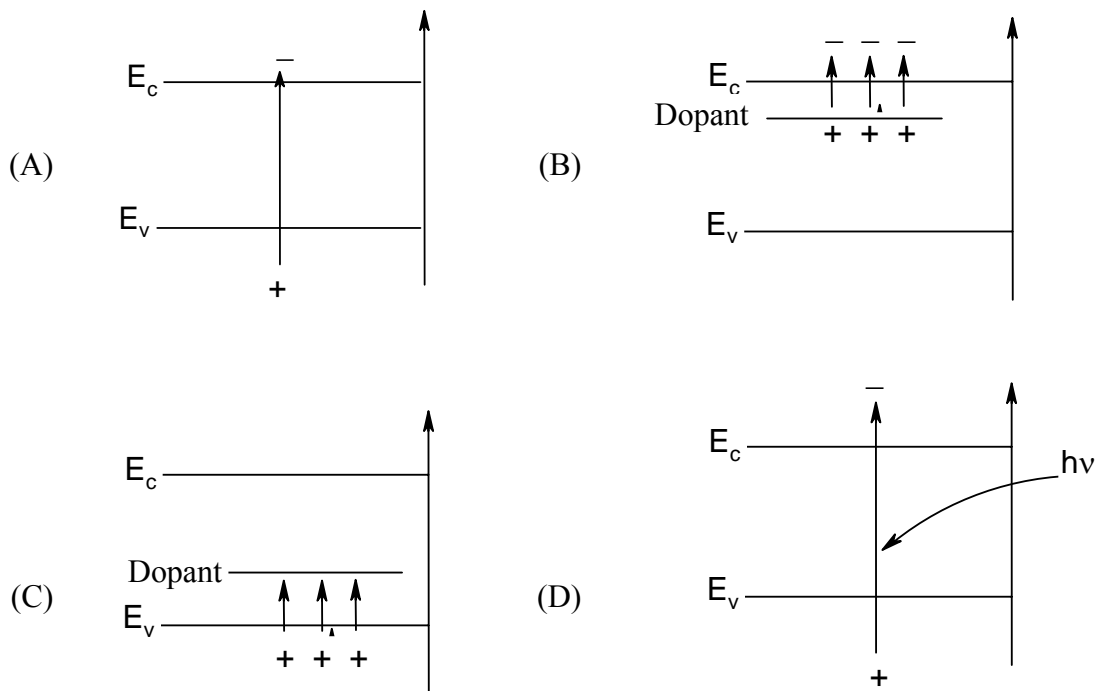


Figure (1.3): Mechanisms of charge carrier generation in a semiconductor, A: Thermal generation, B: n-type doping, C: p-type doping, D: Photo excitation.

1.1.2.3 The Fermi level

Thermodynamically the Fermi level (E_f) is the electrochemical potential of the electron in the solid. An equivalent definition arises from the distribution of electrons among energy levels in a solid. The Fermi level is the hypothetical energy level at which the probability of an energy level being occupied by an electron is exactly 1/2. The Fermi level is an extremely important parameter for metal and semiconductor electrochemistry, since it is the property which is controlled by the externally applied potential.

For semiconductors, the Fermi level resides in the band gap region. The word "level" is misleading in that it implies the existence of an actual energy level, but neither the thermodynamic nor the statistical definition requires one. For n-type doping, the Fermi level shifts toward the conduction band lowest edge, while p-type doping shifts it towards the valence band highest edge [9].

1.1.2.4 Photo-effect

A doped semiconductor has an enormous disparity in the concentrations of two types of charge carriers. Consequently, when light absorption generates a population of excited holes and electrons, the majority carrier concentration changes relatively little and minority carrier concentration is greatly enhanced.

Initial approximation photo-effects switch on as the wavelength of incident light decreases below λ_{bg} . With wavelengths longer than λ_{bg} the electrode is relatively insensitive to light. The dependence of photocurrent on excitation wavelength provides information about the bandgap energy.

Another phenomenon, important to photo-effects, is recombination. The excited hole and electron, resulting from excitation, annihilate one another with the evolution of heat or photon.

Photocurrent at n-type arises from the flux of holes (minority carriers) arriving at the surface. After light absorption generates an electron-hole pair in the depletion layer, the electric field in the depletion layer separates the two charge carriers, with the electron moving toward the bulk of the crystal and the hole migrating toward the surface, Figure (1.4) [6].

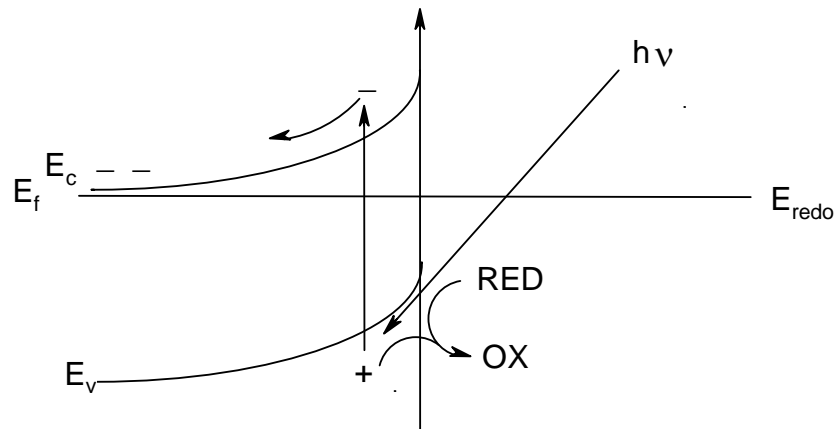


Figure (1.4): Photocurrent generation at n-type semiconductor

1.2 NANOCRYSTALS

1.2.1 Introduction

Nanotechnology is the development and utilization of structures and devices with a size range from 1 nm (molecular scale) to 100 nm, where physical, chemical and biological properties occur as compared to bulk materials [10]. The new properties are generally realized at the nanoparticle or nanocrystal level, and assembling of precursor nanoparticles is the most generic route to nanostructured materials. A main issue is how the scientific paradigm changes will translate into novel concepts in

manufacturing processes. Nanoparticles are used either as precursors to generate more complex structures and devices, or modifiers (enhancing or changing) of physical phenomena, chemical or biological processes. Nanoparticle manufacturing processes aim to take advantage of two kinds of effects:

- (a) New physical, chemical or biological processes and laws that are caused by the reduced size of the particles, tubes, layers, or other nanostructures. Smaller particle size dictates larger relative surface area quantum-confinement and transport size effects. New properties appear as size is reduced.
- (b) Generation of new atomic, molecular and macromolecular structures of materials by using either chemistry (e.g. macromolecular structures and self-assembling techniques), nanofabrication (e.g. creating nanostructures on surfaces), or biotechnology (e.g. evolutionary approach) routes [11].

Few nanoparticle synthesis processes have developed their scientific base decades ago, long time before other nanotechnology areas have emerged. We find in this category the pyrolysis process for carbon black and flame reactions for pigments [12], particle polymerization techniques [13-15], self-assembly micelles [16], and chemistry self-assembly [17]. Several kinds of nanoparticles are routinely produced for commercial use via aerosol and colloidal reactors in the U.S, Japan and Europe. The challenge is to control the nanoparticle size, morphology and properties, assemble them for a given purpose, and to do this with a variety of materials. Nanoparticle processing into functional structures has recently

received more attention. Main areas of relevance are advanced materials and manufacturing, electronics, biotechnology, pharmaceuticals and sensors.

1.2.2 Manufacturing processes

Nanoparticle systems, including nano-clusters, nano-tubes, nanostructured particles, and three-dimensional structures are seen as tailored precursors for nanostructured materials and devices. The improved properties are obtained in this dimension range as a function of material. Powder processing (sintering, extrusion, plasma activation, etc.) is the most general method to prepare nanostructured materials and devices.

Nanoparticle manufacturing processes may be grouped into four categories:

- (1) Nanoparticle synthesis: this includes precipitation from solutions (colloids), gas condensation (aerosols), chemical, plasma, combustion, spray pyrolysis, laser ablation expansion of supercritical fluids, polymerization, mechanical attrition, molecular self-assembly, hydrodynamic activation and other processes. The selection of the most suitable method is generally based on several criteria related to (a) the desired product: size distribution (particle size, monodispersity), particle generation flow rate, and (b) the particle production facility: its complexity, operation conditions (temperature, pressure, toxicity, etc.), and cost [18-20].
- (2) Processing nanoparticles into nanostructured materials (such as advanced ceramics), nanocomponents (such as thin layers), and nanodevices (such as sensors). Examples of processing

methods include sintering [21], creation of nanostructures on surfaces, evolutionary biotechnology [22], and self-assembly techniques [17].

- (3) Utilization of nanoparticles to create or enhance an effect or a phenomenon. This includes processes of mechanical (erosion resistance, friction reduction, sintering aids, etc.), chemical (catalysts, sensors, filtration agents, etc.), optical (pigmentation, filters, waveguides, etc.), electrical (quantum dots, superconductors, insulation, electroceramics with nonlinear electrical response, etc.), magnetic (giant magnetoresistive, superparamagnetic effects) and biological (separation and filtration, active agents, etc.) nature. Examples of more frequently used manufacturing processes of this kind are (a) Nanoparticle deposition and removal from surfaces, with relevance to microcontamination and chemical vapor deposition; (b) use of particles for surface modification, such as in chemical-mechanical polishing (CMP); (c) separation processes, including filtration, mass spectroscopy, and bioseparation; (d) Nanoparticle emission and control, including combustion pollution control; (e) biomedical applications, including drug delivery and health diagnostics; (f) and use of Nanoparticles as catalysts in chemical plants [23].
- (4) Process control and instrumentation aspects. This includes off- and on-line measuring techniques for fine particles and their structures. Besides the better known characterization

methods for particle size, shape and composition, new instruments are developed to measure particle interaction forces, their roughness, electrical, magnetic and thermal properties. A special attention is given to scanning probes, optical and laser-based diagnostic techniques. For example, the previously developed Raman spectroscopic analysis applicable to larger particles has been extended to nanoparticles [24]. An increase in the measurements sensitivity has been achieved by electro-dynamically trapping and illuminating the assembly of trapped particles. Scanning thermal microscopy has been developed [25] using thermal sensors mounted on Atomic Force Microscope (AFM) tips. A spatial resolution of 25 nm has been obtained for temperature measurements on solid surfaces. The scanning Joule expansion microscopy is an improvement of the technique that simplifies the fabrication of the sensor and enhances the resolution to about 10 nm [26].

1.2.3 The nanostructured electrode

Nanostructured electrodes may be prepared by successively breaking up an ideal single crystal (or epitaxial layer) into smaller and smaller interconnected crystals. It is obvious that for a given amount of electrode material the interfacial surface area is increasing in this process of subdividing the single crystal and making it more porous. Finally we reach the limiting case “ the Ångström region “ where further subdivision is not possible without breaking up the structure totally into small molecules and atoms. On the molecular level, the size of the elements building up the

three-dimensional semiconductor network is so small. We can no longer describe the electrode material with macroscopic physical model, where a space charge layer is formed. The Schottky barrier model, normally used to describe a macroscopic single crystal electrode in contact with an electrolyte, is no longer relevant. Quantum size effects must be considered and will be increasingly important as the size of the elements, building the network and forming an interface with the electrolyte, approach the molecular level.

Moreover, the charge transfer and the chemistry at the semiconductor electrode interface (SEI) will be very important for the performance of the electrode [27]. The interfacial kinetics, and the ability to transfer charge through the nanostructured semiconductor and the nanopores without losses will be a ruling factor for the electrode performance. In fact, already in a semiconducting electrode, where the size of the building blocks is several tenths of nanometers, these factors start to be important. A model making use of a macroscopic depletion layer in the semiconductor fails to describe the system. Nevertheless, the nanostructured electrode must be regarded as one unit made up of particles, and pores filled with electrolyte. The physical boundaries of interest in this unit are the back contact, and the interface between the nanostructured semiconductor electrode and the bulk of the electrolyte. There is of course no sharp transition between a nanostructured electrode and an ideal single crystal. Much of the anomalous behavior of polycrystalline electrodes can certainly be ascribed to their (fractal) structure and their porosity.

While the losses due to the impurities in the bulk of a semiconductor are not easily affected, the loss at the SEI can readily be varied by varying

the composition of the electrolyte. Reversible and irreversible processes at the SEI can be studied. The ability to change the composition of the electrolyte gives us an experimental key to deeper understanding of the nanostructured electrode system.

A porous nanostructured semiconducting material would certainly twenty years ago be regarded as a hopeless candidate for any kind of solar cell application. Today we know that dye-sensitized nanostructured electrodes work with surprisingly high efficiencies. An intriguing problem is therefore to understand how such nanostructured systems separate and transport photoinduced charges without major current losses [28]. An important part in the system is the electrolyte. We can define an ideal nanostructured electrode as an electrode built up by electrically interconnected nanometer sized particles in which the electrolyte penetrate the electrode from the semiconductor bulk-electrolyte interface, all the way up to the back contact. We have called such an electrode material "nanoporous-nanocrystalline".

1.2.4 Applications of nanocrystals

Electrochemical techniques have been used in the synthesis and processing of nanostructured films of metals, alloys semiconductors, superconducting compounds, and conducting polymers. In addition, researchers have begun to explore possible applications for these materials in electrochemistry. Application of nanostructured materials in solar energy conversion, electrochemical storage, catalysis, electronics, and sensors are currently being explored [29-30].

Recently, devices combining to some extent properties of conventional TiO₂ films and those of powder or colloidal photocatalysts are attracting major interest. Such highly porous nanocrystalline films, consisting of a fine powder or colloid deposited on a conducting substrate, have first been successfully applied in dye-sensitized wet photovoltaic devices. When submitted to direct bandgap illumination in the presence of redox species in the solution, the porous nanocrystalline films exhibit a series of quite peculiar properties. Particularly usual is their high selectivity towards some photooxidation reactions, especially those involving small organic molecules.

1.3 TITANIUM DIOXIDE

1.3.1 Introduction

The impetus for current extensive research efforts in semiconductor electrochemistry is solar energy conversion. TiO₂ is one of the first nanoparticle semiconductors to be recognized for such purposes. The key point which distinguishes TiO₂ from other semiconductors is the stability and ease of manufacturing polycrystalline electrodes.

Although TiO₂ has wide-spread recognition, because of the facts mentioned above, its wide band gap (3.2 eV) sets a low ceiling to the maximum possible efficiency of solar conversion. Only 3% of natural sunlight can be absorbed by TiO₂ [31], as UV excitation is required in order that the photochemical processes may proceed conveniently [32-34].

TiO₂ may be prepared by different methods. The wet method involves bulk precipitation, sol-gel, inverse micelle, spray, electrospray or tubular templates. The gas-phase method involves evaporation, condensation,

deposition or combustion. The vacuum techniques involve sputtering, laser ablation and ionized beam deposition. Mechanical and self-assembly techniques are also known [35-36].

1.3.2 TiO₂ bulk properties

1.3.2.1 Crystal phases

TiO₂ has three naturally occurring crystal phases: rutile, anatase and brookite.

Both rutile and anatase have tetragonal unit cells, Figure (1.5) [6], with slightly distorted TiO₂ octahedral. The relative crystallographic parameters are listed in Table (1). The bond lengths for rutile and anatase are similar, but the anatase octahedra exhibit greater distortion in bond angles. Consequently anatase has a somewhat more open structure with a higher molar volume and a lower density.

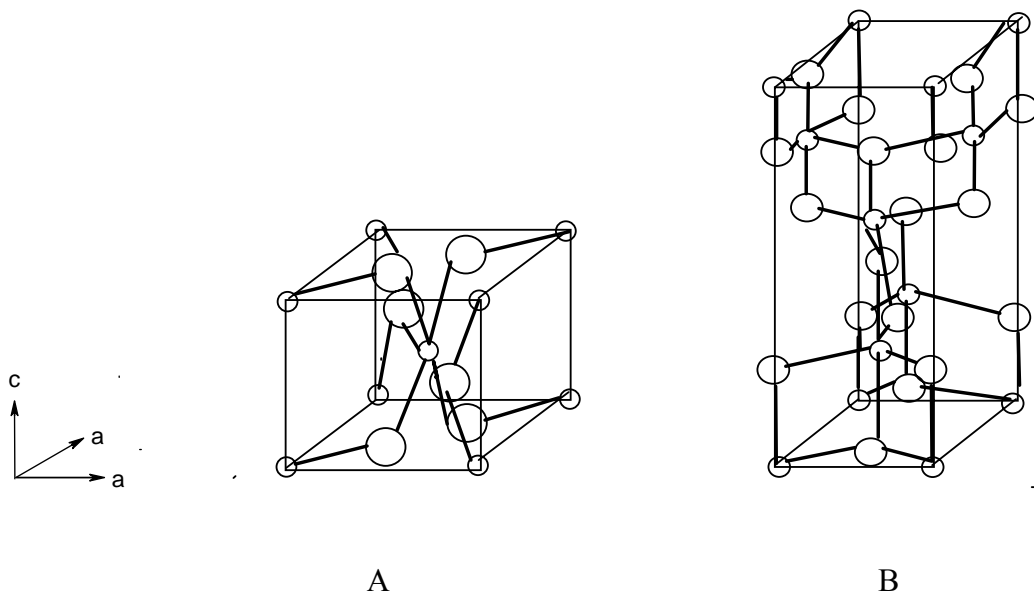


Figure (1.5): TiO₂ crystal structures. A: The unit cell for rutile, B: The unit cell for anatase. The small circles are the Ti cations and the large circles are the O anions.

Small cations and anions can migrate relatively rapidly through channels in the two lattices, a process that affects the uniformity of doping and the density of recombination centers.

The channel in rutile lies parallel to the c-axis (perpendicular to the (001) face). It has roughly circular dimensions with an approximate radius of 0.8Å, based on ionic radii of 0.6Å and 1.3Å for Ti and O respectively. In contrast, the channels in anatase run perpendicularly to the c-axis and to each other. There are three oblong channels with a minimum diameter of 0.7Å which penetrate the (100) face.

Table (1): Crystallographic parameters for rutile and anatase TiO₂ [37- 38]

Rutile	Anatase
2 TiO ₂ formula units per unit cell	4 TiO ₂ formula units per unit cell
Unique Ti coordinates (0,0,0) and (a/2,a/2,c/2)	Unique Ti coordinates (0,0,0), (a/2,a/2,c/2), (a/2,0,c/4) and (0,a/2,3c/4)
Unique O coordinates (±ax, ±ax, 0) and (±a (0.5 +x), ±a (0.5-x), c/2).	Unique O coordinates (0,0, ±cx), (a/2,a/2,c(0.5±x)), (a/2,0,c(0.25±x)), (0,a/2,c(0.75±x))
a= 4.59366, c= 2.95868Å, x= 0.3048	a= 3.7842, c= 9.514Å, x=0.208
Ti—O bond lengths: 1.949Å (4 per octahedron) and 1.980Å (2 per octahedron)	Ti—O bond lengths: 1.9336Å (4 per octahedron) and 1.9800Å (2 per octahedron)
O—Ti—O bond angles: 90°, 81.21° and 98.79°	O—Ti—O bond angles 90°, 78.10°, 101.90°
Molar volume: 18.80 cm ³ /mol	Molar volume: 20.52 cm ³ /mol
Density: 4.250 g/cm ³	Density: 3.894 g/cm ³

1.3.2.2 Optical properties

The absorption and reflection properties of TiO₂ have been studied extensively. At 4K, the short wavelength absorption edge is 410 nm [35-36, 39]. TiO₂ is transparent through the visible and near infrared; lattice absorptions starting at ca. 8 microns. Indices of refraction in the visible

have been reported by Cronemeyer [32] and are rather high (2.4- 2.8). The lowest energy electronic absorption at 3.03eV is an indirect transition with a slight polarization and orientation dependence [40-42].

It has π - π^* character [40], suggesting that the e_g -like band dominates the lower part of the conduction band. A direct transition, polarized perpendicularly to the c-axis, occurs at 3.45- 3.6eV [41-43].

1.3.2.3 Electrical properties

Electrical properties of TiO₂ necessarily refer to doped materials due to high resistivity of undoped TiO₂. Doped TiO₂ is always n-type. A substantial difference in the electrical properties would be expected for the directions parallel and perpendicular to the c-axis. Indeed the early measurements of dielectric constant and conductivity in TiO₂ meet this expectation [39].

1.3.3 Applications of TiO₂

Specific characteristics of nanoporous TiO₂ films are their transparent nature, high internal surface area, surface anchoring abilities and possibility to tune the potential of the conduction band edge. Dye-sensitized TiO₂ electrodes have shown strikingly high photovoltaic conversion efficiencies. The transparent nature of these films allows for the direct monitoring of electron transfer process by spectroscopic means.

TiO₂ has been used in many photoelectrochemical applications:

1. Device manufacturing:

Modern devices such as photovoltaic devices, and electrochromic devices are manufactured.

2. Solar energy conversion devices:

Dye-sensitized photochemical solar cell systems based on highly porous nanocrystalline films of TiO_2 are of considerable technological interest, (Grätzel cell).

3. Water Purification:

TiO_2 has greatly been used for the purpose of water purification processes; it has been used widely as a naked semiconductor in the photodegradation of organic and inorganic contaminants, Table (2). Sensitized TiO_2 surfaces have been prepared and characterized [44-45]. The modified TiO_2 surface has also been used in the degradation of organic and inorganic contaminants. In literature there are many examples of modified TiO_2 surfaces, Table (2). TiO_2 , supported onto insoluble materials such as activated carbon (AC), glass bead, zeolite, silica, and Ti-6Al-4V alloy, have recently been prepared, Table (2). Activated carbon loaded with ruthium oxide as a capacitor has been also used, where ruthium oxide is used in order to increase the capacitance of the activated carbon [46].

Earlier works on water purification

There are numerous reports on this topic, scientists degrade many contaminants either inorganic or organic contaminants.

Inorganic contaminants:

Wen-Yan Lin and others reduced Cr (VI) at TiO_2 in aqueous basic media [47]. The thermodynamic aspects of the photocatalytic reduction of Cr (VI) at TiO_2 are first discussed and contrasted for $\text{pH}=0$, and $\text{pH}=10$ aqueous media. The photo-corrosion of TiO_2 is shown to be thermodynamically less favorable in basic media. A scheme for the one-

step removal of Cr(VI) at TiO₂ via its reduction and subsequent immobilization [as Cr(OH)₃] is demonstrated for pH=10 chromate solutions. Dissolved oxygen is shown to inhibit the reduction of Cr (VI). A preliminary kinetics analysis reveals adherence of the initial rate of Cr (VI) reduction to the simple Langmuir model.

Wen-Yan Lin and others had after then studied the photo-catalytic removal of Nickel (Ni (II)) from aqueous solutions using ultraviolet – irradiated TiO₂ [48]. The photo-catalytic reaction is shown to be electron mediated, and occurs both via direct electron transfer from photo-excited TiO₂ particles to Ni (II), and an indirect route. The latter requires the presence of an organic additive (acetate, formate, or methanol) that generates an intermediate radical reductant via an initial hole-mediated reaction. The effects of inorganic anions (chloride, sulfate) on the rate of Ni (II) removal are described as are those of other variables including TiO₂ dose and solution pH. The direct electron-transfer route is shown to be kinetically sluggish, although it can be made fast by the addition of facile hole acceptors. The dark adsorption of Ni (II) on the TiO₂ (anatase) surface is also quantified in a chloride medium.

Organic contaminants

J. Anthony Byrne and others degraded organic pollutants and reduced metals from waste waters [49]. Photo-anodes were prepared by immobilizing TiO₂ powder on the surface of Ti-6Al-4V alloy. The TiO₂ electrode was incorporated into the anode compartment of a two compartment photo-electrochemical cell and short circuited to a copper wire counter electrode in the cathode compartment. The anode compartment contained oxalate solution and the cathode compartment

contained copper sulfate solution. On illumination of TiO_2 anode oxalate was photo-oxidized at the surface of the TiO_2 and the photo-generated electrons moved via the external circuit to the counter electrode where copper ions were reduced. Ninety-seven per cent of the copper in solution was recovered after 120 min of irradiation.

A. Abdel Wahab and A. Gaber oxidized some heterocyclic sulfur compounds [50]. Polynuclear-heterocyclic sulfides (I-IV) were oxidized dominantly to the corresponding sulfoxides and sulfones via TiO_2 -mediated photo-catalytic oxidation in aerated acetonitrile. Also methylene group in IV and V and active methylene groups in VI have been readily oxidized to carbonyl one in a high yield under the same prevailing conditions. A plausible electron transfer mechanism, in which an electron-hole pair is generated on the surface of TiO_2 by illumination, is suggested for the semiconductor-mediated photo-catalysis.

P. Calza and others decomposed bromomethanes in irradiated aqueous solutions [51]. The decomposition of bromomethanes has been studied by homogeneous photolysis and by heterogeneous photo-catalysis. The photolytic degradation of tetrabromomethane has been investigated also for the effect of pH and oxygen presence. The photo-catalytic degradation of CBr_4 , CHBr_3 and CH_2Br_2 over irradiated TiO_2 has been investigated at pH=5.5 under aerobic and anaerobic conditions.

Bromomethanes degrade through combined reductive and oxidative processes. The importance of reductive pathways decreases from CBr_4 to CHBr_3 and CH_2Br_2 . Brominated and oxygenated intermediates have been quantified until complete degradation or debromination was achieved.

Reactions accounting for the observations were presented based on presumed transient species and identified intermediates.

The effect of hole and electron scavengers was evaluated on CHBr_3 and CH_2Br_2 to elucidate the importance of reductive and oxidative pathways. Electron scavengers as periodate, enhance the rate of disappearance for CH_2Br_2 . The hole scavengers as alcohols, have limited effect on the degradation rate of CHBr_3 but interestingly, have different effects on the degradation rate of CH_2Br_2 , tet-Butanol does not significantly affect the degradation rate whilst methanol increases it. Methanol generates radicals efficiently react with CH_2Br_2 , notably if the system is oxygen-free.

K. Wang and others degraded 2-chloro and 2-nitrophenol by titanium dioxide suspensions in aqueous solutions [52]. This investigation used a specifically built jacketed cylindrical type reactor with suspended titanium dioxide under UV-light 365 nm for feasibility studies of decomposition of mono-substituted phenols. The factors to be studied were the effects of pH, anion additives and the influence of co-existing reactants competing for reaction. Finally, the degree of mineralization of reactants was conducted in order to survey the effectiveness of treatment.

From experimental results, under the condition of 7.5g/l TiO_2 , pH=3, and light intensity of $2.25\text{mW}/\text{cm}^2$, 0.1 mM of substituted phenol could be completely decomposed in 2 h. The reaction was found to be apparent first-order following Langmuir-Hinshelwood model. In the presence of chloride ions, a significant inhibition of reaction was found at pH=3, but not at higher pH levels. At pH=3, a slight inhibition was found for nitrate

ions, but uncertain for sulfate ions. For the experiment with co-existing 2-chloro and 2-nitrophenol, the result differed from that of the individual specie. In the mineralization experiments, substitution in the phenol ring had no applicable influence on the reaction rate, however, complete mineralization to carbon dioxide could not be completed within 9h.

K. Wang and others had after then degraded trichloroethylene (TCE) in gas phase over TiO_2 supported on glass bead [53]. In this investigation, a packed bed filled with coated titanium dioxide glass beads to study the kinetics of photo-catalytic degradation of trichloroethylene under irradiation of 365 nm UV light. In the range of 100-500 ml/min of flowrate, the reaction rate for 6 μM TCE increased with an increasing flowrate up to 300ml/min, while was not affected by the flowrate at the values higher than 300ml/min. For moisture in the range of 9.4-1222.2 μM , the reaction rate of TCE was decreased with an increasing humidity. The adsorbed water on the catalyst surface could compete with the adsorption of TCE on the sites. The reaction rate of 6 μM TCE increased as the light intensity increased, and was proportional to the 0.61 order of the light intensity.

I. Ilisz and A. Dombi decomposed phenol in near-UV-irradiated aqueous TiO_2 suspensions [54]. The photo-degradation of phenol was investigated in the presence of TiO_2 (anatase) as photo-catalyst in near-UV-irradiated aqueous unbuffered suspensions. The distribution of degradation products and a reduction in total organic carbon are reported, focusing on the influence of charge-trapping species (O_2 , Ag^+ and H_2O_2). In the presence of dissolved O_2 , the degradation proceeds predominantly via OH^\cdot , where hydroxylated aromatics were detected: catechol,

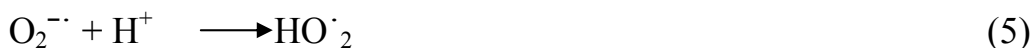
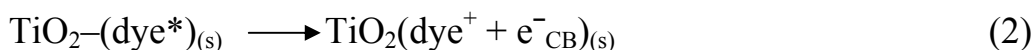
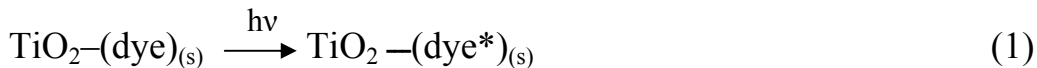
hydroquinone and 1,2,4-trihydroxybenzene; in the presence of Ag^+ , the direct hole oxidation dominates, with p-benzoquinone as the only identified transient product; in the presence of H_2O_2 , both OH^\cdot and direct oxidation by positive holes contribute to the degradation of phenol. Besides the identified compounds, the formation of presumed ring-opening products occurs simultaneously. In contrast with the general view, it is pointed out that the appearance of aliphatic products in the early stage of the oxidation process is not unambiguous proof of the participation of direct hole oxidation in the degradation mechanism.

J. Matos, and others degraded phenol on a suspended mixture of titania and activated carbon [55]. The photo-catalytic degradation of phenol has been performed at room temperature (20°C) in contact with a suspended mixture of titania and activated carbon (AC). Non-additive adsorption capacities were observed when the solids were mixed, and this was ascribed to a strong interaction, involving half of the surface of titania and ca. 14% of that of AC. A synergy effect was observed with an increase of the first order rate constant by a factor of 2.5. As for neat titania, the same main intermediate products (hydroquinone and benzoquinone) were found but in much smaller quantities and during a much smaller lifetime, suggesting that the same reaction mechanism occurred in the presence of photo-inactive AC. The synergy effect was ascribed to an extended adsorption of phenol on AC followed by a transfer to titania where it is photo-catalytically degraded. The synergy effect could not be improved by previous physical treatments of the solid mixture such as grinding and sonication. Some phenol remained adsorbed on AC when no traces of organic compounds were detected in the purified water. This adsorbed

phenol could be destroyed by illuminated titania while maintaining UV-irradiation.

D. Chaterjee and A. Mahata degraded organic pollutants on the surface modified TiO₂ semiconductor [56]. Photo-assisted decomposition of phenol, chlorophenol, and trichloethylene in waste water has been achieved on the surface of TiO₂ semiconductor modified with 8-hydroxyquinoline (HOQ) by using visible light. After 5h of irradiation with a 50 W tungsten lamp, over 70-80% degradation of pollutants is achieved. A working mechanism involving excitation of surface bound dye, followed by charge injection into the TiO₂ conduction band is proposed.

-The suggested mechanism is [56]:



P= contaminants

Table (2): Photochemical water purification processes using TiO₂ catalysts.

Catalyst	contaminant	Cond.	Result	Ref
Naked TiO ₂	Bromomethanes	UV-light	Degradation is O ₂ and pH dependent	51
Naked TiO ₂	2,4-dichlorophenoxy-acetic acid	UV-light	disappeared within 1hr	57
Naked TiO ₂	Benzofuran	UV-light	Degradation is O ₃ dependence	58
Naked TiO ₂	Formaldehyde	UV-light	Decomposed completely	59
Naked TiO ₂	Oxalate	UV-light	Degradation is O ₂ and Fe ³⁺ dependent	60
Naked TiO ₂	Salicylic acid	UV-light	Decomposed completely	54
Naked TiO ₂	Chromium	UV-light	O ₂ inhibits the reduction of Cr (VI)	47
Naked TiO ₂	Nickel	UV-light	Ni (II) adsorption is Cl ⁻¹ dependent	48
Naked TiO ₂	Cupric ion	UV-light	Reduction is formic acid dependents	55
Naked TiO ₂	2-chloro and 2-nitro-phenol	UV-light	complete mineralization to carbon dioxide could not be completed withen 9h	52
Sensitized TiO ₂	RB*	UV-&Vis.	Aromatics needs O ₂ in visible light	62
Sensitized TiO ₂	Heterocyclic sulfides in acetonitrile	UV-light	Sulfoxide and sulfone production	50
Sensitized TiO ₂	Phenol	Vis. light	70–80% degradation is achieved	56
AC/TiO ₂	Phenol	UV-light	The rate increases by a factor of 2.5	55
Glass/TiO ₂	Trichloroethylene	UV-light	It depends on flow rate and humidity	63
Ti-6Al-4V alloy/ TiO ₂	17-β-oestradiol	UV-light	98% were destroyed in 3.5 hr	64
Ti-6Al-4V alloy/ TiO ₂	Oxalate and cupric ion	UV-light	97% of copper was recovered in 120 min	49
ZSM-5 zeolite/ TiO ₂	NO	UV-light	33% of NO converse to N ₂	65

Silica/ TiO ₂	Trichloroethylene	UV-light	Degradation is temperature and silica content dependent	53
Dye/ zeolite Y/ TiO ₂	Propoxur (pesticide)	UV-light	Almost complete disappearance	66

* *RB: rhodamine B(NNNN'-tetraethyl-rhodamine)*

1.3.4 Objectives of the present work

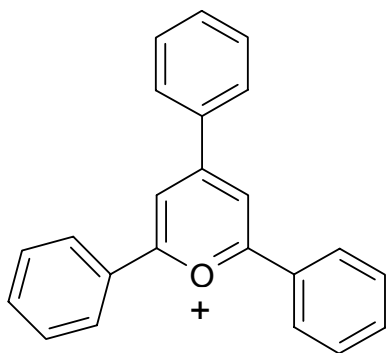
The presence of contaminants (organic pollutants, and pesticides) in ground waters, surface waters, and other sources of drinking water has recently become a great environmental concern. Most of these compounds are considered toxic or potentially carcinogenic and mutagenic to mammals and aquatic life.

Titanium dioxide remains the most frequently investigated semiconductor electrode (in the form of thin films) and photocatalyst (in the form of high surface area powders). This is principally due to its good resistance against photo corrosion in various media as well as to the high photo conversion efficiencies generally attained with polycrystalline TiO₂ films, and tubes [67-68].

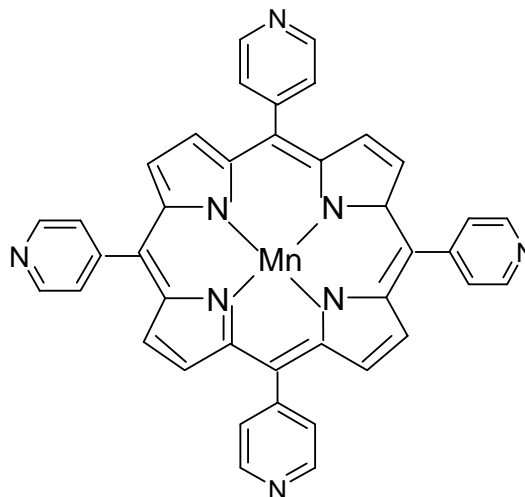
The main objectives of this work are:

- (1) To investigate the effect of naked TiO₂ surfaces in the degradation of water contaminants. UV light is needed here.
- (2) To prepare dye modified TiO₂ surfaces and study their catalytic efficiency in photo-degradation of water contaminants, using UV and visible regions. Two dyes will be studied; 2,4,6-triphenylpyrylium hydrogen sulfate (Scheme I),

and tetra-4-pyridylporphyrinatomanganese(III) complex (Scheme II).



Scheme (I)



Scheme (II)

- (3) To support naked TiO_2 and dye-modified TiO_2 particles onto activated carbon surfaces. This will yield AC/ TiO_2 and AC/ TiO_2 /dye systems. The dye is 2,4,6-triphenylpyrylium hydrogen sulfate, or tetra-4-pyridylporphyrinatomanganese(III) complex. These systems will be used as catalysts for photo-degradation of water contaminants using UV and visible radiations.

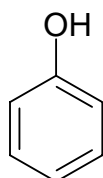
Three types of water contaminants will be degraded, which are phenol, benzoic acid, and Tamaron.

1.3.5 Hypothesis

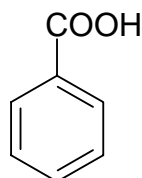
The work presented here is based on the following assumptions:

- 1) That naked TiO_2 will catalyze organic contaminant degradation by UV light in water. This is due to the large band gap of TiO_2 , 3.05

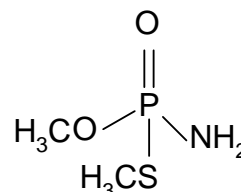
eV. When TiO_2 is irradiated with UV, the highly energetic holes, with high positive potential and high oxidizing power, created in the valence band, will oxidize all contaminants described here, phenol, Scheme (III), benzoic acid, Scheme (IV) and Tamaron Scheme (V). Scheme (VI) describes such processes. On the other hand, due to its large band gap, naked TiO_2 will not be able to photo-degrade contaminants, even unstable ones like Tamaron, in the visible region.



Scheme III



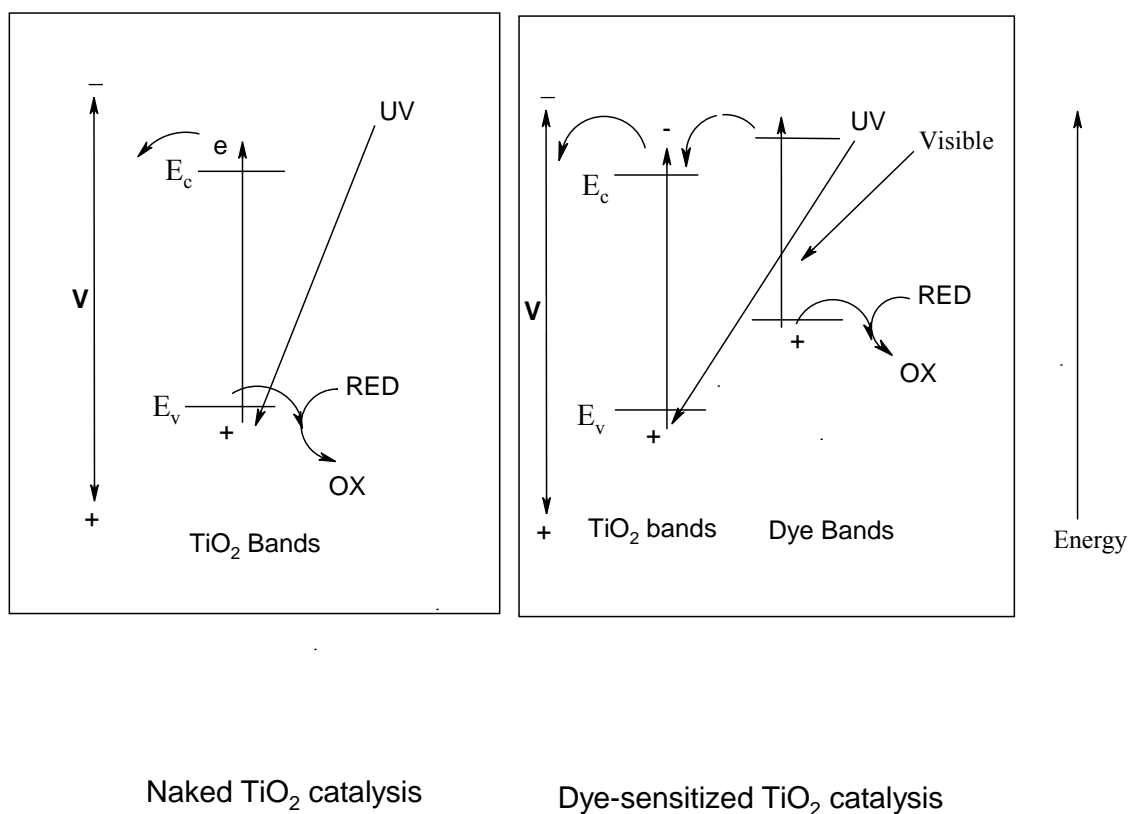
Scheme IV



Scheme V

- 2) That TiO_2 modified with special dyes, like 2,4,6-triphenylpyrilium ion or metalloporphyrines, may activate TiO_2 as catalyst for photo-degradation, in the visible region, for unstable contaminants, such as Tamaron, but the modified system will again fail to degrade stable contaminants (phenol and benzoic acid). This is because the holes created by visible irradiation, in valence band of the dye are not energetic enough (low positive potentials) to oxidize stable contaminants, Scheme (VI). The influence of the dyes on enhancing catalytic activity of TiO_2 in case of UV will be investigated, with the possibility of behaving as charge transfer catalysts.
- 3) That supporting TiO_2 onto insoluble supports, like activated charcoal, will not affect its optical or electrical properties, but will enhance its catalytic activity if conditions are met. Graphite is

assumed to adsorb contaminant molecules, and to bring them into close proximity to the TiO_2 catalytic sites. Such behavior is expected to enhance the catalytic activity of naked and modified TiO_2 . Therefore, it is assumed that the catalytic activity of naked and modified TiO_2 , in degrading phenol, benzoic acid and Tamaron, by UV, will be enhanced. It is also assumed that Tamaron degradation by visible light, with modified TiO_2 , will also be enhanced.



Scheme (VI)

REFERENCES

- 1) W. Brattain, and C. Garrell, "Physical theory of semiconductor surfaces", *Bell System Tech. J.*, **34**, (1955) 125.
- 2) W. Brattain, and P. Boddy, "The Distribution of Potential across the Low-Index Crystal Planes of Germanium Contacting an Aqueous Solution", *J. Electrochem. Soc.*, **109**, (1962) 514-518.
- 3) A. Fujishima, and K. Honda, "Electrochemical photolysis of water at a semiconductor", *Nature*, **238**, (1972) 37.
- 4) M. Williams, and S. Loyalka, "Experiments on the interface between Germanium and electrolyte", *Aerosol Science: Theory and Practice*, (1991) 129-176.
- 5) D. Montgomery, S. Kocha, and J. Nozik, "III-V Ternary semiconductors as light-gathering systems for the photoelectrochemical production of hydrogen from water", *J. Electroanal. Chem.*, **27**, (1991) 367.
- 6) H. Finklea, "Semiconductor electrodes", *Elsevier*, (1988) 4-46.
- 7) O. Carp, C. Huisman, and A. Reller, "Photoinduced reactivity of TiO₂", *Progress in Solid State Chemistry*, **32**, (2004) 33-177.
- 8) S. Kocha, D. Montgomery, and J. Tumer, "Direct conversion systems based on GaInP₂", *Phys. Rev.*, **B45**, (1992) 11173-11191.
- 9) S. Huang, G. Schlichthörl, B. Lee, A. Nozik, M. Grätzel, and A. Frank, "Charge recombination in dye-sensitized nanocrystalline TiO₂ solar cells", *J. Phys. Chem.*, (1996).

- 10) K. Zhang, I. Alexandrov, and R. Valiev, "The structural characterization of nanocrystalline Cu by means of the X-ray diffraction", *J. Appl. Phys.* **80**, (1996) 5617-5624.
- 11) C. Crowe, W. Babcock, P. Willoughby, "Drag coefficient for particle in rarefied, low mach number flows", *Prog. Heat and mass Trans.*, **6**, (1973) 419.
- 12) M. Peters, "A nonequilibrium molecular dynamics simulation of free molecule flows in complex geometries: Application to the Brownian motion of aggregate aerosols", *Phys. Rev.*, **E 50**, (1994) 4609-4617.
- 13) E. Kobatake, "A Fluoroimmunoassay based on immunoliposomes containing genetically engineered lipid-tagged antibody", *Analytical Chemistry*, **69**, (1997) 1295-1298.
- 14) N. Noskova, E. Ponomaeva, I. Pereturina, and V. Kuznetsov, "Strength and plasticity of a Pd-Cu-Si alloy in the amorphous and nanocrystalline states", *Phys. Met. and Metallogr.*, **81**, (1996) 121-138.
- 15) N. Noskova, E. Ponomaeva, A. Glazer, V. Lukshina, and A. Potapov, "The effect of preliminary deformation and low-temperature annealing on grain size in nanocrystalline $\text{Fe}_{73,5}\text{Cu}_1\text{Nb}_3\text{Si}_{13,5}\text{B}_9$ alloy produced by crystallization of amorphous ribbons", *Phys. Met. and Metallogr.*, **76**, (1993) 171-173.
- 16) R. Siegel, and G. Fougere, " Mechanical properties of nanophase metals", *Nano-Structured Materials*, **6**, (1995) 205-216.
- 17) N. Noskova, "The structure and properties of nanocrystalline polyphases alloys", *Nano-Structured Materials*, **9**, (1997) 505-508.

- 18) R. Andrievskii, A. Vikhrev, V. Ivanove, R. Kuznetsov, N. Noskova, and V. Sazonova, "Magnetic-pulse and high-pressure shear-strain compaction of nanocrystalline titanium nitride", *phys. Met. and Metallogr.*, **81**, (1996) 92-97.
- 19) A. Olofinjana, and H. Davies, "Preparation and mechanical properties Fe-Si-B-Nb-Cu nanocrystalline alloy wire" *Nano-Structured Materials*, **6**, (1995) 465-468.
- 20) R. Valiev, A. Korznikov, and R. Mulykov, "Structure and properties of ultrafine-grained materials produced by severe plastic deformation", *Materials science and engineering*, **A 168**, (1993) 141-148.
- 21) C. Koch, and Y. Cho, "Nanocrystals by high energy ball milling", *Nano-Structured Materials*, **1**, (1992) 207-212.
- 22) R. Valiev, "Approach to nanostructured solids through the studies of submicron grained polycrystals", *Nano-Structured Materials*, **6**, (1995) 73-82.
- 23) R. Valiev, N. Krasilnikov, and N. Tsenev, "Plastic deformation of alloys with submicrograin structure", *Mater. Sci. Enginer.*, **A137**, (1991) 35-40.
- 24) A. Korsnikov, Y. Ivanisenko, D. Laptionok, I. Safarov, V. Pilyugin, and R. Valiev, "Influence of severe plastic deformation on structure and phase composition of carbon steel", *Nano-Structured Materials*, **4**, (1994) 159-167.
- 25) H. Shen, B. Guenther, A. Korsnikov, and R. Valiev, " Influence of powder consolidation methods on the structural and thermal

- properties of a nanophase Cu-50%Ag alloy", *Nano-Structured Materials*, **6**, (1995) 385-388.
- 26) R. Valiev, V. Gertsman, and O. Kaibyshev, "Structure of grain boundaries subjected to internal influences", *Phys. Stat. Solidi*, **A97**, (1986) 11-32.
- 27) W. Wunderlich, Y. Ishida, and R. Maurer, "High resolution electron microscopy of nanocrystalline materials", *Scr. Metall. Mater.*, **24**, (1990) 403-408.
- 28) R. Islamgaliev, and R. Valiev, "Electron microscopy investigations of grain boundaries in ultrafine-grained germanium", *Solid State Physics*, **37**, (1995) 417-426.
- 29) R. Valiev, and R. Musalimov, " High resolution electron microscopy of nanocrystalline materials", *Phys. Metals Metallogr.*, **78**, (1994) 114-121.
- 30) I. Alexandrov, K. Zhang, and R. Valiev, "Comparative X-ray analysis of nanocrystalline materials, processed by severe plastic deformation", *Nano-Structured Materials*, **9**, (1997) 347-354.
- 31) F. Grant, "Properties of Rutile Titanium Dioxide", *Rev. Modern Phys.*, **31**, (1959) 646-674.
- 32) N. Daude, C. Gout, and C. Jouanim, "Electronic band structure of titanium dioxide ", *Phys. Rev.*, **B 15**, (1977) 3229-3235.
- 33) S. Munnix, and M. Schmeits, "Electronic densities of states of defect-free TiO₂(110) and TiO₂ (001) surfaces", *Phys. Rev.*, **B 28**, (1983) 7342-7345.

- 34) R. Hull, J. Bean "Germanium Silicon: Physics and Materials. Semiconductors and Semimetals", *Academic Press*, **56**, 1999.
- 35) H. Ihrig, "The phase stability of BaTiO₃ as a function of doped 3d elements: an experimental study", *J. Phys. C: Solid State Phys.*, **11**, (1978) 819-827.
- 36) S. Petal, M. Grätzel, and J. Moser, "Femtosecond Dynamics of Interfacial and intermolecular Electron Transfer at Eosin-Sensitized Metal Oxide Nanoparticles", *J. Phys. Chem. B.*, **107**, (2003) 3215-3224.
- 37) C. Howard, T. Sabine and F. Dickson, " Structural and thermal parameters for rutile and anatase", *Acta Cryst.*, **B47**, (1991) 462-468
- 38) K. Vos, and H. Krusemeyer, "Reflectance and electroreflectance of TiO₂ single crystals. I. Optical spectra", *J. Phys.*, **C 10**, (1977) 3893-3915 and 3917-3939.
- 39) B. O'Regan, and M. Grätzel, "A low cost, high-sensitized colloidal TiO₂ films", *Nature*, (1990) 737-740.
- 40) M. Nazeeruddin, A. Kay, I. Rodicio, R. Humphry-Baker, E. Müller, P. Liska, N. Vlachopoulos, and M. Grätzel, "Conversion of light to electricity by cis-X₂Bis(2,2'-bipyridyl-4,4'-dicarboxylate)ruthium(II) charge-transfer sensitizers (X = Cl⁻, Br⁻, I, CN, and SCN) on nanocrystalline TiO₂ electrodes", *J. Am. Chem. Soc.*, **115**, (1993) 6382-3-6390.
- 41) M. Ben Farah, F. Lapique, and Matlosz, "Electrical characterization of the semiconducting properties of n-TiO₂", *J. Electrochem. Soc.*, **145 (10)**, (1998) 3550-3556.

- 42) A. Kay, and M. Grätzel, "Artificial photosynthesis. Photosensitization of TiO₂ solar cells with chlorophyll derivatives and related natural porphyrins", *J. Phys. Chem.*, **97**, (1993) 6272-6277.
- 43) O. Schwarz, D. Luyen, S. Lochusch, N. Turro, and H. Dürr, "Preparation and application of new ruthenium (II) polypyridyl complexes as sensitizers for nanocrystalline TiO₂", *Photochemistry and Photobiology A: Chemistry*, **132**, (2000) 91-98.
- 44) Q. Zhang, L. Gao, and J. Guo, "Effects of calcinations on the photocatalytic properties of nanosized TiO₂ powders prepared by TiCl₄ hydrolysis", *Appl. Cat. B: Environmental*, **26**, (2000) 207-215.
- 45) A. Chemseddine, and T. Moritz, "Nanostructuring Titania: Control over nanocrystal structure, size, shape, and organization", *Eur. J. Inorg. Chem.*, (1999) 235-245.
- 46) Y. Sato, K. Yomogida, T. Nanaumi, K. Kobayakawa, Y. Ohsawa, and M. Kawai, "Electrochemical behavior of activated-carbon capacitor materials loaded with ruthenium oxide", *Electrochem. And solid-state letters*, **3 (3)**, (2000) 113-116.
- 47) W. Lin, C. Wei, and K. Rajeshwar, "Photolytic reduction and immobilization of hexavalent chromium at TiO₂ in aqueous basic media", *J. Electrochem. Soc.*, **140**, (1993) 2477-2482.
- 48) W. Lin, and K. Rajeshwar, "Photocatalytic removal of Nickel from aqueous solutions using ultra violet-irradiation TiO₂", *J. Electrochem. Soc.*, **144**, (1997) 2751-2756.
- 49) J. Byrne, B. Eiggins, W. Byers, and N. Brown, "Photoelectrochemical cell for the combined photocatalytic

oxidation of organic pollutants and the recovery of metals from waste waters", *appl. Cat. B: Environmental*, **20**, (1999) L85-L89.

- 50) J. Byrne and B. Eggins, N. Brown, B. McKinny, and M. Rouse, "Immobilization of TiO₂ powder for the treatment of polluted water", *Applied Catalysis B: Environmental*, **17**, (1998) 25-36.
- 51) P. Calza, C. Minero, A. Hiskia, E. Papacostantinou, and E. Pelizzetti, "Photolytic and photocatalytic decomposition of bromomethanes in irradiated aqueous solutions", *Applied Catalysis B: Environmental*, **21**, (1999) 191-202.
- 52) K. Wang, Y. Hieh, M. Chou, and C. Chang, "Photocatalytic degradation of 2-chloro and 2-nitrophenol by titanium dioxide suspensions in aqueous solution", *Catalysis B: Environmental*, **21**, (1999) 1-8.
- 53) K. Jung, and S. Park, "Enhanced photoactivity of silica-embedded titania particles prepared by sol-gel process for the decomposition of trichloroethylene", *Applied Catalysis B: Environmental*, **25**, (2000) 249-256.
- 54) R. Matthews, "Purification of water with near u.v. illuminated suspensions of titanium dioxide", *Water research*, **24 (5)**, (1990) 653-660.
- 55) J. Matos, J. Laine, and J. Herrmann, "Synergy effect in the photocatalytic degradation of phenol on a suspended mixture titania and activated carbon", *Applied Catalysis B: Environmental*, **18**, (1998) 281-291.

- 56) D. Chatterjee, and, A. Mahata, "Photo-assisted detoxification of organic pollutants on the surface modified TiO₂ semiconductor particulate system", *Catalysis communications*, **2**, (2001) 1-3.
- 57) E. Piera, J. Calpe, E. Brillas, X. Domènech, and J. Peral, "2,4-Dichlorophenoxyacetic acid and degradation by catalyzed ozonation: TiO₂/UVA/O₃ systems", *Applied Catalysis B: Environmental*, **27**, (2000) 169-177.
- 58) J. Marie, J. Didier, P. Pichat, S. Malato, and J. Blanco, "TiO₂-based solar photocatalytic detoxification of water containing organic pollutants, case studies of 2,4-dichlorophenoxyacetic acid (2,4-D) and of benzofuran", *Applied Catalysis B: Environmental*, **17**, (1998) 15-23.
- 59) E. Shine, R. Senthurchelvan, J. Munoz, S. Basak, and K. Rajeshwar, "Photolytic and photocatalytic destruction of formaldehyde in aqueous media", *J. Electrochem. Soc.*, **143**, (1996) 1562-1570.
- 60) J. Byrne and B. Eggins, "Photoelectrochemistry of oxalate on particulate TiO₂ electrodes", *J. Electroanalytical chemistry*, **457**, (1998) 61-72.
- 61) T. Kanki, H. Yonida, N. Sano, A. Toyoda, and C. Nagai, "Photocatalytic reduction and deposition of metallic ions in aqueous phase", *Chemical Engineering Journal*, **97**, (2004) 77-81.
- 62) P. Qu, J. Zhao, T. Shen, and H. Hidaka, "TiO₂-assisted photodegradation of dyes: A study of two competitive primary processes in the degradation of RB in an aqueous TiO₂ colloidal solution", *Journal of Molecular Catalysis A: Chemical*, **129**, (1998) 257-268.

- 63) K. Wang, H. Tsai, and Y. Hsieh, "The kinetics of photocatalytic degradation of trichloroethylene in gas phase over TiO₂ supported on glass bead", *Applied Catalysis B: Environmental*, **17**, (1998) 313-320.
- 64) H. Coleman, B. Eggins, J. Byrne, F. Palmer, and E. King, "Photocatalytic degradation of 17- β -oestradiol on immobilized TiO₂" *Applied Catalysis B: Environmental*, **612**, (1999) 1-5.
- 65) S. Zhang, N. Fujii, and Y. Nosaka, "The dispersion effect of TiO₂ loaded over ZSM-5 zeolite", *J. Mol. Cat.*, **129**, (1998) 219-224.
- 66) A. Sanjuán, G. Aguirre, M. Àlvaro, H. Gracia, and J. Scaiano, "degradation of propoxur in water using 2,4,6-triphenylpyrylium-Zeolite Y as photo-catalyst product study and laser flash photolysis", *Appl. Cat. B: Environmental*, **25**, (2000) 257-265.
- 67) D. Dionysiou, A. Khodadoust, A. Kern, M. Suidan I. Baudin, and J. Laîne, "Continuous-mode photocatalytic degradation of chlorinated phenols and pesticides in water using a bench-scale TiO₂ rotating disc reactor", *Applied Catalysis B: Environmental*, **24**, (2000) 139-155.
- 68) D. Dumitriu, A. Bally, C. Ballif, P. Hones, P. Schmid, R. Sanjinés, F. Lévy, and V. Pârvulescu, "Photocatalytic degradation of phenol by thin films prepared by sputterin", *Applied Catalysis B: Environmental*, **25**, (2000) 83-92.

CHAPTER 2

EXPERIMENTAL

2.1 Reagents

All common chemicals, used in this work (anatase TiO_2 , 2,4,6-triphenylpyrylium hydrogen sulfate (H_2TPyP), activated carbon (AC), KBr, and manganese(II)-sulfate) were purchased from Aldrich. Organic solvents (methanol, DMF, and chloroform) were obtained from Reidel- DeHaën in a pure form.

2.2 Equipment

2.2.1 Reactor

The reactor, Figure (2.1), used in this work was of a two-necked round-bottomed flask. A test tube was inserted in one neck. The tip of the fiber optical bundle of the lamp was inserted in the tube. Sample solutions were taken for analysis from the other neck. The flask was covered with an aluminum foil for the purpose of (a) protecting personnel from the harmful UV- light and (b) reflecting back all the light to the solution. The solution was stirred magnetically.

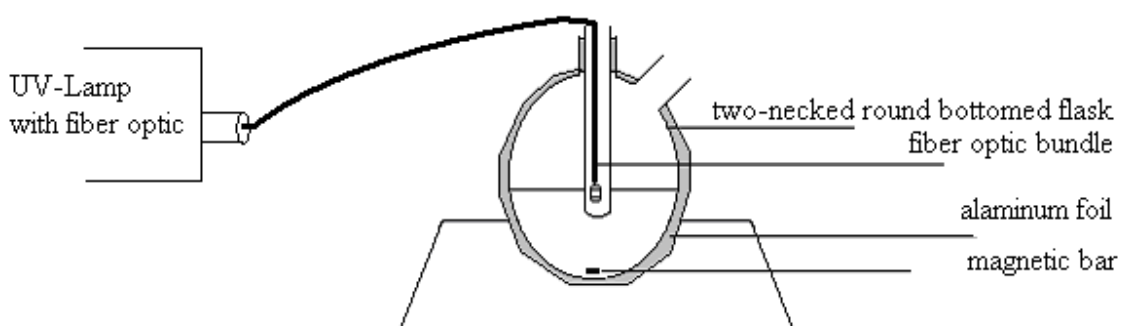


Figure (2.1): Schematic photodegradation reactor

2.2.2 Measuring Devices

HPLC

Waters 2695/ Separation Module, Photodiode Array Detector at 254 nm, and Empower software were used for HPLC determinations. The injected volume was 20 μ L. Mobile phase was 20% acetic acid (pH= 3) solution, Analysis were performed on 250 \times 4 mm I.D. Merck Lichrospher 100 RP-18 (5 μ m) column fitted with guard column.

GC/MS

GC-MS (QP5000, SHIMADZU Corporation. Japan) was used during the present work. It was supported with auto injector (AOC-17), Class 5000 software and capillary column DB-SMS (5%- phenyl) Methylopolysiloxane 0.25 μ m film thickness, with 30 meters length and 0.25 mm I.D. (Available from J&W SCIENTIFIC). Chromatographic analysis was performed as follows: injector was set up at 250°C, GC-MS interface at 280°C, and helium carrier gas at a flow rate of 0.80 mL/min at 25°C. The sample (2 μ l) was injected in the splitless injection mode. The oven temperature was programmed as follows: 100°C for 1 min, raised to 320°C (5°C/min), and hold for 10 min at 320°C.

UV/vis spectrophotometer

The absorption spectra of Mn^(III)TPyP, and PhOH concentration were measured on a Shimadzu UV-1601 spectrophotometer

FTIR

Furrier Transform Infrared Spectrophotometer (Shimadzu FTIR-8201PC) was used for the catalyst analysis

2.2.3 Light Sources

Illumination in the UV- range was carried out using a 500W Hg/Xe lamp (Oriel instruments, Universal Arc Lamp Housing, Model 66901) equipped with a fiber bundle inserted inside the reactor through a tube. The lamp specifications are shown in Table (3), and the output spectrum is shown in Figure (2.2) [1]. Unless otherwise stated the lamp was operated at 150W power.

Table (3): Arc lamp description [2]

Model no.	Description	Average life (hours)	Suggested power range (W)	Typical voltage (VDC)	Typical current (ADC)
Oriel-66142	500 watt Hg (Xe)	400	400-500	26	19

Illumination in the visible range was carried out using a 50W xenon lamp equipped with housing and a concentrating lens (Leybold Didactic Company, model 45064). The lamp has a high stability and an intense coverage of wide spectrum, Figure (2.3), [1]. The light intensity at the electrode surface was measured and was 8500 Lux (0.301 W/cm^2) [3].

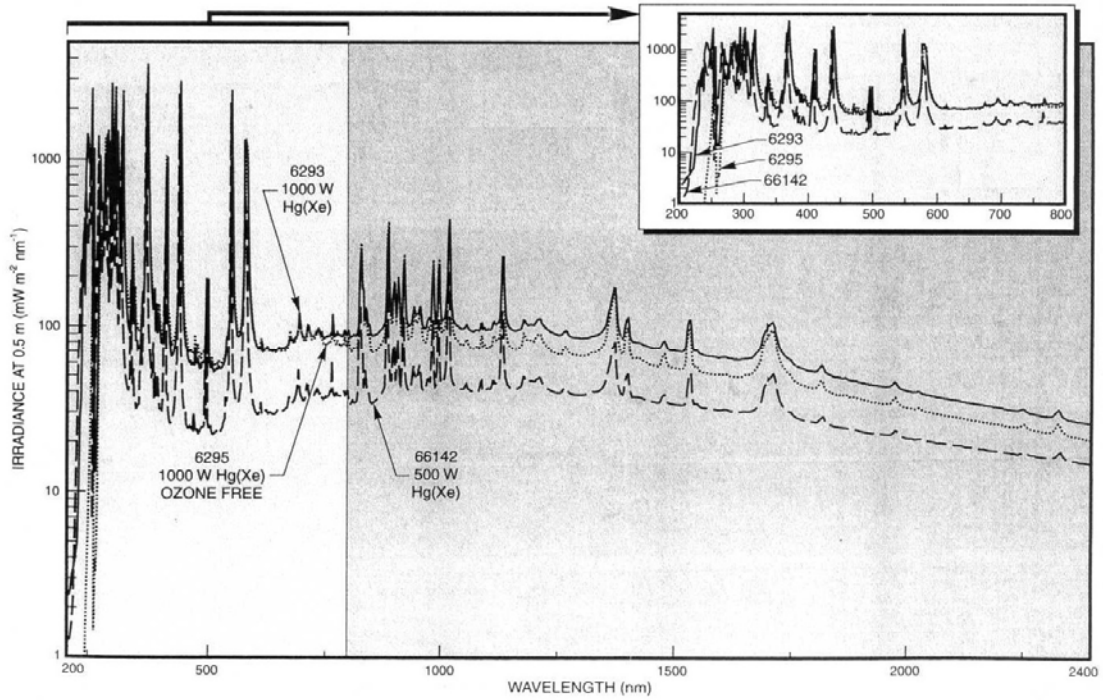


Figure (2.2): Spectral irradiance of various Arc Lamps.

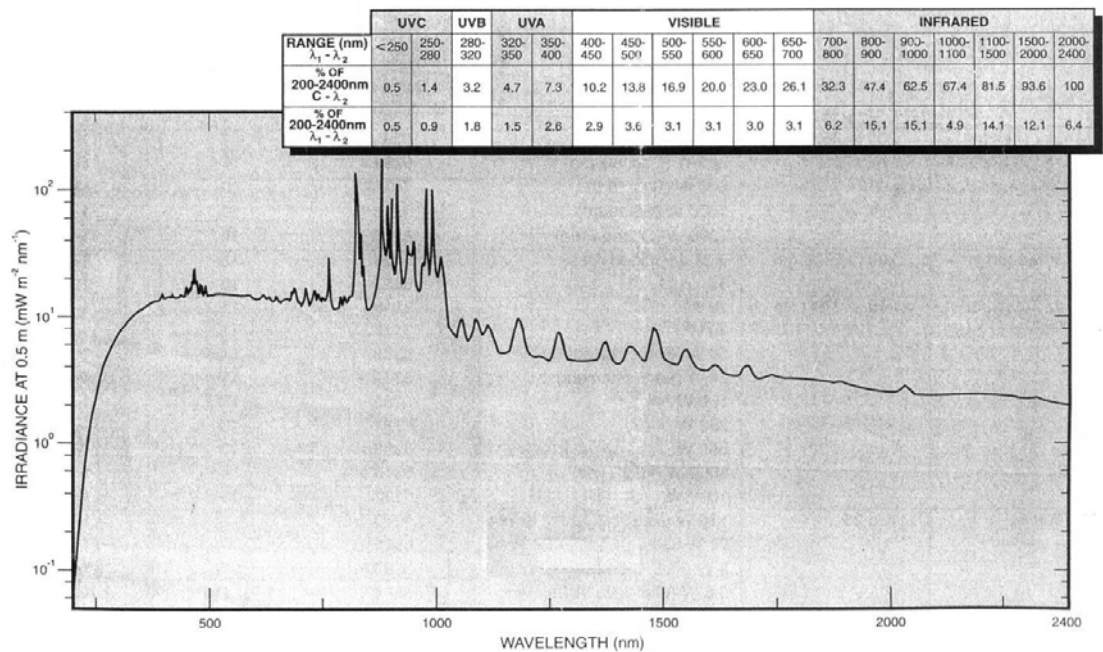


Figure (2.3): Typical spectral irradiance of 150 W Xe Lamp, showing % of total irradiance in specific UV, VIS and NiR spectral ranges.

2.3 MnP preparation and characterization

The tetra-4-pyridylporphyrinatomanganese(III) sulfate [$\text{Mn}^{\text{III}}\text{P}$] [4]. H_2TPyP (81.7 mg, 0.132 mmol) was vigorously refluxed with manganese (II) sulfate (1.53 mg, 0.91mmol) in DMF (60 ml) for approximately 15 hr. Air was bubbled through the reaction mixture to oxidize $\text{Mn}^{\text{(II)}}$ to $\text{Mn}^{\text{(III)}}$. The reaction mixture was then chromatographed over active neutral alumina (Bio- Rad. AGF, 100-200 mesh) using DMF as eluant. The MnP was further separated from the DMF by chromatography over neutral alumina using methanol and chloroform (5: 95 vol. /vol.) [5]. The spectra were measured and showed three characteristic bands: 462, and 569 nm characteristic for the $\text{Mn}^{\text{(III)}}$ complex, Figure (2.4). The band at 374 nm also indicates the presence of the $\text{Mn}^{\text{(II)}}$ complex. Testing indicates that the MnP complex is a mixture of $\text{Mn}^{\text{(II)P}}$ and $\text{Mn}^{\text{(III)P}}$, but the ratio $\text{Mn}^{\text{(III)P}}$ to $\text{Mn}^{\text{(II)P}}$ is $\gg 1$. It was noticed that the ratio becomes larger as the mixture is exposed to air.

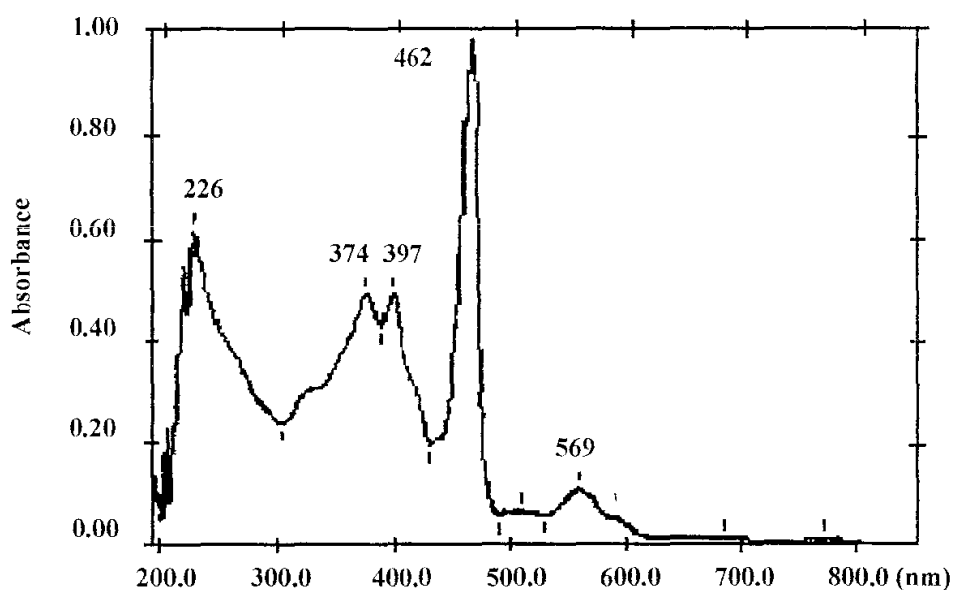


Figure (2.4): The electronic absorption spectra in the UV/visible region for MnP solution in methanol.

2.4 Surface area measurement

Surface areas for TiO₂ and AC were measured using the BET method [6], but here we used the method of acetic acid adsorption on the surface of TiO₂ and/ or AC [7].

Seven dry and clean flasks were used, and 1.0g of AC (or TiO₂) was added to each. A standardized solution of approximately 0.2 M acetic acid was diluted to 100 ml of different molarities (0.150, 0.120, 0.090, 0.075, 0.060, 0.030, and 0.015) and added to each flask. The flasks were stoppered and shaken in a thermostat at 25±2°C for at least one hour to establish equilibrium. The samples were filtered and then titrated with a 0.100 M standardized NaOH solution, using phenolphthalein as an indicator.

The surface area results for TiO₂ and AC were calculated to be 98.8 m² and 845.4 m² respectively according to the following Tables:

Table (4): Surface area of TiO₂

V	C	N1	N2	(N2-N1)/0.5g	N = (N2-N1)/1.0g	C / N
17.5	0.14525	0.002905	0.003	9.5E-05	0.00019	764.4737
14	0.1162	0.002324	0.0024	7.6E-05	0.000152	764.4737
10.5	0.08715	0.001743	0.0018	5.7E-05	0.000114	764.4737
8.7	0.07221	0.0014442	0.0015	5.58E-05	0.000112	647.043
7.1	0.05893	0.0011786	0.0012	2.14E-05	4.28E-05	1376.869
3.5	0.02905	0.000581	0.0006	1.9E-05	3.8E-05	764.4737
1.7	0.01411	0.0002822	0.0003	1.78E-05	3.56E-05	396.3483

Table (5): Surface area of activated carbon (AC)

V	C	N ₁	N ₂	(N ₂ - N ₁)/0.5g	N = (N ₂ - N ₁)/1.0g	C / N
15.3	0.12699	0.0025398	0.003	0.0004602	0.00092	137.9726
12.1	0.10043	0.0020086	0.0024	0.0003914	0.000783	128.2959
8.9	0.07387	0.0014774	0.0018	0.0003226	0.000645	114.4916
7.5	0.06225	0.001245	0.0015	0.000255	0.00051	122.0588
6	0.0498	0.000996	0.0012	0.000204	0.000408	122.0588
3	0.0249	0.000498	0.0006	0.000102	0.000204	122.0588
1.5	0.01245	0.000249	0.0003	0.000051	0.000102	122.0588

V: volume of NaOH_{aq} used in the titration.

C: Concentration of acetic acid (calculated using $M_1V_1 = M_2V_2$).

N₁: Number of moles of free acetic acid that remain after adsorption.

N₂: Number of moles of acetic acid before adsorption.

N: Number of moles of acetic acid adsorbed per 1.0g AC or TiO₂.

The equation, used to calculate the surface area, is (Langmuir adsorption isotherm):

$$C/N = C/N_m + 1/KN_m$$

Where N_m: Number of moles of acetic acid per gram required to form a monolayer.

A plot C/N vs. C was therefore constructed for the TiO₂ Figure (2.4) and the slope (1/N_m) was then calculated.

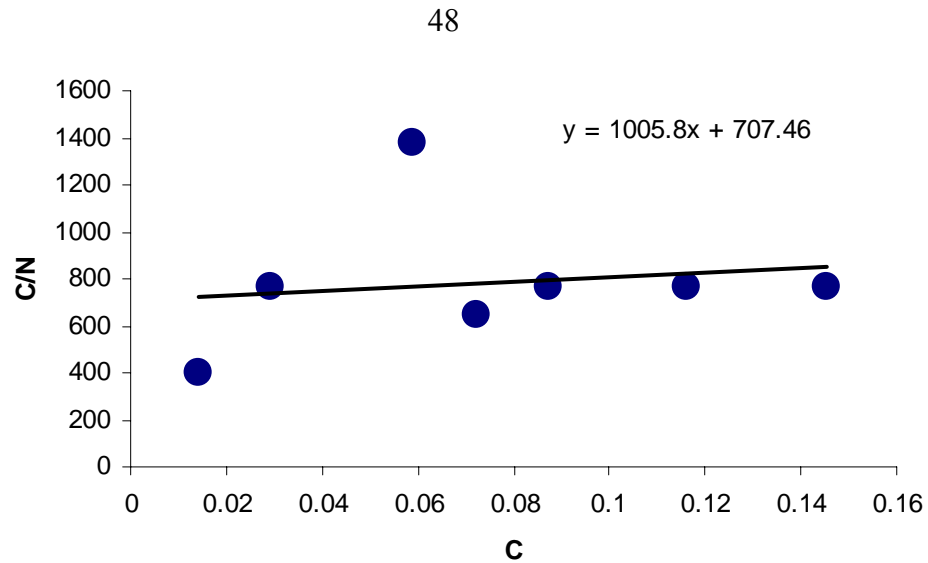


Figure (2.5): A plot of C/N vs. C for TiO₂ surface

From the calculated number of moles of acetic acid, adsorbed onto 1.0g TiO₂, the number of molecules (per gram TiO₂), assuming a monolayer) was then calculated. This was multiplied by the area of 1.0 molecule acetic acid to yield the relative surface area (m²/g) TiO₂. The measured relative surface area for TiO₂ used here was 125.691m²/g, Table (6).

Similarly the AC surface area was calculated from C/N_m vs. C plots, Figure (2.5). The AC surface area was found to be 10076.006 m²/g, Table (6).

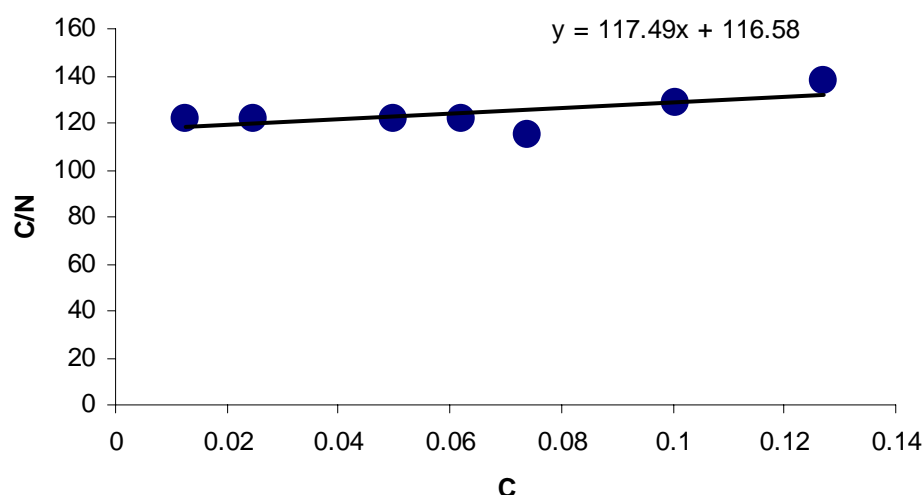


Figure (2.6): A plot of C/N_m vs. C for AC

Table (6): Surface area data measured for TiO_2 and AC based on Langmuir plots

Surface	slope	1/slope (no. of moles (M))	Molecule ($6.02E23 \times M$)	Area of acetic acid molecule ($m^2/molecule$)	surface area (m^2/g)
TiO_2	1005.8	0.000994	$5.9853E+20$	$2.1E-19$ [8]	125.691
AC	117.49	0.008511	$5.12E+21$	$2.1E-19$ [8]	1076.006

2.5 Photolysis experiments

2.5.1 Naked TiO_2 as catalyst

Anatase TiO_2 (0.5g, 0.0063 mol) was added to 100 ml of pollutant aqueous solution with a known concentration. The mixture was then exposed to the light source as explained earlier in Figure (2.1). Sample aliquots were taken every 30 min. and analyzed. The reaction mixture was magnetically stirred during photolysis.

2.5.2 Dye as catalyst

2,4,6-triphenylpyrylium hydrogen sulfate (TPPHS) dye (0.003g, 7.38×10^{-6} mol) was added to 100 ml of pollutant solution. The solution was

treated as described above to study the catalytic effect of TPPHS alone with no added TiO₂.

2.5.3 TiO₂/TPPHS catalyst

TiO₂ (0.5g, 0.0063 mol) was stirred with TPPHS dye (0.003g, 7.38×10^{-6} mol) in approximately 10.0 ml of water for 4 hr in the dark [9]. After filtering the mixture through a sintered-glass funnel, the solid was placed in the reactor. A 100 ml aliquot of pollutant solution was added to it, and the catalytic experiment was then started as explained above.

2.5.4 AC/TiO₂/TPPHS catalyst

TiO₂ (0.5g, 0.0063 mol) was stirred with TPPHS dye (0.006g, 1.476×10^{-5} mol) in aqueous solution for 4 hr in the dark, then the TiO₂/TPPHS filtered and stirred again with AC (0.1g, 0.0083 mol) for 1 hr [10]. The procedure was continued as described above. Before exposure to light, the reaction mixture (catalyst and pollutant solution) was stirred for 1 hr more in the dark, to allow maximum adsorption of contaminant (equilibrium conditions).

2.5.5 Metalloporphyrin (MnP) modified TiO₂ catalyst

A 0.04 ml aliquot of MnP (4×10^{-3} M) was stirred with TiO₂ (2.0g, 0.0252 mol), in approximately 10 ml DMF, in the dark for 5 hr [4]. The colored solid (brown) was filtered and washed with distilled water several times. The pollutant solution (100 ml) was then added to the solid. The photolysis experiment was then started.

To prepare AC/TiO₂/MnP system, TiO₂ (2.0g, 0.0252 mol) was stirred with AC (0.4g, 0.033 mol) in aqueous solution for 1 hr in dark. The

contaminant solution (100 ml) was then added, and the photolysis experiment started.

2.5.6 Control experiments

Control experiments were conducted. Photolysis experiments were carried out with no catalyst, while using activated carbon (AC) alone. In these experiments the pollutant concentrations didn't significantly change after prolonged times (3h).

Control experiments were also conducted in the dark, to study the effect of light. There was no significant change in pollutant concentrations in the dark. Only up to 3% contaminant loss was observed due to adsorption on AC surfaces. Control experiments were conducted in each contaminant study, as described later in Chapters 4-5.

2.5.7 Reuse experiments

After the end of the photocatalytic experiment, the catalyst was filtered and washed with distilled water, and then reused as a catalyst for a new experiment. The reuse procedure was repeated for four times. In the fourth reuse, fresh amount of TPPHS dye (0.006g, 1.476×10^{-5} mol) was added.

2.5.8 Catalyst analysis

2.5.8.1 Using FT-IR

Solid state FT-IR spectra were recorded for TiO_2 , TPPHS, $\text{TiO}_2/\text{TPPHS}$, and $\text{AC}/\text{TiO}_2/\text{TPPHS}$ as KBr pellets.

2.5.8.2 Thermal Gravimetric analysis (TGA)

TGA analysis was done in the SCA-CNKS laboratory (Service Central d'Analysis), France. TGA apparatus of the type TA Instrument 2950HR V5-3 was used. Two kinds of software under Windows NT and XP were used, the first one is for acquisition: instrument control V 3.03, and the other one is for reprocessing universal analysis 2000 V 3.7. Under-air heating was started at room temperature and ended at 1000°C, with temperature increase rate of 5°C/min.

AC/TiO₂/TPPHS samples recovered from phenol photo-degradation experiments, and fresh AC/TiO₂/TPPHS samples, were analyzed using TGA. The TGA showed a 20% weight loss in each of the two samples, attributed to AC burning, Figures (2.6-2.7). The 20% weight loss due to carbon burning is parallel to the mass percentage of carbon in the AC/TiO₂/TPPHS system preparation. This indicates that the TiO₂ content in the AC/TiO₂/TPPHS remained unchanged under photo-degradation conditions, with no significant leaching of TiO₂ from the support during reaction.

Fresh TiO₂/TPPHS samples showed no significant weight loss by heating, Figure (2.8). This is presumably due to the small weight ratio of the TPPHS in the modified system. Similarly, the recovered TiO₂/TPPHS showed no significant TPPHS loss in the TGA, Figure (2.9).

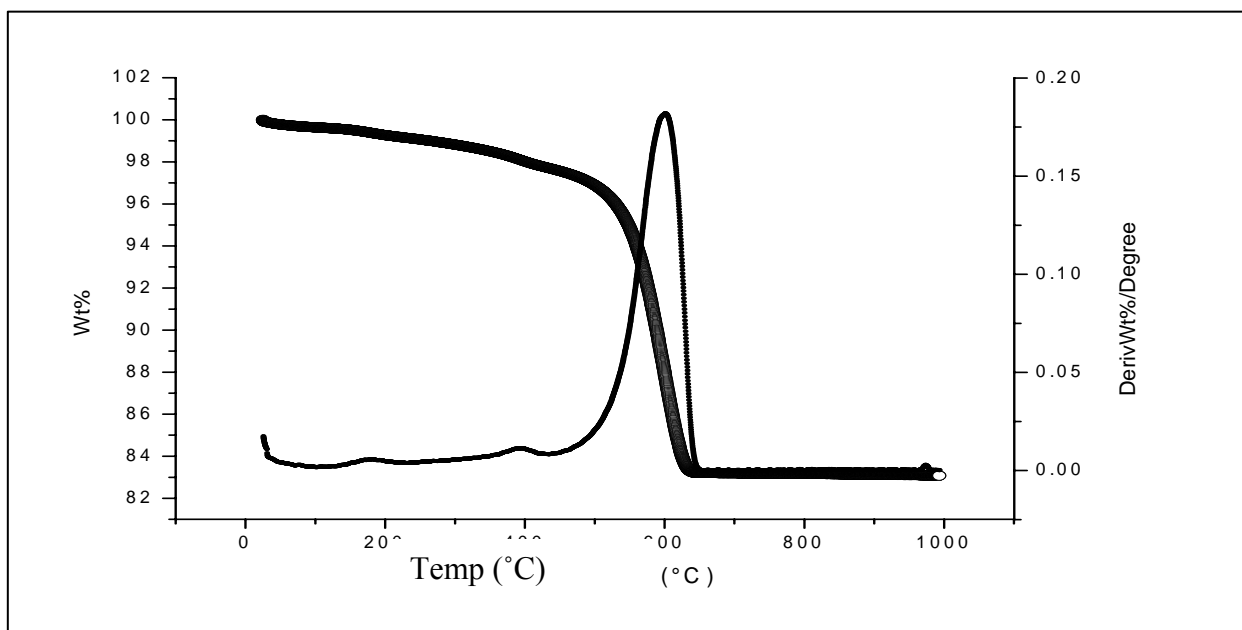


Figure (2.7): TGA results for a fresh AC/TiO₂/TPPHS sample.

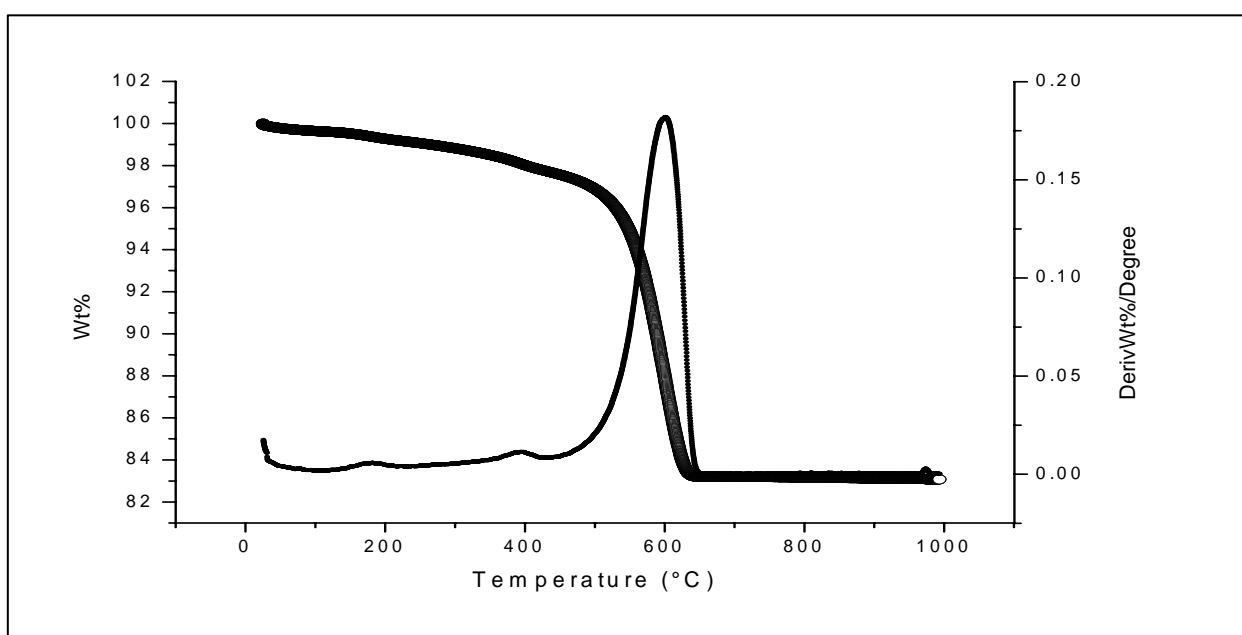


Figure (2.8): TGA results for a sample of AC/TiO₂/TPPHS recovered from phenol photo-degradation reaction.

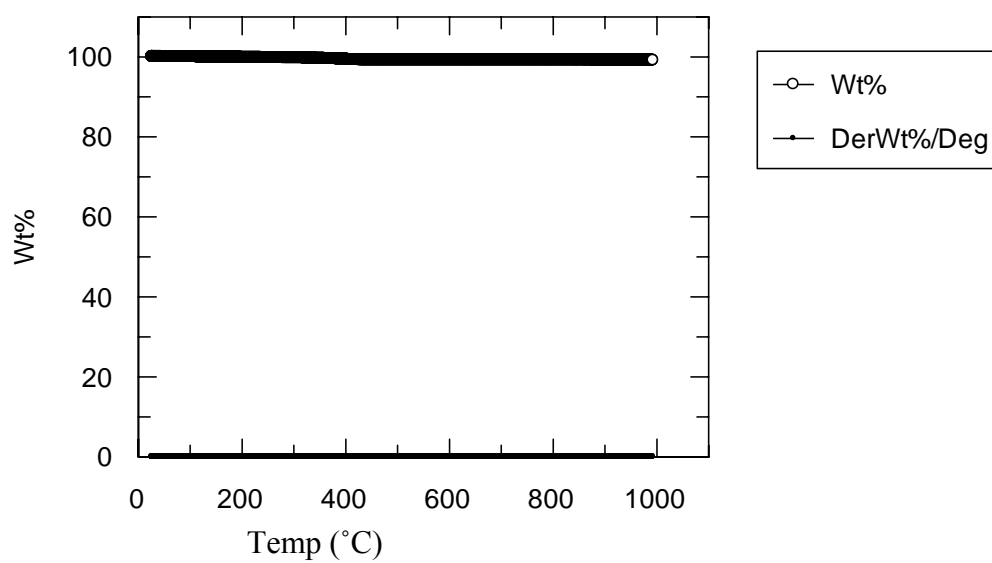


Figure (2.9): TGA results for a fresh TiO₂/TPPHS sample.

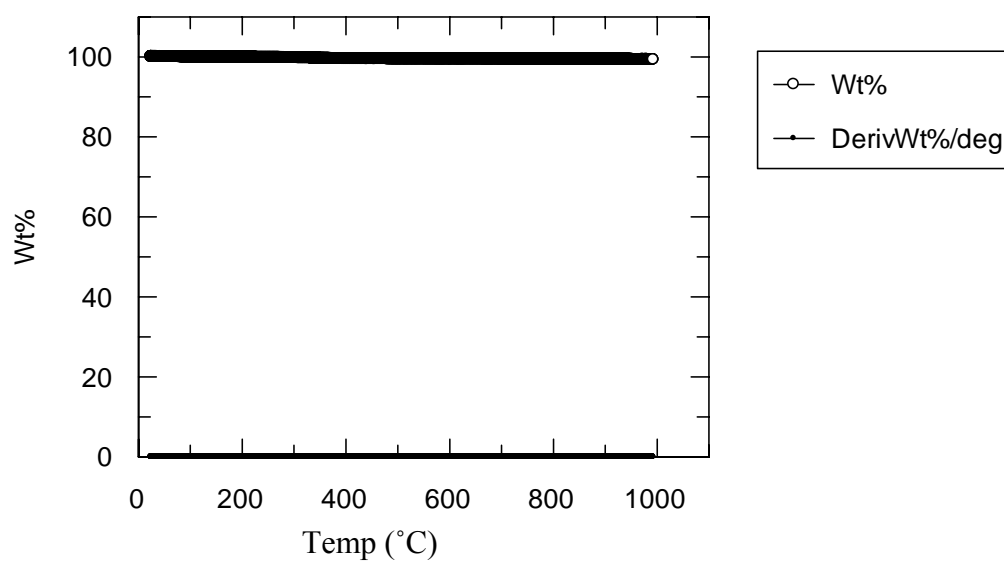


Figure (2.10): TGA results for a sample of TiO_2 /TPPHS recovered from phenol photo-degradation reaction.

REFERENCES

- 1) The Book of Photon Tools, Oriel Instruments, Stratford, CT, USA, p. 44, 50.
- 2) Thermo Oriel: 500 W Xenon/Mercury (Xenon) ARC Lamp Power Supply Model 68911.
- 3) N. Kobayashi, H. Seiki, and T. Osa, "Catalytic electro-reduction of molecular oxygen using 5,10,20-tetrakis-(1-methylpyridinium-4-yl)porphinatomanganese", *Chem. Lett.*, **125**, (1985) 1917.
- 4) A. Alder, F. Longo, F. Campas, and J. Kim, "On the preparation of metalloporphyrins", *J. Inorg. Nucl. Chem.*, **32**, (1970) 2443-2445.
- 5) A. Harriman, and G. Porter, "Photochemistry of manganese porphyrins", *J. Chem. Soc. Faraday Trans II*, **75**, (1979) 1532-1542.
- 6) F. Ahnert, H. Arafat, and N. Pinto, "A Study of the Influence of Hydrophobicity of Activated Carbon on the Adsorption Equilibrium of Aromatics in Non-Aqueous Media" *Adsorption*, **9**, (2003) 311–319.
- 7) S. Glasstone, and D. Lewis, "Elementary physical chemistry", *The Machillan press Ltd.*, **2nd edition**, (1983), 566.
- 8) D. Shoemaker, C. Garland, and J. Nibler, "Experiments in physical chemistry", *McGraw-Hill, Inc.*, **5th edition**, (1989).
- 9) D. Chatterjee, and, A. Mahata, "Photo-assisted detoxification of organic pollutants on the surface modified TiO₂ semiconductor particulate system", *Catalysis communications*, **2**, (2001) 1-3.

- 10) J. Matos, J. Laine, and J. Herrmann, "Synergy effect in the photocatalytic degradation of phenol on a suspended mixture titania and activated carbon", *Applied Catalysis B: Environmental*, **18**, (1998) 281-291.

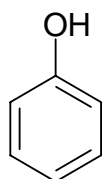
CHAPTER 3

PHOTO-DEGRADATION OF PHENOL

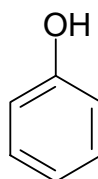
3.1 Introduction

Phenols are compounds of the general formula ArOH, where Ar is phenyl, substituted phenyl, or one of the other aryl groups. Phenols differ from alcohols in having the —OH group attached directly to an aromatic ring. Phenols are generally named as derivatives of the simplest member of the family, phenol.

Phenol is a low melting solid (m.pt. = 41°C), because of hydrogen bonding, it has quite high boiling point (b.pt. = 182°C) [1]. It is somewhat soluble in water (9.3g/ 100g H₂O), presumably because of hydrogen bonding with the water. It is stable since it contains a benzene ring, and involves hybrids of the Kekulé structures, Schemes VII and VIII.

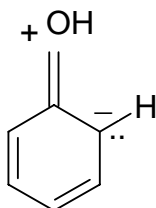


VII

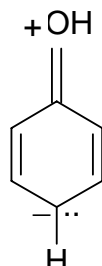


VIII

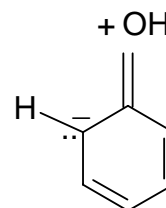
However, there are additional structures to be considered. Being basic, oxygen may share more than a pair of electrons with the ring, structures, Schemes (IX – XI).



IX



X



XI

In humans, the effects of inhaling phenol are not known. People who had skin exposure to high levels may experience liver damage, diarrhea, dark urine, and hemolytic anemia. In animals, inhaling high levels of phenol results in lung irritation. Repeated exposures led to muscle tremors and loss of coordination. Exposure to high levels of phenol for several weeks caused paralysis and severe injury to the heart, liver, kidneys, and lungs, and in some cases, death. Children exposed to phenol experience higher risk of accidentally ingesting home products that contain phenol. The effects of exposure to phenol on the human fetus are not known. Pregnant animals that drink water containing high concentrations of phenol gave birth to babies that had low birth weights and minor birth defects [2].

It is not known if phenol causes cancer in humans. Cancer occurred in mice when phenol was applied to the skin several times a week for the lifetime of the animal. Phenol did not cause cancer in mice or rats when they drank water containing it for 2 years.

Phenol is an example of the compounds that are difficult to degrade by conventional chemical and/or biological methods in water, so photo-electrochemical methods are used to degrade such compounds. Naked, and/or modified TiO_2 surfaces, such as: (a) $\text{TiO}_2/\text{TPPHS}$, and (b) supported $\text{TiO}_2/\text{TPPHS}$ onto insoluble materials such as activated carbon (AC) were used for such degradation purposes [3-9].

3.2 Experimental

3.2.1 Chemicals

Chemicals (phenol, 4-aminoantipyrine, K_2HPO_4 , KH_2PO_4 , and $K_3Fe(CN)_6$) were purchased from Aldrich. Organic solvents (NH_4OH , and ether) were obtained from Reidel- DeHaën in a pure form.

Stock solution preparations

The following solutions were needed and prepared:

- Stock phenol solution: 1.00 g (0.0106 mol) of phenol was dissolved in freshly boiled and cooled distilled water, then it was diluted to 1.0 L, to make the final concentration 0.0106M.
- Ammonium hydroxide (NH_4OH , 0.5N): 35 ml of fresh conc. NH_4OH (14.8M) were diluted to 1.0 L with distilled water.
- Phosphate buffer solution: 104.5 g (0.600575 mol) of K_2HPO_4 and 72.3 g (0.531618 mol) of KH_2PO_4 were dissolved in distilled water and diluted making final volume 1.0 L.
- 4-Aminoantipyrine solution: 2.0 g (0.009843 mol) of 4-aminoantipyrine were dissolved in distilled water and diluted to 100 ml making final concentration 0.0984M, A fresh solution of 4-aminoantipyrine was prepared when ever needed.
- Potassium ferricyanide solution: 8.00 g (0.0243 mol) of $K_3Fe(CN)_6$ were dissolved in distilled water and the solution was diluted to 100 ml making final concentration 0.2432M. The solution was stored in a brown glass bottle, and was prepared only within a few days prior to use.

3.2.2 Equipment

A Shimadzu UV-1601 spectrophotometer was used for absorbance measurements. A pH meter and a Gas Chromatograph Mass Spectrometer (Shimadzu GCMS- QP 5000, with a column (J and W Scientific DB-5MS, and of 30m length) were used to analyze the degradation products.

3.2.3 Photo-degradation experiments

The reactor, the light source, the catalyst analysis and the photolysis experiments of phenol were discussed in Chapter 2. Here product analysis methods are presented.

An aqueous sample was taken from the reaction system and then extracted with an organic solvent (ether). The organic layer was tested using GC-MS. Other than unreacted phenol in the sample no organic compounds were detected. This is in accordance with literature [10]. Therefore, phenol degradation products are only CO₂ and H₂O, which are not detected by GC-MS.

3.2.4 Concentration measurements

Phenol was analyzed spectrophotometrically as explained in literature [10]. A calibration curve was constructed for this purpose. Phenol solutions (100ml each) with different concentrations were prepared from the original stock solution. 0.0, 0.1, 0.2, 0.3, 0.4, and 0.5ml aliquots were placed in 6 different 100ml volumetric flasks. Each flask contents were then transferred to a 400ml beaker. To each beaker was added 2.5 ml of NH₄OH (5.0N), followed by phosphate buffer to make pH 7.9 ± 0.1. Then 4-aminoantipyrine (1.0 ml) was added to each beaker, followed by 1.0ml of K₃Fe(CN)₆ solution. After 15 min waiting time, the spectra were measured for each beaker at $\lambda = 500$ nm.

3.3 Results

3.3.1 Calibration curve

The absorbance vs. concentration calibration curve was used to measure the unreacted phenol concentrations with time during degradation experiments. Figure (3.1) shows the calibration curve used.

3.3.2 Control experiments

Control experiments were conducted, using aqueous phenol solutions, in the absence of light and in the absence of catalyst. Control experiments were also conducted using aqueous phenol solutions in the absence of catalyst while using activated carbon (AC). It was found that in all photolysis experiments, carried out with no catalyst, or no light, phenol concentrations didn't change after prolonged times (3h), Figure (3.2). Phenol loss due to adsorption on AC surface was less than 3% at most.

3.3.3 Naked TiO₂ and naked TPPHS dye

Phenol degradation experiments were conducted in the UV using TiO₂ and TPPHS separately. Only little change in phenol concentrations were observed when TiO₂ or TPPHS were used separately, Figure (3.3).

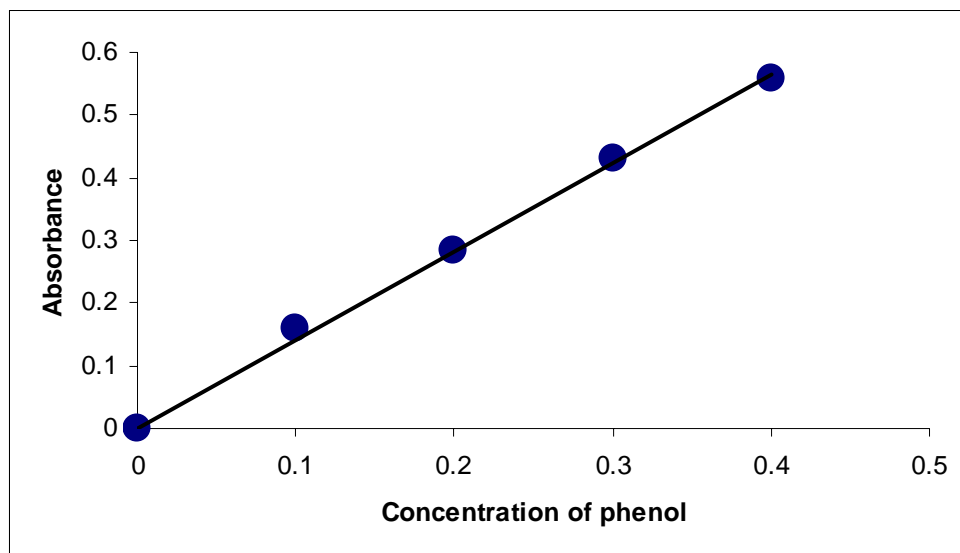


Figure (3.1): A calibration curve showing a plot of absorbance vs. phenol concentration (M). Measurements were conducted in aqueous media, at room temperature.

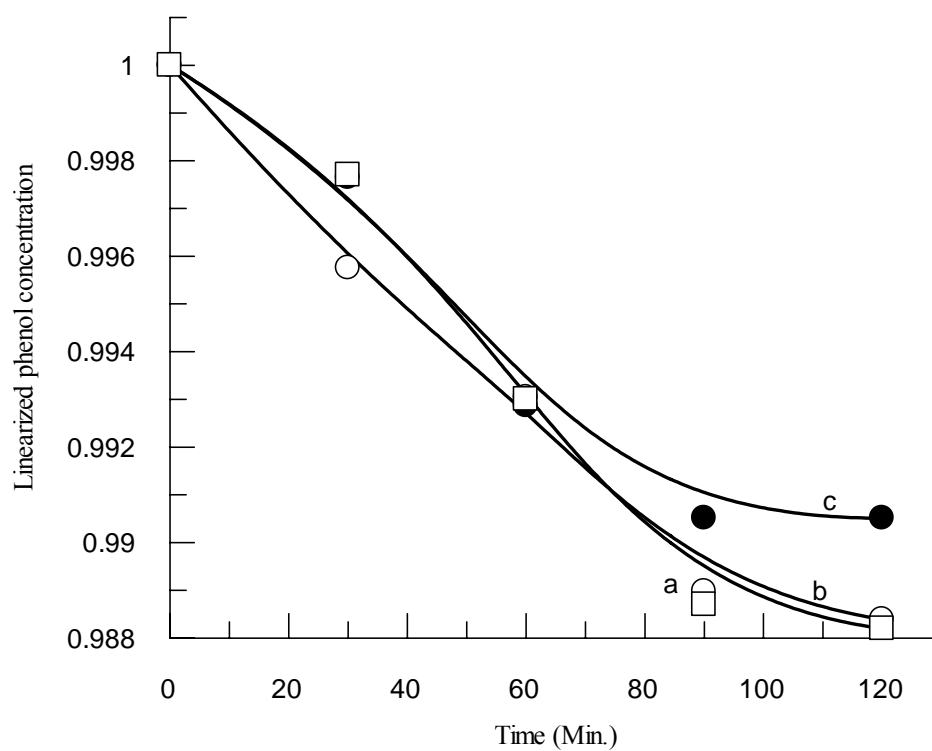


Figure (3.2): Plots of remaining phenol concentration (M) vs. time in phenol degradation experiments showing the control experiments. (a) AC alone, (b) UV light with no catalyst ($\text{TiO}_2/\text{TPPHS}$), (c) catalyst with no UV light, using 0.3M phenol concentration.

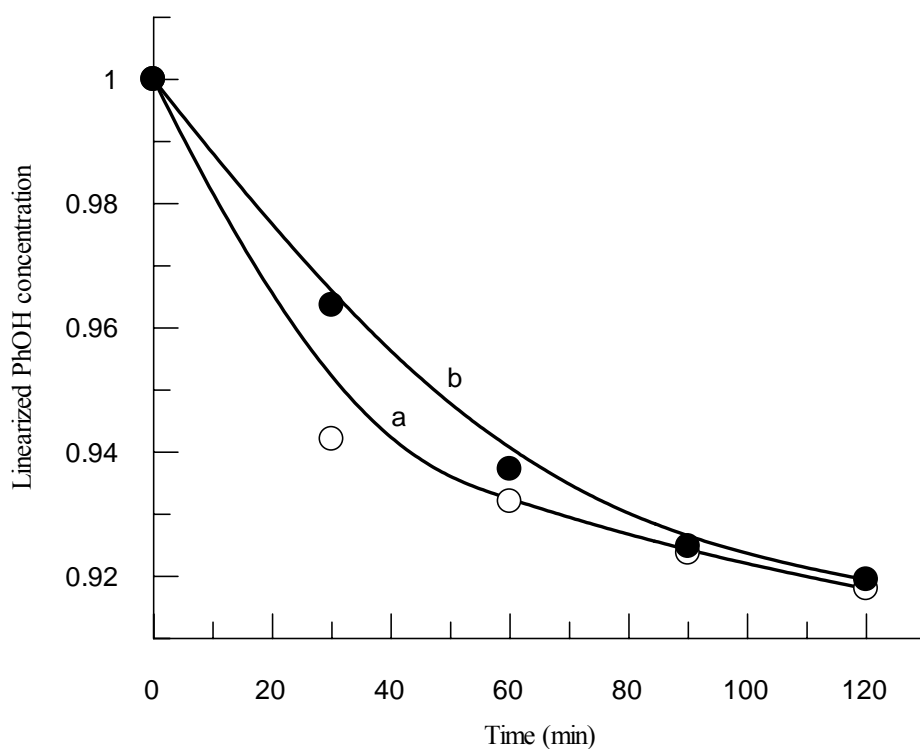


Figure (3.3): Plots of remaining phenol concentration (M) vs. time in phenol degradation experiments. (a) Naked dye (TPPHS) (0.003g, 0.738×10^{-5} mol), (b) Naked TiO_2 (0.5g). Experiments were conducted in the UV at room temperature.

3.3.4 TiO₂/TPPHS catalyst

TiO₂, combined together with TPPHS, were used to degrade phenol in the UV region. Unlike separate TiO₂ or TPPHS systems, the combined TiO₂/TPPHS showed higher catalytic activity in the UV region.

Effect of initial contaminant concentration

Effect of initial phenol concentration on initial rate of phenol degradation was studied. No significant change on rate, due to initial concentration change, was observed, Figure (3.4).

Effect of oxygen concentration

The effect of oxygen exposure, on phenol degradation was studied. Experiments were conducted using reactors that are open to air, closed to air or bubbled with air. Figure (3.5) shows that the reaction system, which was kept open to oxygen with no bubbling, was the fastest system. On the other hand the reaction was significantly hindered by air bubbling. The reaction conducted in a closed system was faster than that conducted with bubbling, but slower than the open reactor.

The results indicate that oxygen is needed by the reaction but may also inhibit it when used at higher concentrations. Therefore, unless otherwise stated, all degradation experiments were conducted in an open reactor with no air bubbling.

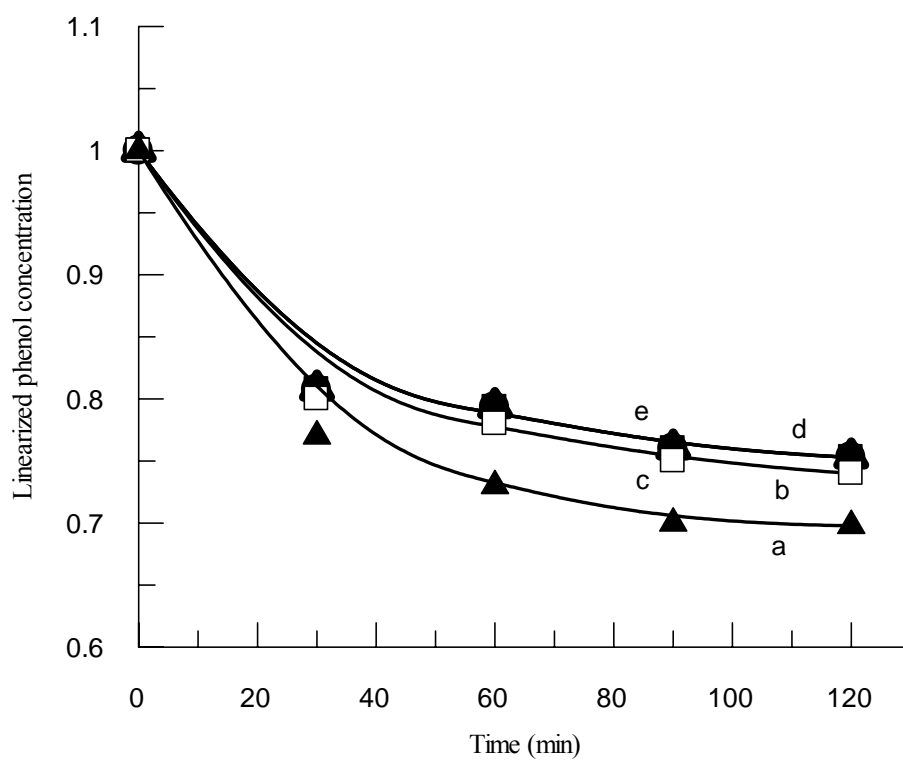


Figure (3.4): Plots of remaining phenol concentration (M) vs. time in phenol degradation experiments showing the effect of initial phenol concentration, (a) 0.1, (b) 0.08, (c) 0.06, (d) 0.04, (e) 0.01M. Linearized concentration = concentration / initial concentration.

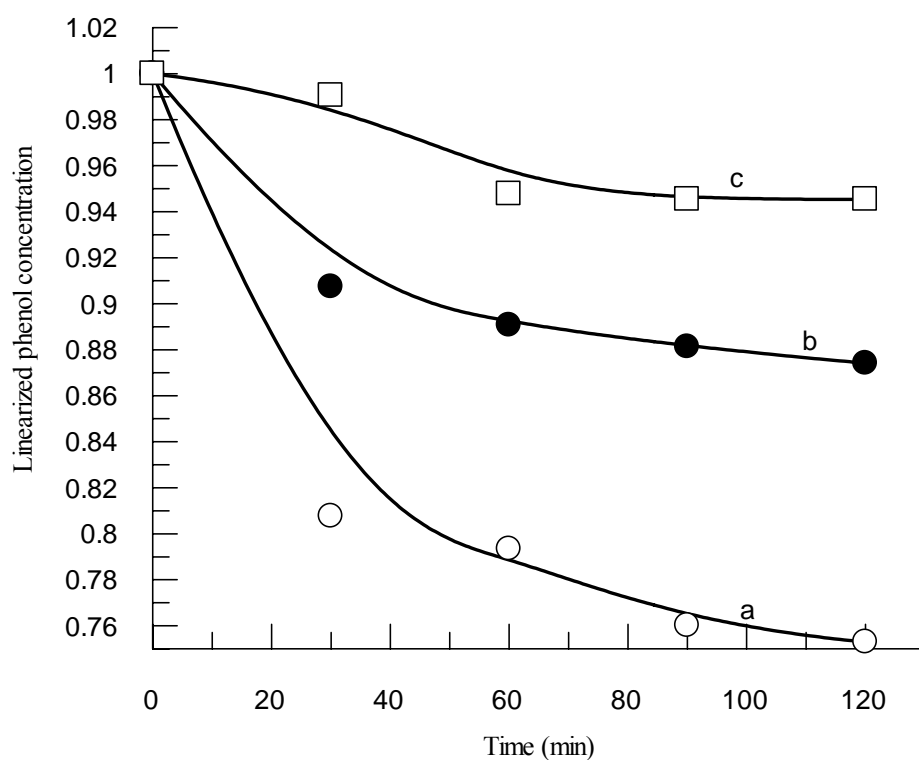


Figure (3.5): Plots of remaining phenol concentration (M) vs. time in phenol degradation experiments showing the effect of oxygen concentration, TiO_2 (0.5g), dye (TPPHS) (0.003g , 0.738×10^{-5} mol). (a), open reactor, (b) reactor closed, (c) bubbles of air. Experiments were conducted in the UV region at room temperature, using 0.3M phenol concentration.

Effect of dye concentration

The effects of TiO₂ and TPPHS concentrations, on rate of phenol degradation, were investigated. TiO₂ concentration showed no effect. Nominal TPPHS concentrations did not affect rate, because TiO₂ surface was saturated with TPPHS even at extremely low concentrations. Therefore, actual TPPHS concentration was always constant and did not affect rate. Figure (3.6) summarizes these observations.

Effect of type of radiation

The TiO₂/TPPHS system was employed to catalyze phenol degradation using UV and visible light. Figure (3.7) shows that UV is much more efficient than the visible light. Therefore unless otherwise stated, all phenol degradation experiments were conducted using UV radiation. This result indicates that the TPPHS failed to sensitize TiO₂ in the visible region. The fact that TPPHS enhanced catalytic efficiency of TiO₂ in the UV will be further discussed at a later stage.

3.3.5 AC supported TiO₂/TPPHS catalyst

TiO₂/TPPHS was supported onto AC. The AC/TiO₂/TPPHS system was used to photo-degrade phenol in the UV. The system showed higher catalytic activity than the un-supported TiO₂/TPPHS. Different concentrations of TiO₂ and/or TPPHS were studied. The rate of degradation was independent of TiO₂ or TPPHS concentrations, as shown in Figures (3.8-3.9).

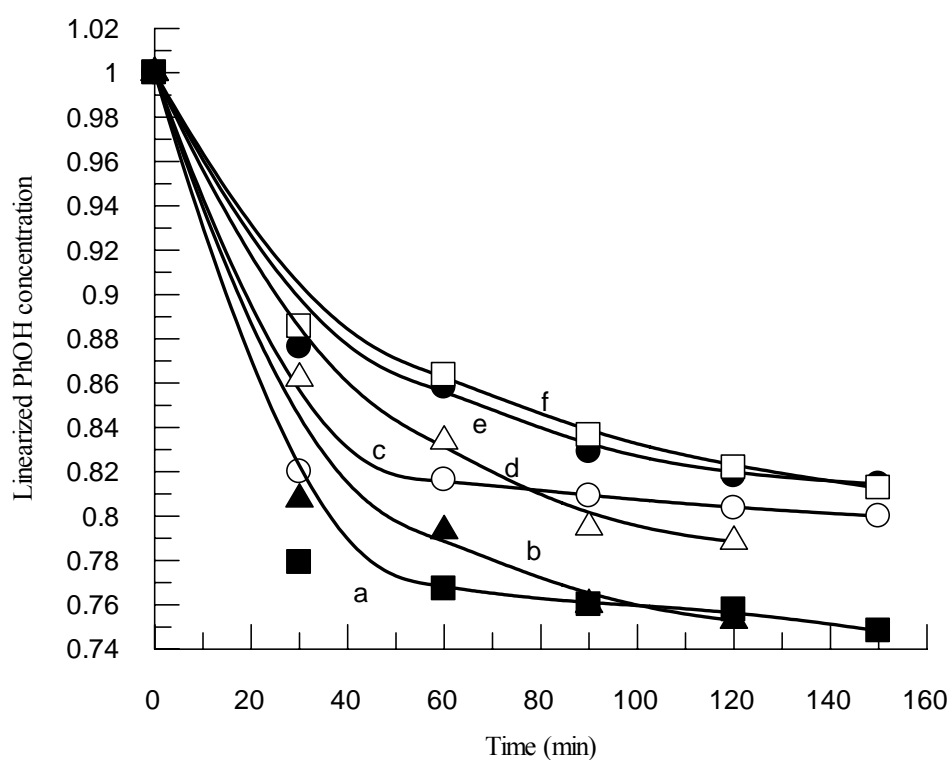


Figure (3.6): Plots of remaining phenol concentration (M) vs. time in phenol degradation experiments showing the effect of nominal dye (TPPHS) concentration, (a) 0.005g, 1.23×10^{-5} mol, (b) 0.003g, 0.738×10^{-5} mol, (c) 0.004g, 0.984×10^{-5} mol, (d) 0.01g, 2.46×10^{-5} mol, (e) 0.006g, 1.476×10^{-5} mol, (f) 0.007g, 1.772×10^{-5} mol. All experiments were conducted in the UV region at room temperature, using TiO_2 (0.5g), and 0.3M phenol concentration.

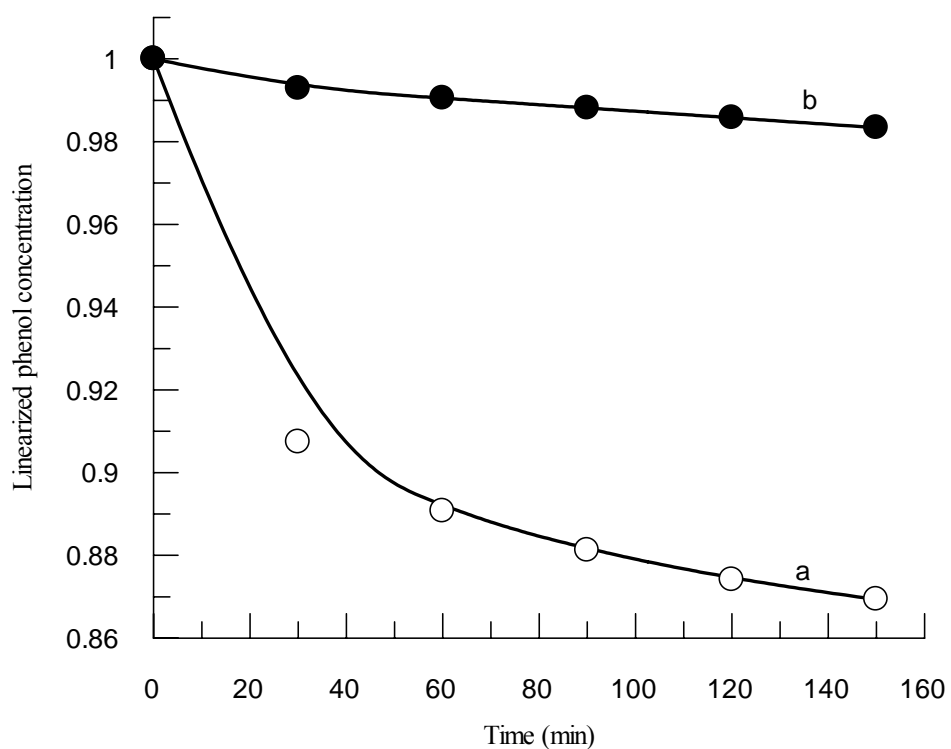


Figure (3.7): Plots of remaining phenol concentration (M) vs. time, in phenol degradation experiments showing the effect of radiation, (a), UV- light, (b) visible light. Experiments were conducted at room temperature, using TiO_2 (0.5g), TPPHS (0.003g , 0.738×10^{-5} mol), and 0.3M phenol concentration.

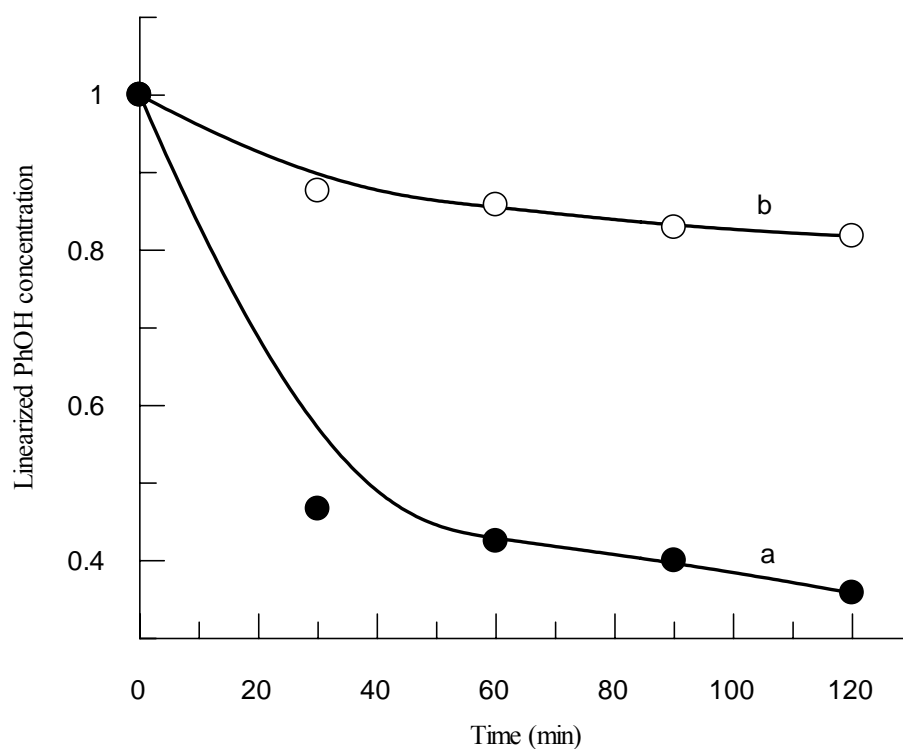


Figure (3.8): Plots of remaining phenol concentration (M) vs. time, in phenol degradation experiments showing the effect of AC, (a) with AC (0.1g), (b) no AC. All experiments were conducted in the UV at room temperature, using TiO_2 (0.5g), TPPHS (0.006g, 1.476×10^{-5} mol), and 0.3M phenol concentration.

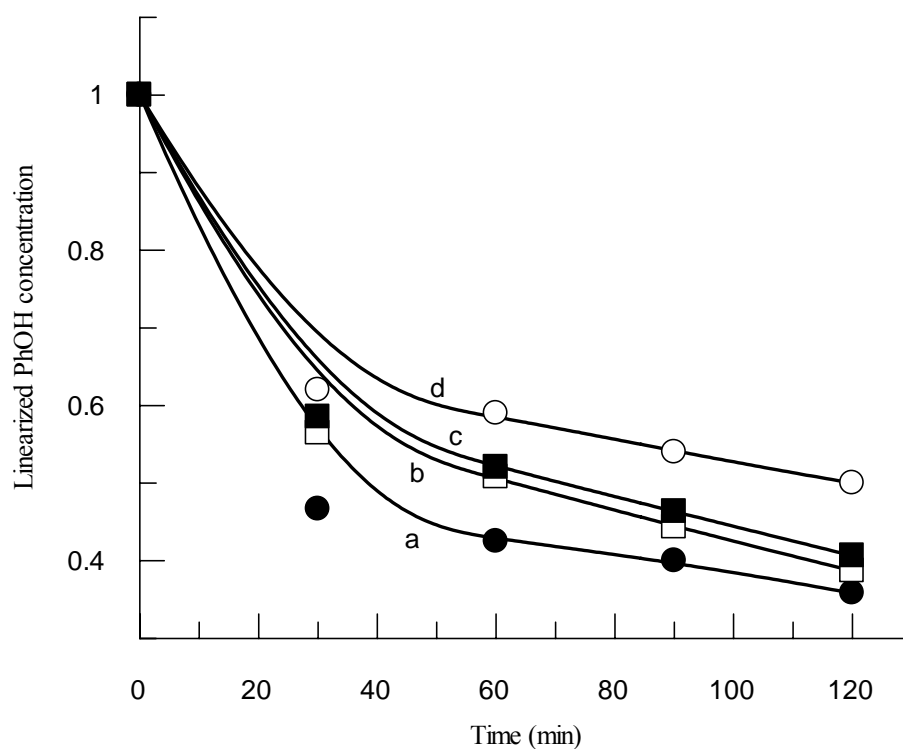


Figure (3.9): Plots of remaining phenol concentration (M) vs. time, in phenol degradation experiments showing the effect of TPPHS nominal concentration, (a) 0.006g, 1.476×10^{-5} mol, (b) 0.01g, 2.46×10^{-5} mol, (c) 0.012g, 2.0952×10^{-5} mol, (d) 0.003g, 0.738×10^{-5} mol. All experiments were conducted in the UV region at room temperature, using TiO_2 (0.5g), AC (0.1g), and 0.3M phenol concentration.

Effect of type of radiation

The AC/TiO₂/TPPHS system was employed to catalyze phenol using UV and visible regions. Parallel to TiO₂/TPPHS system, the AC/TiO₂/TPPHS showed much higher efficiency in the UV region than in the visible region, as shown in Figure (3.10).

Effect of temperature

The effect of temperature on AC/TiO₂/TPPHS catalyst activity was investigated. There was no significant temperature effect on catalyst efficiency, and the 20°C temperature was slightly more favorable than higher temperatures, Figure (3.11).

Effect of catalyst concentration

The effect of catalyst concentration on AC/TiO₂/TPPHS catalyst activity was investigated. There was no increase in activity as concentration of the catalyst (AC/TiO₂/TPPHS) increases, Figure (3.12).

Effect of speed of stirring

Different speeds of stirring were used in the UV degradation of phenol by AC/TiO₂/TPPHS system. Stirring speed showed no significant effect on phenol degradation, Figure (3.13)

3.3.6 Reuse experiments

The activity of used AC/TiO₂/TPPHS catalyst was examined for fresh phenol samples, Figure (3.14). While fresh AC/TiO₂/TPPHS systems caused higher than 60% degradation of phenol, using UV, the reused catalytic samples failed to degrade more than 10% of fresh phenol used, Figure (3.14, a-c). Addition of fresh TPPHS to the recovered system did not enhance the catalytic efficiency, Figure (3.14, d).

3.3.7 Metalloporphyrin (MnP) modified TiO₂ catalyst

MnP modified TiO₂ catalytic systems were prepared and studied in catalyzing phenol degradation in the UV. The TiO₂/MnP system showed no catalytic activity in the UV, and only little changes in phenol concentrations were noticed.

The TiO₂/MnP was also supported onto AC. The AC/TiO₂/MnP system was used in phenol degradation in the UV. The supported system showed no significant catalytic activity.

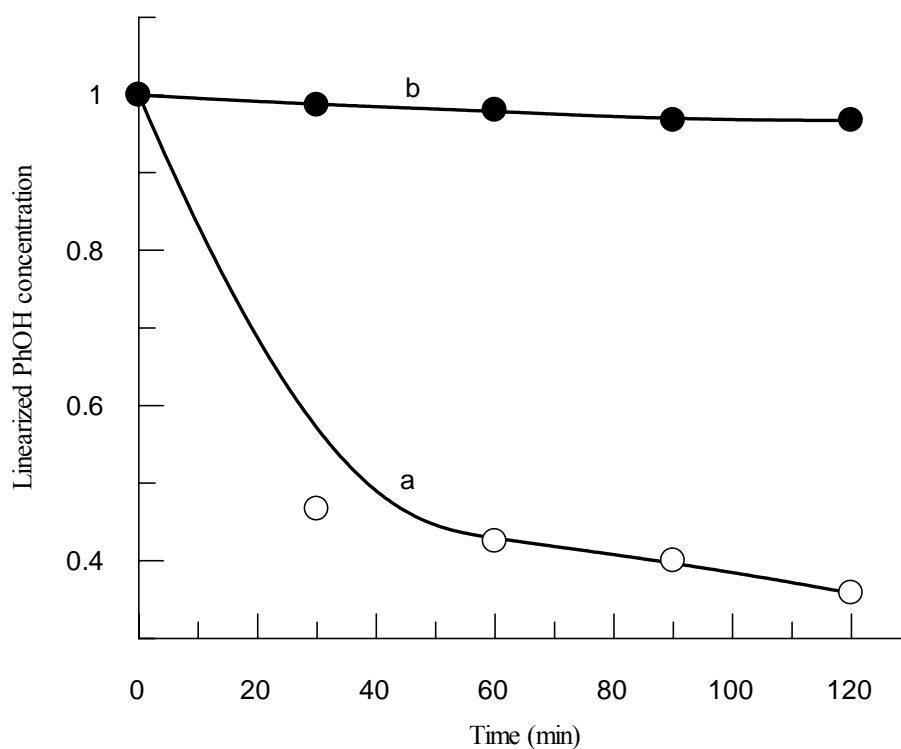


Figure (3.10): Plots of remaining phenol concentration (M) vs. time in phenol degradation experiments showing the effect of radiation, TiO_2 (0.5g), dye (TPPHS) (0.006g , 1.476×10^{-5} mol), AC (0.1g). (a) UV-light, (b) visible light. Experiments were conducted at room temperature, using 0.3M phenol concentration.

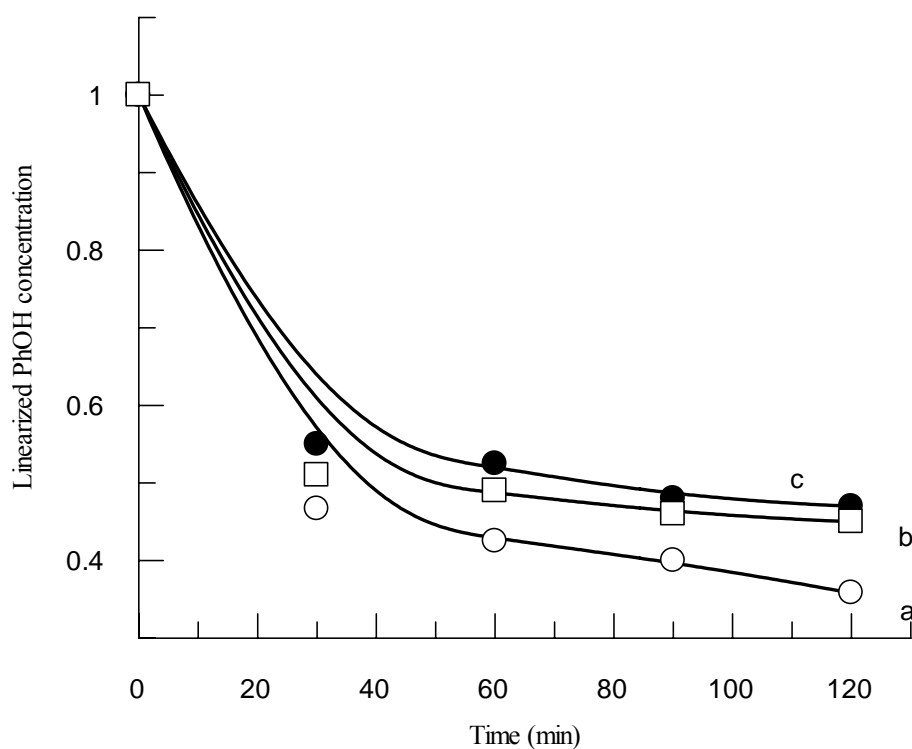


Figure (3.11): Plots of remaining phenol concentration (M) vs. time in phenol degradation experiments, showing the effect of temperature (a), 20°C, (b) 40°C, (c) 30°C. Experiments were conducted in the UV region, using AC/TiO₂/TPPHS catalyst, TiO₂ (0.5g), dye (TPPHS) (0.006g, 1.476×10^{-5} mol), AC (0.1g), and 0.3M phenol concentration.

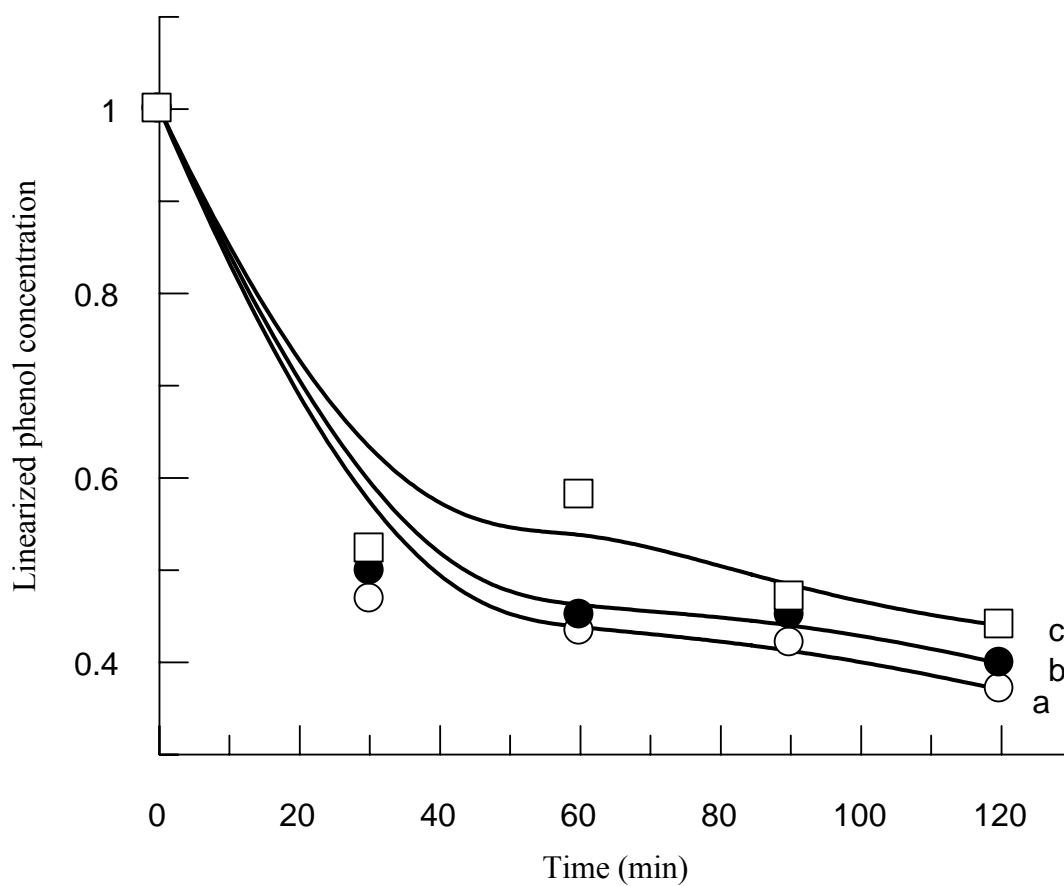


Figure (3.12): Plots of remaining phenol concentration (M) vs. time in phenol degradation experiments, showing the effect of AC/TiO₂/TPPHS catalyst concentration. (a) 1.0g catalyst, (b) 0.6g catalyst, (c) 0.3g catalyst. Experiments were conducted in the UV at room temperature, using 0.3M phenol concentration.

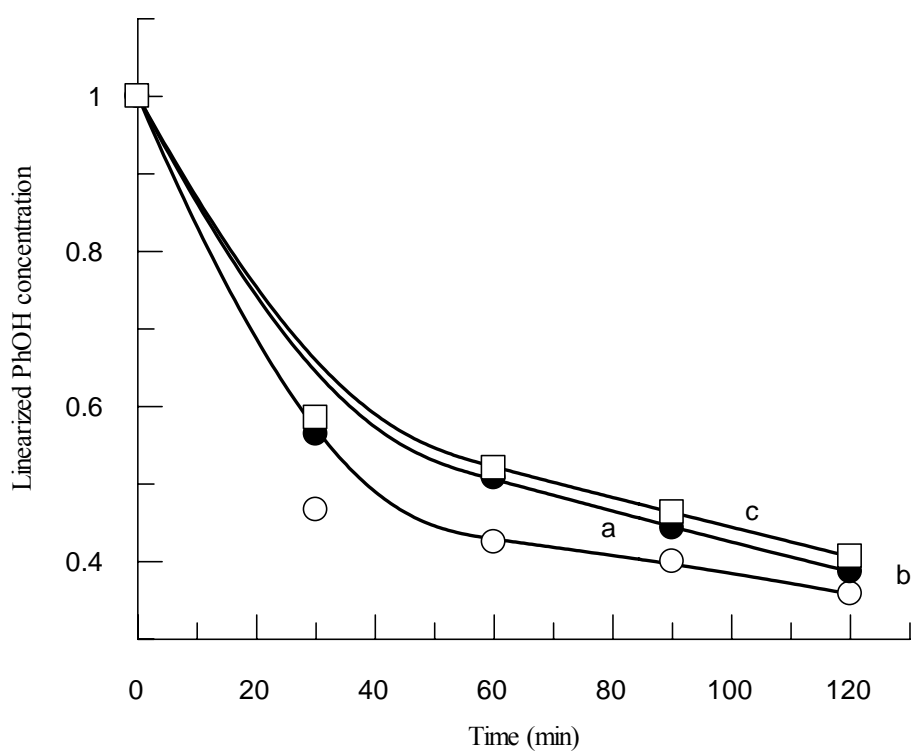


Figure (3.13): Plots of remaining phenol concentration (M) vs. time in phenol degradation experiments, showing different speeds of stirring (a) Low speed, (b) moderate speed, (c) high speed. All experiments were conducted in the UV at room temperature, using TiO_2 (0.5g), dye (TPPHS) (0.006g , 1.476×10^{-5} mol), AC (0.1g), and 0.3M phenol concentration.

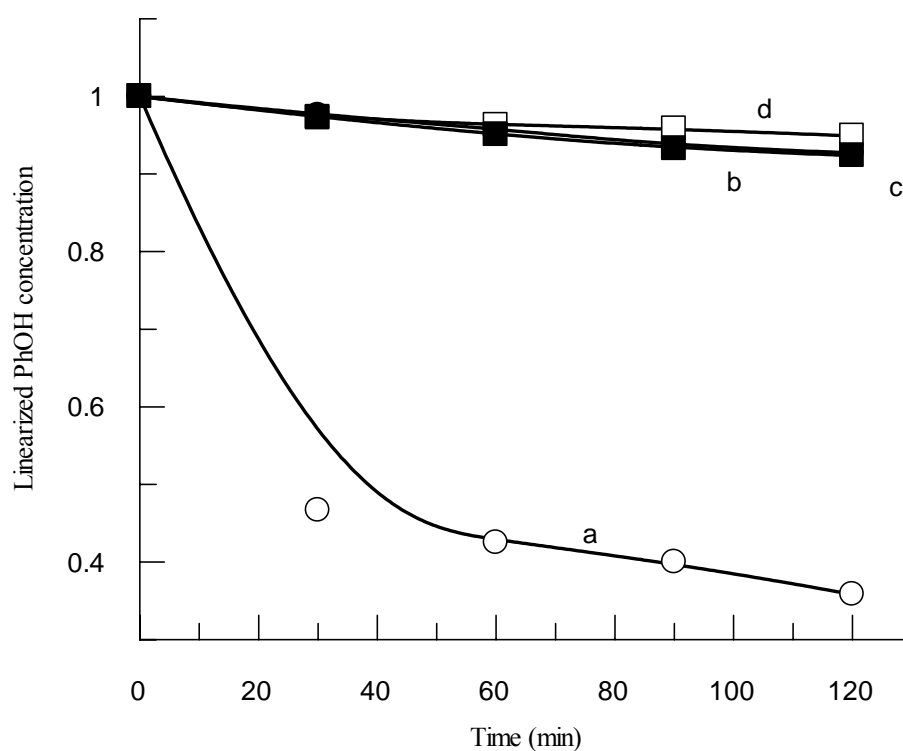


Figure (3.14): Plots of remaining phenol concentration (M) vs. time in phenol degradation experiments, showing the reuse experiments, (a) First time, (b) second time, (c) third time, (d) fourth time with a fresh dye sample (0.006g , 1.476×10^{-5} mol) added. Experiments were conducted in the UV at room temperature, using AC/TiO₂/TPPHS, AC (0.1g), TiO₂ (0.5g), dye (TPPHS) (0.006g , 1.476×10^{-5} mol), and 0.3M phenol concentration.

3.4 Discussion

3.4.1 Introduction

TiO₂ is widely investigated as photo-catalyst in water purification. This is due to many features, mainly its non-hazardous nature, stability and low cost. On the other hand, TiO₂ suffers two drawbacks. It has a wide band gap, 3.2 eV, which demands UV light for excitation. Moreover, TiO₂ is difficult to isolate from aqueous mixtures, which adds to the technical difficulties of using it. TiO₂ advantages and disadvantages have been discussed earlier.

To overcome the first difficulty, research is focused to photosensitize TiO₂ in the visible by different sensitizers, as explained earlier. For this purpose, TPPHS has been investigated here as possible photosensitizer for TiO₂ in phenol degradation. The other difficulty may possibly be solved out by supporting TiO₂ catalyst onto other insoluble materials which are hydrophobic in nature, such as AC. By such a technique, it is assumed that the supported TiO₂ will be easily separated from aqueous mixtures by simple filtration. For this purpose, naked and modified TiO₂ particles have been supported onto AC surfaces, and investigated in phenol degradation processes.

Model for dye-sensitized TiO₂

Scheme (XII) shows the energetics at the interface between TiO₂ and attached dye molecules. The band gaps, band edges and excitation processes are explained schematically therein. The Scheme shows that UV is needed to excite TiO₂ with its high band gap (3.2 eV), whereas the dye molecules need only visible light for excitation.

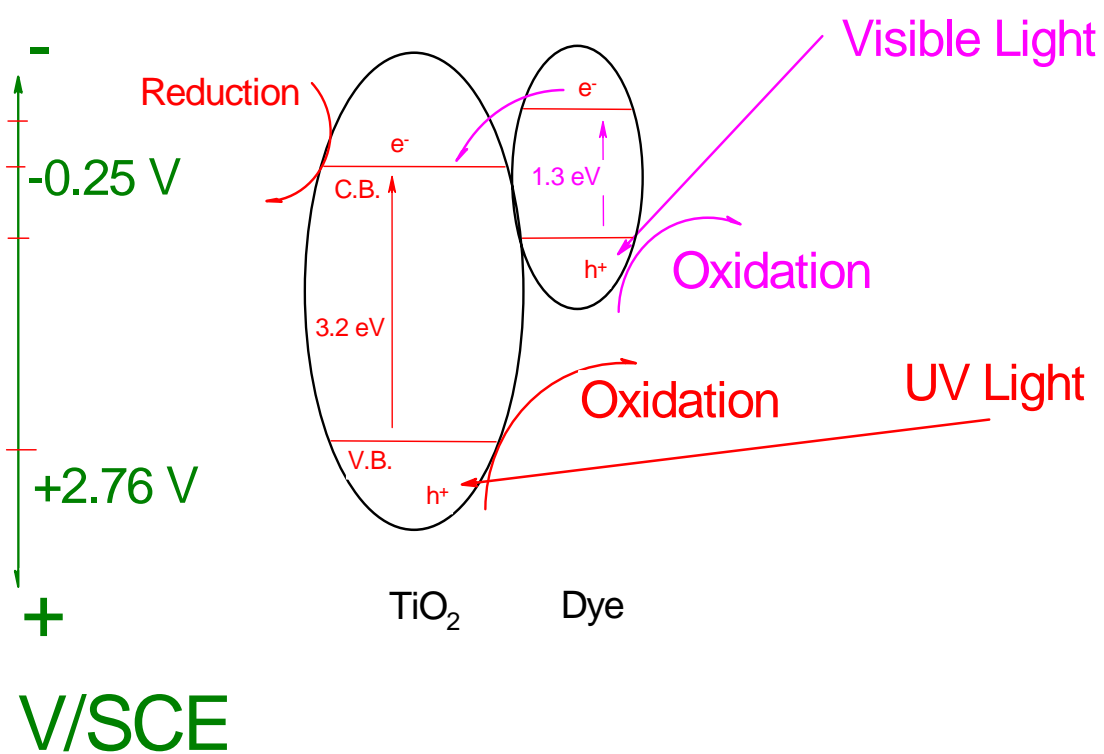
The concept of sensitization is explained in Scheme (XII). In a sensitization process, the dye molecules are themselves excited in the visible, creating electrons and holes. The electrons immigrate from the dye conduction band to the TiO_2 conduction band. The electrons would then reduce species (such as oxygen) at the TiO_2 back surface. At the front face of the dye, the holes remain at the dye valence band edge, where they oxidize species (contaminants). If a species has a moderate oxidation potential, i.e. comparable or less positive than the dye valence band edge, then the species will readily be oxidized by the dye holes. Such a process is called dye-sensitized oxidation process, and is shown separately in Scheme (XIII).

On the other hand, if the species has oxidative potential more positive than the dye valence band edge, then it will not be oxidized by the dye holes. In such a case, sensitization will not affect the degradation process. The only way, for such species to be oxidized, will be to excite the TiO_2 itself. When TiO_2 is excited, with UV, the resulting holes will have high oxidizing power as they occur in the highly positive valence band. Thermodynamically speaking, such holes have very high oxidizing power. Nevermind this thermodynamic factor, the oxidation process may occur slowly. To speed up such a process, a charge-transfer catalyst may be needed. The charge-transfer catalyst would intermediate in the hole transfer between the TiO_2 valence band and the species, as shown in Scheme (XIV).

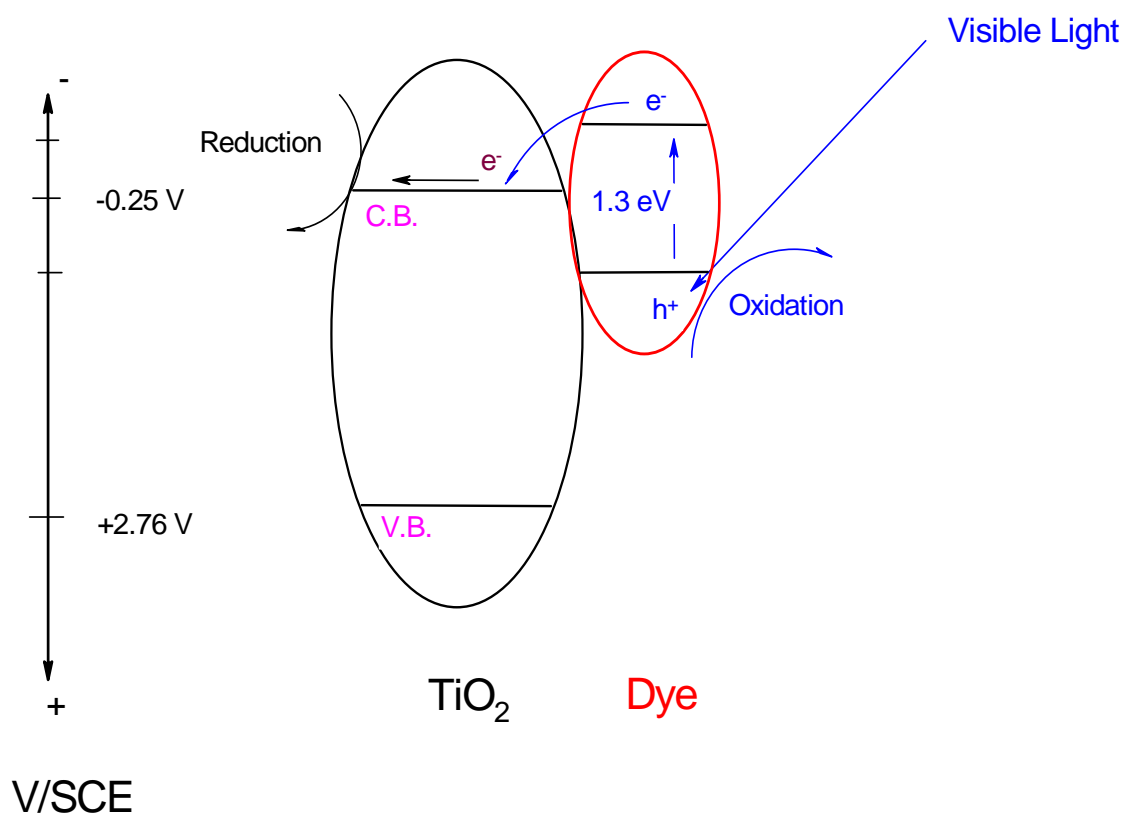
Therefore, one should be careful before deciding if a process is a sensitization or a charge-transfer one. If the process occurs readily in the visible region, it is then called a sensitization process. On the other hand, if

UV is needed, and the dye speeds up the process, it is called a charge-transfer process.

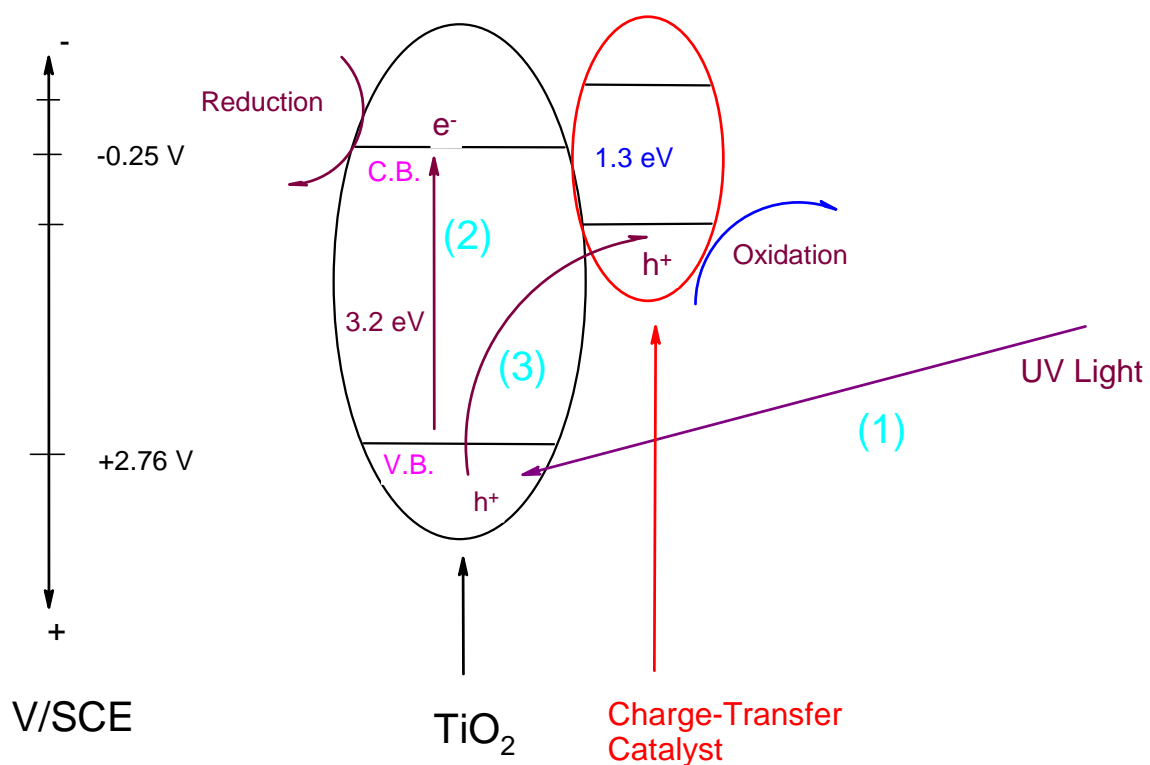
Therefore, TPPHS was used here in combination with TiO_2 to degrade phenol in the UV and visible regions. Effect of dye, temperature, oxygen, carbon support and other parameters have been studied together with other parameters. Plots of remaining phenol concentrations were used to show degree of degradation as was presented in Figures (3.2-3.13). For further clarification of catalyst efficiency in degradation process, turn-over number values were calculated by dividing number of moles of reacted phenol by number of moles of dye, after 120 min. Values of turn-over number are shown in Table (7).



Scheme XII: Effect of dye in TiO_2 sensitization and in charge-transfer catalytic processes



Scheme XIII: Effect of dye in TiO_2 Sensitization process. Note that only visible light is needed to produce low oxidation power holes.



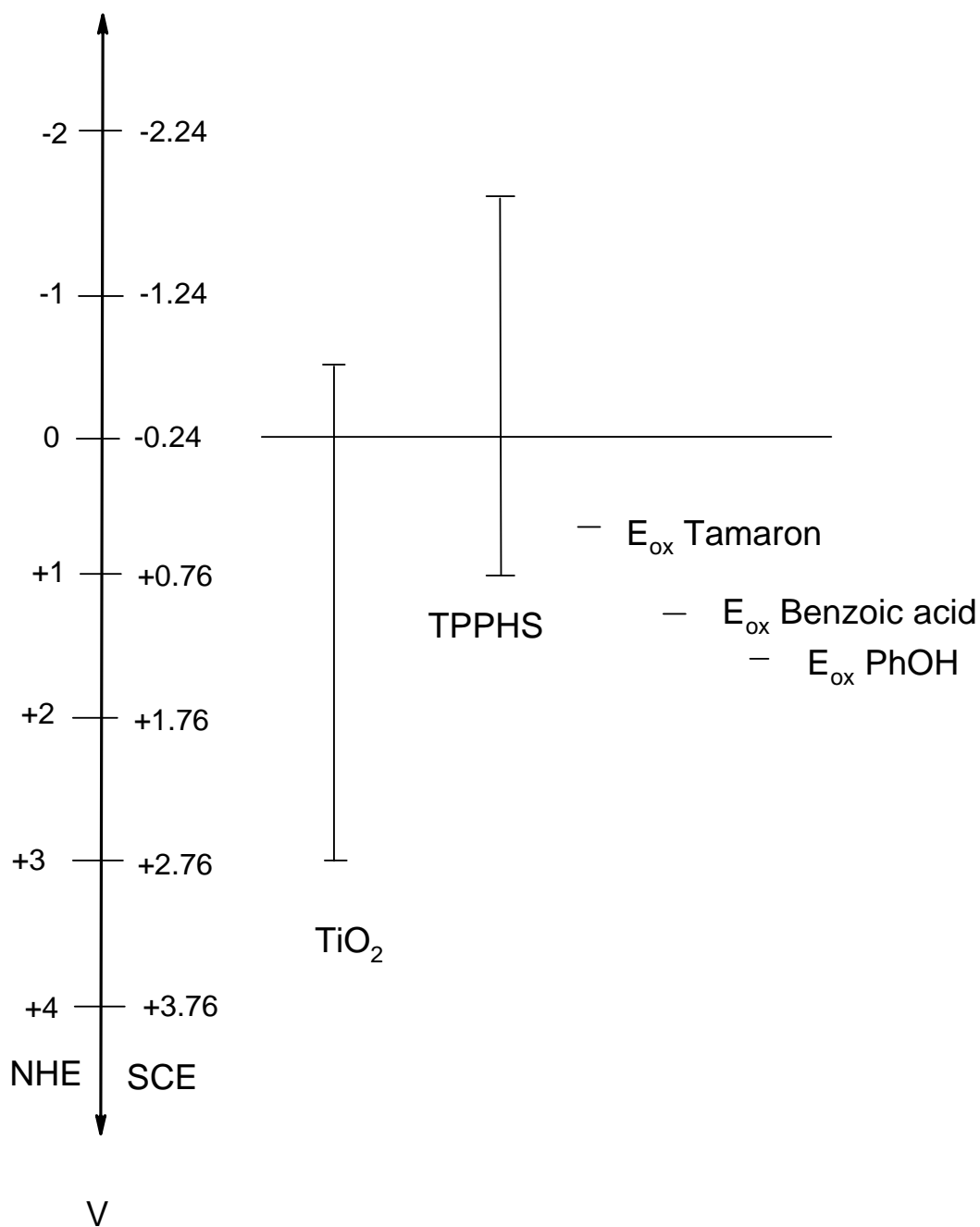
Scheme XIV: Effect of dye as a charge transfer catalyst. The dye is not excited itself, but the TiO₂ is excited with UV. The resulting holes are highly oxidizing, and the dye is only a charge transfer catalyst.

3.4.2 Effect of dye

Neither TiO_2 nor TPPHS were catalytically active, when used separately, in phenol photo-degradation, as shown in Figure (3.3) and Table (7). The combined TiO_2 /TPPHS did not catalyze the reaction in the visible region, Figure (3.7). This indicates that the TPPHS failed to sensitize the TiO_2 in the visible region. On the other hand, the TPPHS enhanced the catalytic activity of TiO_2 in the UV. Such enhancement is understandable in terms of charge transfer catalytic activity, Schemes (XIII-XIV).

The lack of sensitization mechanism is due to the holes resulting in the valence band of the dye, by visible excitement, are not positive enough, as the needed oxidation potential for phenol is high, Scheme (XV). TPPHS absorbs light at about 435 nm (band gap ~ 2.85 eV) and the resulting holes are presumably not energetic enough to oxidize phenol in the visible.

The mode of action of TPPHS in enhancing TiO_2 catalytic activity in phenol degradation is best summarized in Scheme (XIV). The mechanism involves TiO_2 excitation by UV, creating an electron-hole pair. The electron is excited to the TiO_2 conduction band, where it reduces oxygen at the back contact. The hole oxidizes the contaminant molecules at the front contact. This step is catalyzed by the TPPHS, which may accept the hole and redirect it to the contaminant molecule. The ability of TPPHS to catalyze charge transfer processes is documented in literature [11-12].



Scheme XV: Band positions (top of valence band and bottom of conduction band) of TiO₂, TPPHS and oxidation potential for phenol, benzoic acid and Tamaron.

Effect of activated carbon

Despite the fact that TiO_2 is the most widely used photo-catalyst for UV driven contaminant degradation processes, it is difficult to isolate from aqueous media after reaction completion. To solve this technical difficulty, research is directed towards supporting naked TiO_2 onto insoluble materials, such as AC [13], glass [14], Ti-6Al-4V alloy [15-16], ZSM-5 zeolite [17], silica [18] and others.

In this work, TiO_2 /TPPHS was prepared and supported onto AC for the first time. To our knowledge, no dye-modified TiO_2 systems were supported onto AC before. In addition to easy separation, the AC/ TiO_2 /TPPHS system showed higher catalytic activity than the TiO_2 /TPPHS, Figure (3.8), and Table (7). AC is expected not to affect TiO_2 /TPPHS optical or electrical properties. Due to its large surface area and hydrophobic nature, the AC is expected to preferentially adsorb organic contaminant molecules. The contaminant molecules are thus brought into close proximity to the TiO_2 catalytic sites, and consequently the degradation process is expected to be enhanced. The effect of AC observed in here is thus understandable by the ability of AC to preferentially adsorb contaminant molecules. An enhanced concentration of contaminant is progressively built up around the TiO_2 sites, leading to a significant increase in reaction rate. Complete mineralization is also expected in the presence of AC. This is because any possible intermediate compounds, resulting from degradation at earlier stages, will be also adsorbed by AC and more exposed to the degradation catalytic sites [11].

Effect of temperature

The temperature showed no significant effect on catalyst efficiency, with more activity observed at lower temperatures, as shown in Figure (3.11). The results are consistent with earlier literature reports, which also showed that photocatalytic oxidation rate is not much affected by changes in temperature. The photo-degradation rate independence of temperature is reflected by its low activation energy (a few kJ/mol) compared to ordinary thermal reactions [11]. Moreover, at higher temperatures, oxygen concentrations in the reaction solution are lowered by increasing temperature. This explains why at 20°C the rate was slightly higher than at higher temperatures.

Effect of oxygen concentration

Oxygen was essential for semiconductor photocatalytic degradation of organic compounds. Dissolved molecular oxygen is strongly electrophilic and thus an increase of its content probably reduces unfavourable electron–hole recombination routes. Experiments conducted in a closed reactor showed low degradation rates, whereas open reactor experiments showed higher rates. Therefore, the presence of reasonable oxygen concentrations is essential for degradation to occur. This is in accordance with literature [11,19]. On the other hand, higher oxygen concentrations, attained by oxygen bubbling, lead to a downturn of the reaction rate as shown in Figure (3.5). Literature also showed similar results, where higher oxygen concentrations inhibited the photo-degradation of organic contaminants [20]. This is attributed to the fact that the TiO₂ surface becomes highly hydroxylated to the extent of inhibiting the adsorption of pollutants at active sites [11, 20].

Therefore, while oxygen is necessary, for the degradation process to occur, by behaving as electron scavenger [19], its high concentrations inhibit the free radical formation processes necessary for degradation [20]. Despite these contradicting effects of oxygen, there seems to be no technical difficulty in degrading contaminants at large scale in the presence of oxygen with moderate concentrations. Keeping the reactor open to oxygen is all one needs for degradation process to occur, as observed here. This is technically important for future processes at large scale, as we will need no oxygen pumping while purifying waters with UV radiation.

Effect of initial contaminant concentration

Initial phenol concentrations did not affect rate of phenol degradation in UV using AC/TiO₂/TPPHS. Two factors might be responsible for this behavior: [11]

- The generation and migration of photo-generated electron-hole pairs and their reaction with organic compounds occur in series. Therefore, each step may become rate-determining for the overall process. At low concentrations, the latter dominates the process and, therefore, the degradation rate increases linearly with concentration. However, at high concentrations, like the ones used here, the former will become the governing step, and the degradation rate increases slowly with concentration, and for a given illumination intensity, a constant degradation rate may be observed as a function of concentration.

- Intermediates generated during the photocatalytic process also affect the rate constant of their parent compounds. A higher initial concentration will yield a higher concentration of adsorbed intermediates, which would affect the overall rate.

Effect of catalyst concentration

Different AC/TiO₂/TPPHS catalyst concentrations on phenol photo-degradation were studied. It was noticed that the rate of phenol degradation was independent of the catalyst concentration. This result is explainable although our expectation is the opposite.

The rate is proportional to number of irradiated catalytic sites at a given time. In suspensions, like the AC/TiO₂/TPPHS system used here, only a fraction of catalytic sites would be exposed to radiation. As higher catalyst concentrations are used, more sites will be hidden away from radiation. Therefore, the number of irradiated catalytic sites at a given time will not increase with increased amount of added catalyst. Therefore, the rate of degradation is not affected by catalyst amount, as shown in Figure (3.12).

Effect of speed of stirring

Different speeds of stirrings were investigated in UV phenol degradation by AC/TiO₂/TPPHS catalyst system. No significant change in phenol degradation was noticed. This rules out any possibility for the reaction to be controlled by diffusion of contaminant molecules.

3.4.3 Effect of MnP dye

MnP modified TiO₂ surfaces were prepared and investigated in phenol decomposition. The TiO₂/MnP system was inefficient in either UV or visible regions. When AC supported TiO₂/MnP was not efficient as well.

The inefficiency of MnP to sensitize TiO₂ for phenol degradation is understandable by the fact that it has only a small band gap (2.68 eV, 463 nm) which is not sufficient for phenol oxidation. Furthermore, the inefficiency of TiO₂/MnP to degrade phenol in the UV is due to inability of MnP to function as a suitable charge transfer catalyst here. Therefore, it is not recommended here to use TiO₂/MnP systems for degradation of stable contaminants like phenol.

Reuse

Due to technical difficulty in separating TiO₂/TPPHS, the used catalyst was not recovered for reuse. The AC/TiO₂/TPPHS was easily recovered by simple filtration over sintered glass. The recovered AC/TiO₂/TPPHS catalyst showed low catalytic activity, in phenol degradation, compared to fresh samples, Figure (3.13). This indicates the failure of the catalyst in reuse studies. This failure is presumably not due to TPPHS decomposition under the photolysis experimental conditions. Literature [12] showed that TPPHS survived similar irradiation conditions for prolonged times.

The other reason, of catalyst deactivation, is possibly the TiO₂/TPPHS burial inside AC. This may occur under reaction stirring conditions, where AC particles undergo shape changes due to mechanical milling. The TiO₂/TPPHS sites are expected to be buried inside AC pores

with no access for contaminant molecules. For confirmation, fresh samples of TPPHS were added to the used AC/TiO₂/TPPHS systems. It is assumed that if catalyst deactivation is due to TPPHS decomposition, then fresh TPPHS would regenerate the catalyst activity. As results show, the fresh TPPHS samples failed to do so, Figure (3.13). This confirms the conclusion that deactivation was due to active site burial inside the AC pores. As such, the freshly added TPPHS did not adhere to buried TiO₂ particles in the recovered catalyst. This means that magnetic stirring should be avoided in future study of AC/TiO₂/TPPHS photocatalytic system.

Table (7): Values of turnover number for different catalytic systems in phenol degradation

Catalyst	TiO ₂ amount g	TPPHS amount g (mol)	Turnover number*
Naked TiO ₂	0.5	0	33**
Dye only	0	0.006 (1.476×10 ⁻⁵)	27
TiO ₂ /TPPHS	0.5	0.01 (2.46×10 ⁻⁵)	163
	0.5	0.005 (1.23×10 ⁻⁵)	129
	1	0.006 (1.476×10 ⁻⁵)	149
	0.5	0.006 (1.467×10 ⁻⁵)	270
	0.5	0.003 (0.738×10 ⁻⁵)	176
	0.5	0.006 (1.476×10 ⁻⁵)	372
AC/TiO ₂ /TPPHS	0.5	0.012 (2.952×10 ⁻⁵)	169
	0.5	0.01 (2.46×10 ⁻⁵)	677
	0.5	0.003 (0.738×10 ⁻⁵)	580
	0.5	0.003 (0.738×10 ⁻⁵)	580

*Turnover number values, (reacted PhOH moles/dye moles) were measured after 120 min reaction time.

** Turnover number value was calculated assuming presence of TPPHS (0.006 g, 1.476×10⁻⁵).

REFERENCES

- 11) R. Morrison, and R. Boyd, "Organic Chemistry", *Allyn and Bacon Inc.*, **4th edition**, (1983), 957-960.
- 12) ATSDR, Agency for Toxic Substances And Disease Registry, June 18- (2005).
- 13) D. Chen, and A. Ray, "Photo-catalytic kinetics of phenol and its derivatives over UV irradiated TiO₂", *App. Catal. B: Env.*, **23**, (1999) 143.
- 14) R. Mathews, "Photo-catalytic oxidation of organic contaminants in water: An aid to environmental preservation", *Pure and Appl. Chem.*, **64 (9)**, (1992) 1285-1290.
- 15) J. Matos, J. Laine, and J. Herrmann, "Synergy effect in the photocatalytic degradation of phenol on a suspended mixture titania and activated carbon", *Applied Catalysis B: Environmental*, **18**, (1998) 281-291.
- 16) D. Chatterjee, "Visible Light Induced Photodegradation of Organic Pollutants on Dye Adsorbed TiO₂ Surface", *Bulletin of the Catalysis Society of India*, **3**, (2004) 56-58.
- 17) D. Dionysiou, A. Khodadoust, A. Kern, M. Suidan I. Baudin, and J. Laîne, "Continuous-mode photocatalytic degradation of chlorinated phenols and pesticides in water using a bench-scale TiO₂ rotating disc reactor", *Applied Catalysis B: Environmental*, **24**, (2000) 139-155.
- 18) D. Dumitriu, A. Bally, C. Ballif, P. Hones, P. Schmid, R. Sanjinés, F. Lévy, and V. Pârvulescu, "Photocatalytic degradation of

phenol by thin films prepared by sputterin", *Applied Catalysis B: Environmental*, **25**, (2000) 83-92.

- 19) D. Chatterjee, and, A. Mahata, "Photo-assisted detoxification of organic pollutants on the surface modified TiO₂ semiconductor particulate system", *Catalysis communications*, **2**, (2001) 1-3.
- 20) AOAC Official Method 979.13, copyright 1998, AOAC International.
- 21) O. Carp, C. Huisman, and A. Reller, "Photoinduced reactivity of TiO₂", *Progress in Solid State Chemistry*, **32**, (2004) 33-177.
- 22) A. Sanjuàn, G. Aguirre, M. Alvaro, And H. García, "2,4,6-Triphenylpyrylium ion encapsulated within γ zeolite as photocatalyst for the degradation of methyl parathion", *Wat. Res.*, **34** (1), (2000) 320-326.
- 23) J. Matos, J. Laine, and J. Herrmann, "Synergy effect in the photocatalytic degradation of phenol on a suspended mixture titania and activated carbon", *Applied Catalysis B: Environmental*, **18**, (1998) 281-291.
- 24) J. Byrne and B. Eggins, N. Brown, B. McKinny, and M. Rouse, "Immobilization of TiO₂ powder for the treatment of polluted water", *Applied Catalysis B: Environmental*, **17**, (1998) 25-36.
- 25) H. Coleman, B. Eggins, J. Byrne, F. Palmer, and E. King, "Photocatalytic degradation of 17- β -oestradiol on immobilized TiO₂" *Applied Catalysis B: Environmental*, **612** (1999) 1-5.
- 26) J. Byrne, B. Eggins, W. Byers, and N. Brown, "Photo-electrochemical cell for the combined photocatalytic oxidation of

organic pollutants and the recovery of metals from waste waters", *Appl. Cat. B: Environmental*, **20**, (1999) L85-L89.

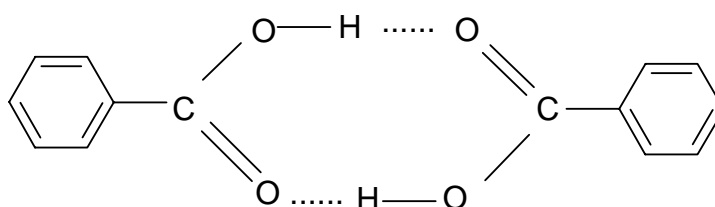
- 27) S. Zhang, N. Fujii, and Y. Nosaka, "The dispersion effect of TiO₂ loaded over ZSM-5 zeolite", *J. Mol. Cat.*, **129**, (1998) 219-224.
- 28) K. Wang, H. Tsai, and Y. Hsieh, "The kinetics of photocatalytic degradation of trichloroethylene in gas phase over TiO₂ supported on glass bead", *Applied Catalysis B: Environmental*, **17**, (1998) 313-320.
- 29) Y. Wang, and C. Hong, " TiO₂-mediated photomineralization of 2-chlorobiphenyl: the role of O₂", *Water Research*, **34 (10)**, (2000), 2791-2797.
- 30) G. Heit, and A. Braun, "VUV-photolysis of aqueous systems: Spatial differentiation between volumes of primary and secondary reactions", *Water Sci. and Tech.*, **35 (4)**, (1997), 25-30.

CHAPTER 4

**PHOTO-DEGRADATION OF BENZOIC
ACID**

4.1 Introduction

Carboxylic acids are compounds that contain a carboxyl group attached to either an alkyl group (R—COOH), or an aryl group (Ar—COOH). The simplest aromatic acid is benzoic acid. It is polar, and its molecules may couple in pairs which form hydrogen bonds to each other. The molecules may also form hydrogen bonds with molecules of other compounds. Its solubility in water is 0.34g/100g H₂O. It is solid at room temperature, with a melting point of 122°C [1]. Benzoic acid has a high boiling point (250°C), due to pairing of molecules. Each pair is held together by two hydrogen bonds, Scheme (XVI).



XVI

Contact with benzoic acid irritates the eyes with possible damage. Inhalation irritates the nose, throat and lungs causing coughing, wheezing and/or shortness of breath. Benzoic acid may also cause a skin allergy. If allergy develops, very low future exposure may cause itching and skin rash [2].

Benzoic acid is difficult to degrade by conventional methods, so photo-electrochemical methods are used to degrade it. As described earlier in Chapter (3), naked, and/or modified TiO₂ surfaces were used [3-9] for such purpose.

4.2 Experimental

4.2.1 Chemicals

Benzoic acid and NaOH were purchased from Aldrich. Acetic acid was obtained from Reidel- DeHaën in a pure form.

Stock solution preparations

The following stock solutions were prepared:

- 1000 ppm benzoic acid solution was prepared by dissolving 1.0g benzoic acid in distilled water then diluting to 1.0 L.
- Approximately 0.1 M NaOH solution was prepared by dissolving 0.4 g of NaOH in distilled water then diluted to 100 ml.
- 20% acetic acid (pH=3) solution was prepared by diluting 200 ml of acetic acid in 1.0 L distilled water, the pH was adjusted with the 0.1M NaOH solution described above.

4.2.2 Equipment

The concentration of benzoic acid was measured using HPLC instrument (Waters 2695/ Separation Module, Photodiode Array Detector) at 254 nm and the mobile phase was 20% acetic acid (pH= 3) solution, the injected volume was 20 μ L. GC-MS was used to analyze possible products which may result from degradation. Details of equipment description are presented earlier (page 42).

4.2.3 Photo-degradation experiments

Reactor, light source, catalyst analysis and photolysis experiments were described earlier, in Chapter 2. For product analysis the following method was used:

A sample was taken from the reaction system and was extracted with an organic solvent, ether. The organic layer was analyzed using GC-MS. Other than remaining benzoic acid in the sample, no organic matter was detected. This indicates that the products of degrading benzoic acid are CO_2 and H_2O . This is in accordance with literature [11].

4.2.4 Concentration measurements

HPLC was used to measure benzoic acid remaining during photo-degradation experiments. Aqueous solutions with different nominal benzoic acid concentrations, 200ppm, 150ppm, 100ppm, and 50ppm, were prepared. HPLC was used, and absorbance vs. concentration calibration curve was constructed, Figure (4.1). The calibration curve was used to analyze remaining benzoic acid through out the course of degradation reaction.

4.3 Results

4.3.1 Calibration curve

The absorbance vs. concentration calibration curve was used to measure the unreacted benzoic acid concentrations with time during degradation experiments. Figure (4.1) shows the calibration curve used.

4.3.2 Control experiments

Control experiments were conducted, using aqueous benzoic acid solutions, in the dark, or in the absence of catalyst, AC adsorption of

benzoic acid was also studied. It was found that in all photolysis experiments, carried out with no catalyst, with no light, or with AC alone, benzoic acid concentrations didn't significantly change after prolonged times (3h), Figure (4.2). Only up to 7% loss of benzoic acid was observed in control experiments.

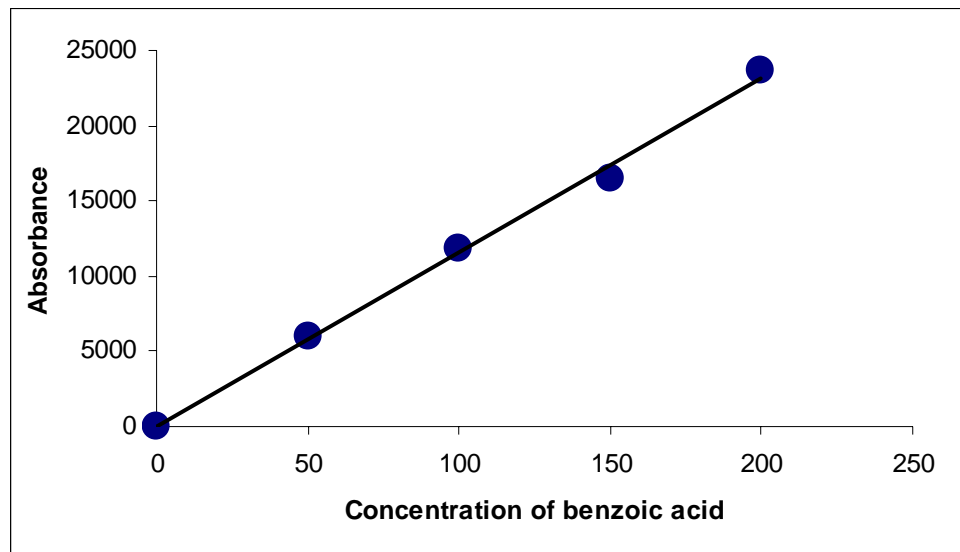


Figure (4.1): A calibration curve showing a plot of absorbance vs. benzoic acid concentration (ppm). Measurements were conducted in aqueous media, at room temperature.

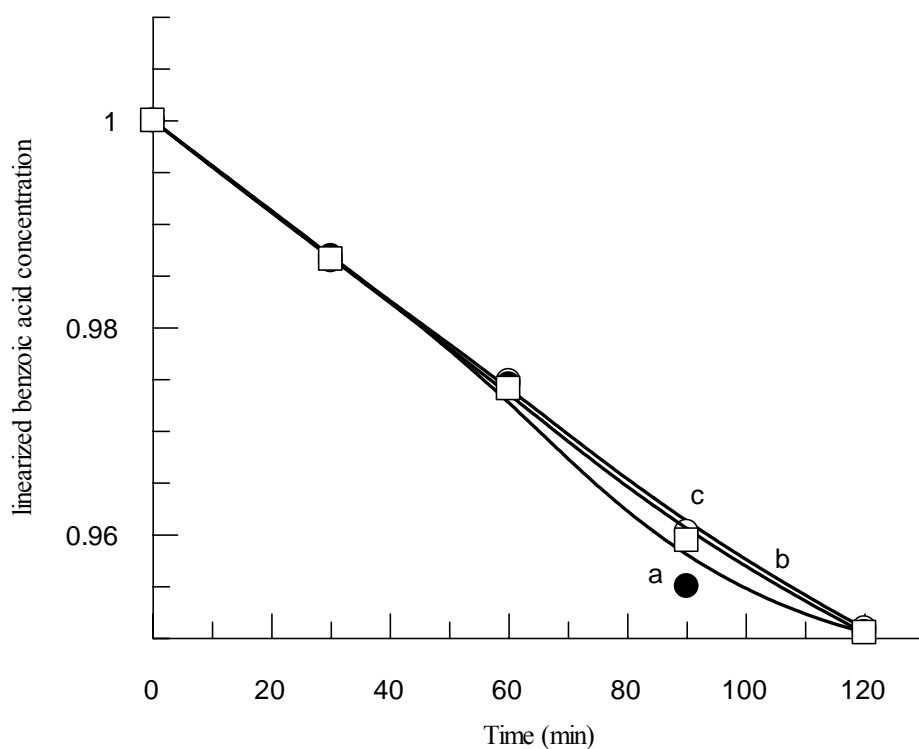


Figure (4.2): Plots of remaining benzoic acid concentration (ppm) vs. time in benzoic acid degradation experiments, showing the control experiments. (a) UV light with no catalyst ($\text{TiO}_2/\text{TPPHS}$), (b) catalyst with no light (UV), (c) AC alone, using TiO_2 (0.5g), TPPHS (0.003g, 0.738×10^{-5} mol), AC (0.1g), and 200 ppm benzoic acid concentration.

4.3.3 Naked TiO₂ and naked TPPHS dye

When TiO₂ was used as catalyst, in the absence of TPPHS, only little loss of benzoic acid occurred under UV or visible. Replacement of TiO₂ with TPPHS, did not enhance benzoic acid degradation, as shown in Figure (4.3). Thus, TiO₂ or TPPHS did not effectively catalyze the reaction while used separately.

4.3.4 TiO₂/TPPHS catalyst

TiO₂, combined with TPPHS, was used in benzoic acid degradation by UV. The combined system showed higher catalytic activity than separate ones.

Effect of initial benzoic acid concentration

Initial benzoic acid concentration was studied and showed slight increase in benzoic acid degradation, Figure (4.4).

Effect of oxygen concentration

The effect of oxygen exposure, on benzoic acid degradation was studied using UV. Experiments were conducted using reactors that are open to air, closed to air or bubbled with air. Figure (4.5) shows that the open reaction system, with no bubbling, was the fastest system. On the other hand the reaction was significantly hindered by air bubbling. The reaction conducted in a closed system was faster than that conducted with bubbling, but slower than the open reactor. Therefore, unless otherwise stated, all degradation experiments were conducted in an open reactor with no air bubbling.

Effect of dye concentration

Different concentrations of TiO₂ and/or TPPHS were used to degrade benzoic acid using UV. The rate of degradation was independent of TiO₂ or TPPHS nominal concentrations after TiO₂ is saturated with TPPHS. Approximately 33% of benzoic acid was degraded within 2.5 h, Figure (4.6).

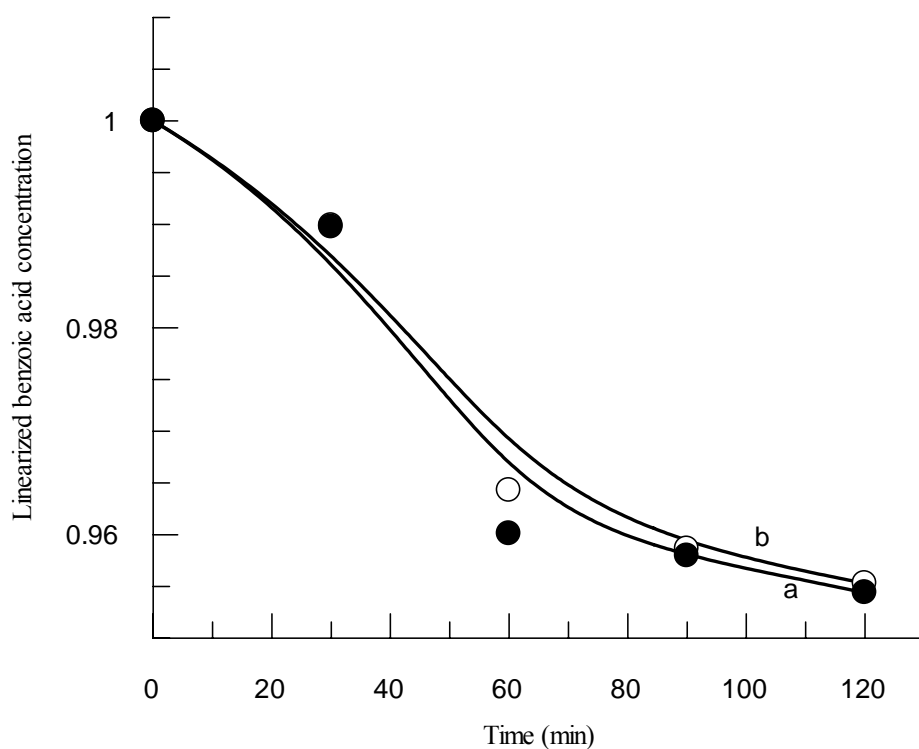


Figure (4.3): Plots of remaining benzoic acid concentration (M) vs. time in benzoic acid degradation experiments. (a) Naked dye (TPPHS), (b) Naked TiO₂. Experiments were conducted in the UV at room temperature, using TiO₂ (0.5g), TPPHS (0.003g, 0.738×10^{-5} mol), and 200 ppm benzoic acid concentration.

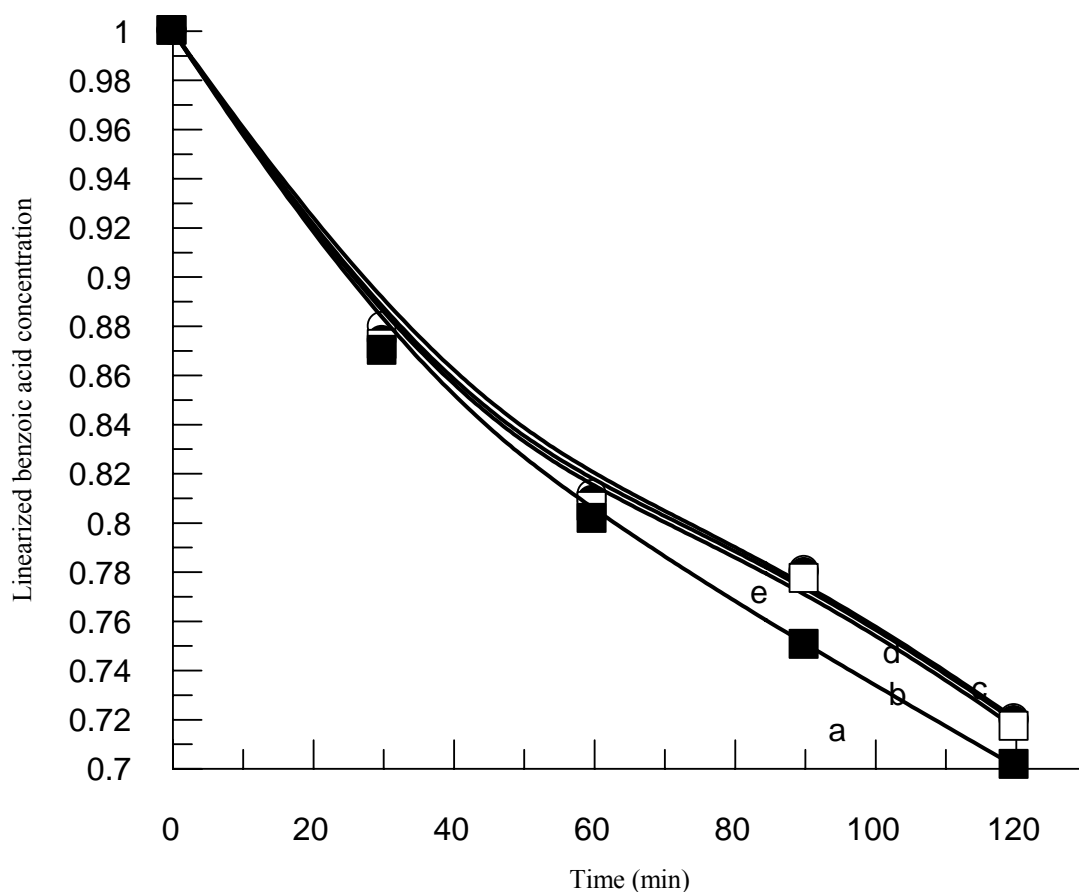


Figure (4.4): Plots of remaining benzoic acid concentration (ppm) vs. time in benzoic acid degradation experiments showing the effect of initial benzoic acid concentration, (a) 200, (b) 150, (c) 100, (d) 70, (e) 20 ppm. All experiments were conducted in the UV at room temperature, using TiO_2 /TPPHS system, TiO_2 (0.5g), TPPHS (0.003g, 0.738×10^{-5} mol).

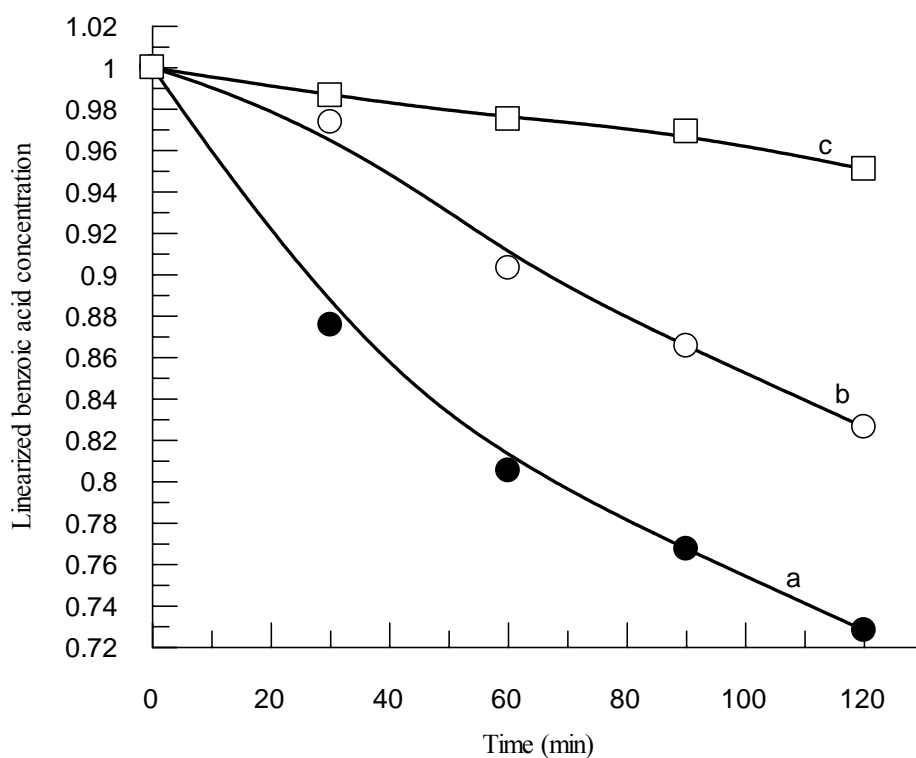


Figure (4.5): Plots of remaining benzoic acid concentration (M) vs. time in benzoic acid degradation experiments showing the effect of oxygen concentration, (a) opened reactor, (b) reactor closed, (c) bubbles of air. Experiments were conducted in the UV region at room temperature, using AC/TiO₂/TPPHS system, TiO₂ (0.5g), TPPHS (0.003g, 0.738×10^{-5} mol), AC (0.1g) and 200 ppm benzoic acid concentration.

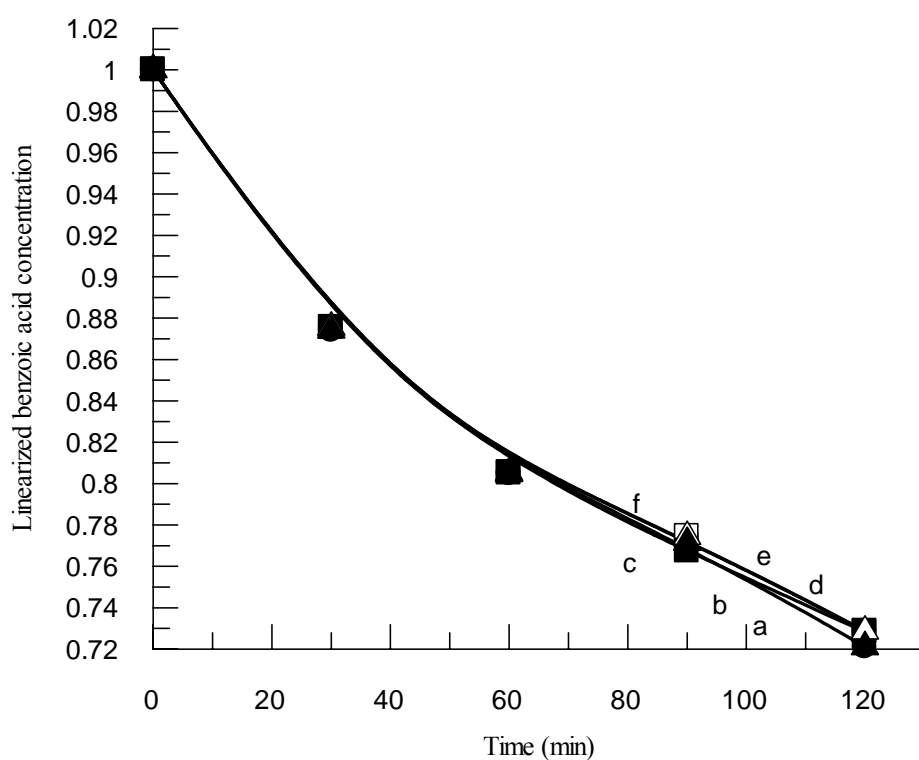


Figure (4.6): Plots of remaining benzoic acid concentration (M) vs. time in benzoic acid degradation experiments showing the effect of nominal dye (TPPHS) concentrations, (a) 0.005g, 1.23×10^{-5} mol, (b) 0.004g, 0.984×10^{-5} mol, (c) 0.006g, 1.476×10^{-5} mol, (d) 0.007g, 1.772×10^{-5} mol, (e) 0.003g, 0.738×10^{-5} mol, (f) 0.01g, 2.46×10^{-5} mol. All experiments were conducted in the UV region at room temperature, using TiO_2 (0.5g), and 200 ppm benzoic acid concentration.

Effect of type of radiation

The TiO₂/TPPHS system was employed to catalyze benzoic acid degradation using UV and visible light. Figure (4.7) shows that UV is much more efficient than the visible light. Therefore unless otherwise stated, all phenol degradation experiments were conducted using the UV radiation.

4.3.5 AC/TiO₂/TPPHS catalyst

TiO₂/TPPHS was prepared and supported onto activated carbon, as described in Chapter (2). The new AC/TiO₂/TPPHS system was used to catalyze benzoic acid degradation in the UV region. More than 50% of benzoic acid was degraded when AC/TiO₂/TPPHS catalyst was used. This shows that AC enhanced the catalytic activity of the combined TiO₂/TPPHS. Different concentrations of TPPHS were studied. The rate of degradation was independent of TPPHS concentration after saturation is reached, Figures (4.8-4.9).

Effect of type of radiation

The AC/TiO₂/TPPHS system was employed to catalyze benzoic acid in the UV and visible regions. Similar to TiO₂/TPPHS system, the AC/TiO₂/TPPHS showed much higher efficiency in the UV than in the visible as shown in Figure (4.10).

Effect of catalyst concentration

The effect of concentration of AC/TiO₂/TPPHS on degradation of benzoic acid was investigated. Only a slight increase in rate was observed as concentration of the catalyst (AC/TiO₂/TPPHS) increases, Figure (4.11).

Effect of temperature

The effect of temperature, on AC/TiO₂/TPPHS catalyst activity was investigated. Within the used temperature range, 20-40°C, there was no significant temperature effect on catalyst efficiency, Figure (4.12).

4.3.6 Metalloporphyrin (MnP) modified TiO₂ catalyst

TiO₂ was modified with tetrapyridylporphyrinatomanganese (III). The TiO₂/MnP system was investigated as catalyst for benzoic acid degradation. The TiO₂/MnP system showed no significant catalytic activity in UV or visible regions.

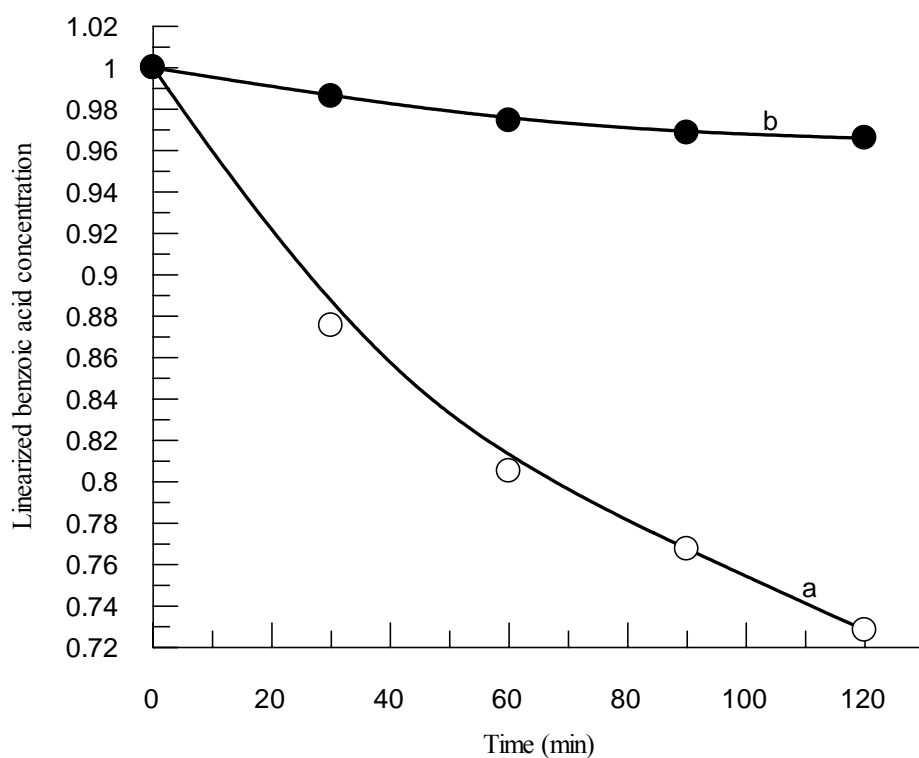


Figure (4.7): Plots of remaining benzoic acid concentration (M) vs. time in benzoic acid degradation experiments showing the effect of radiation, (a) UV-light, (b) visible light. All experiments were conducted at room temperature, using TiO_2 /TPPHS system TiO_2 (0.5g), TPPHS (0.003g, 0.738×10^{-5} mol), and 200 ppm benzoic acid concentration.

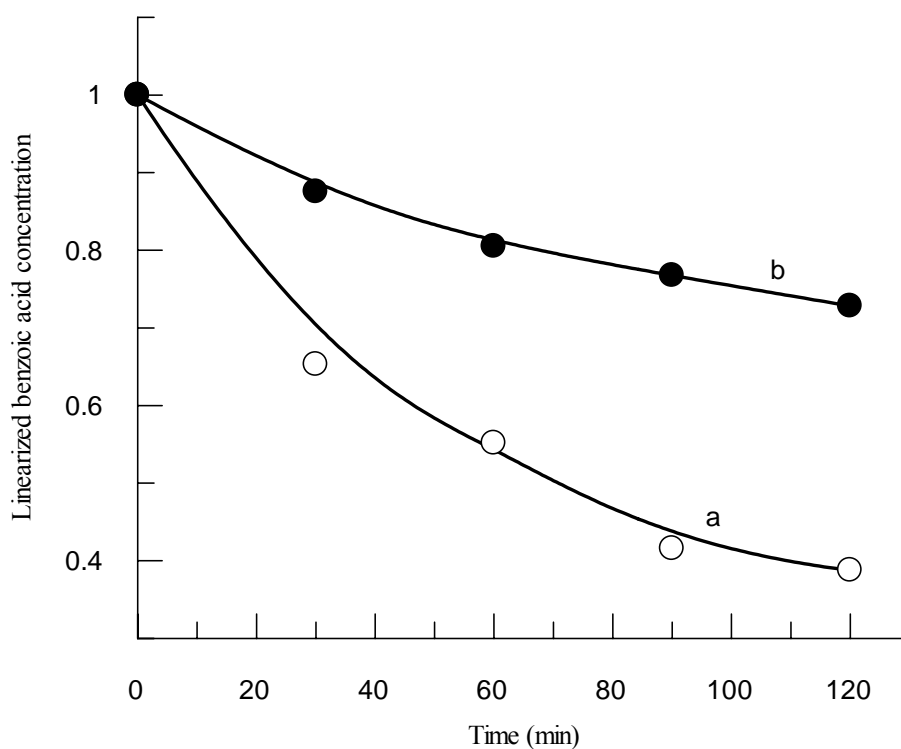


Figure (4.8): Plots of remaining benzoic acid concentration (M) vs. time in benzoic acid degradation experiments showing the effect of AC, (a) With AC (0.1g), (b) with no AC. All experiments were conducted in the UV at room temperature, using TiO_2 (0.5g), and TPPHS (0.006g , 1.476×10^{-5} mol), and 200 ppm benzoic acid concentration.

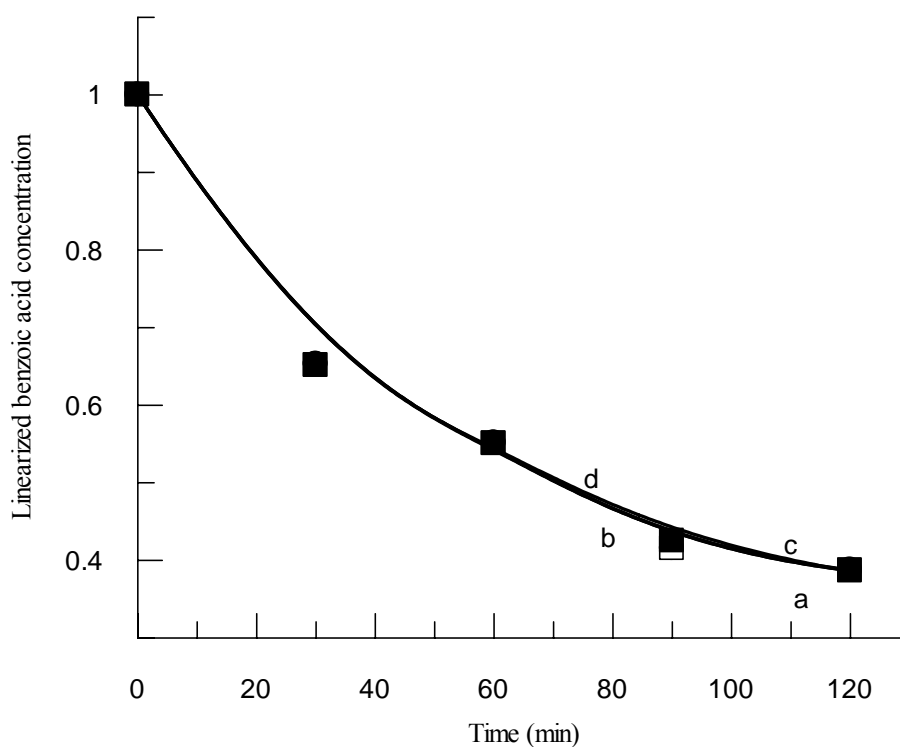


Figure (4.9): Plots of remaining benzoic acid concentration (M) vs. time in benzoic acid degradation experiments showing the effect of nominal dye (TPPHS) concentration, (a) 0.006g, 1.476×10^{-5} mol, (b) 0.01g, 2.46×10^{-5} mol, (c) 0.012g, 2.0952×10^{-5} mol, (d) 0.003g, 0.738×10^{-5} mol. All experiments were conducted in the UV region at room temperature, using AC/TiO₂/TPPHS system TiO₂ (0.5g), AC (0.1g), and 200 ppm benzoic acid concentration.

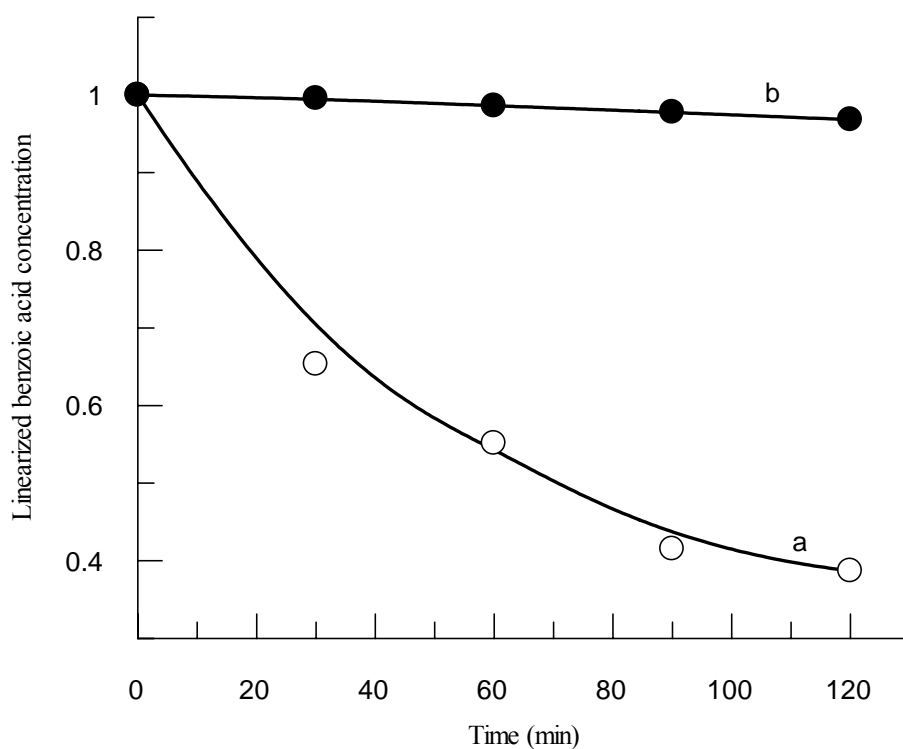


Figure (4.10): Plots of remaining benzoic acid concentration (M) vs. time in benzoic acid degradation experiments showing the effect of radiation, (a) UV-light, (b) visible light. Experiments were conducted at room temperature, using AC/TiO₂/TPPHS system, AC (0.1g), TPPHS (0.006g, 1.476×10^{-5} mol), TiO₂ (0.5g), and 200 ppm benzoic acid concentration.

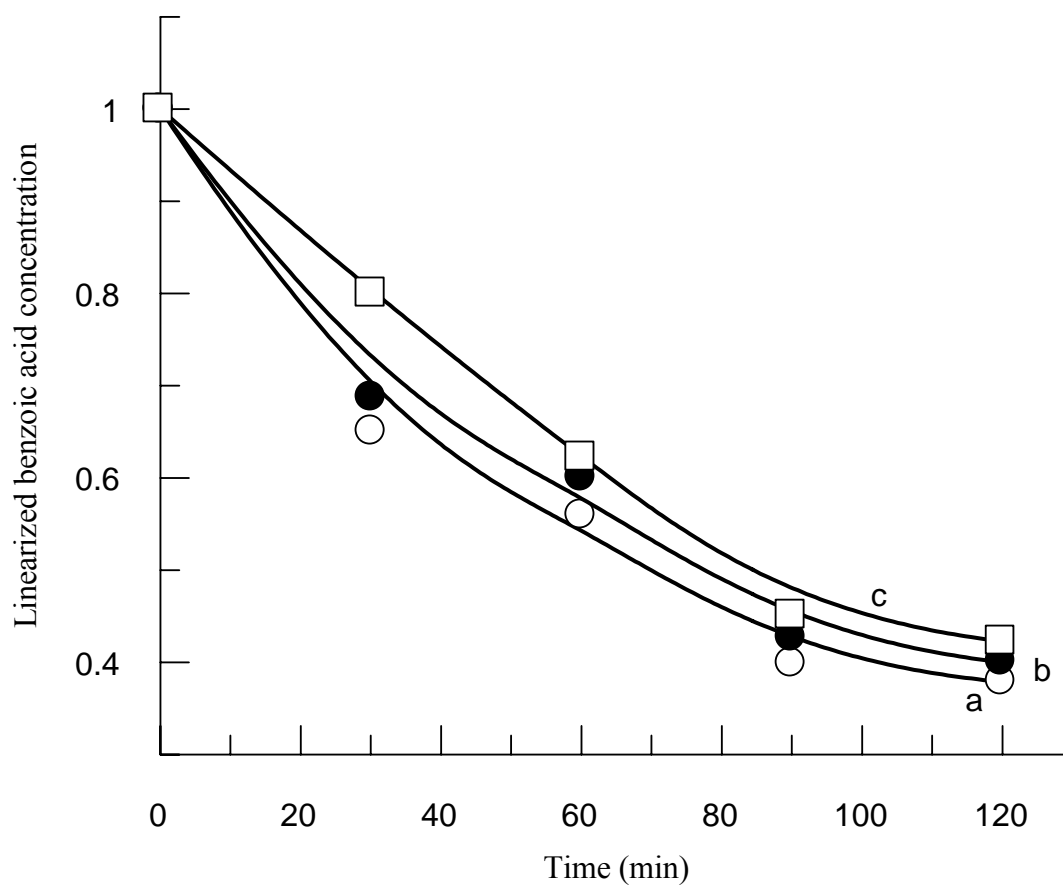


Figure (4.11): Plots of remaining benzoic acid concentration (ppm) vs. time in benzoic acid degradation experiments showing the effect of catalyst (AC/TiO₂/TPPHS) concentration. (a) 1.0g catalyst, (b) 0.6g catalyst, (c) 0.3g catalyst. Experiments were conducted in the UV at room temperature, using AC (0.1g), TPPHS (0.006g, 1.476×10^{-5} mol), TiO₂ (0.5g), and 200 ppm benzoic acid concentration.

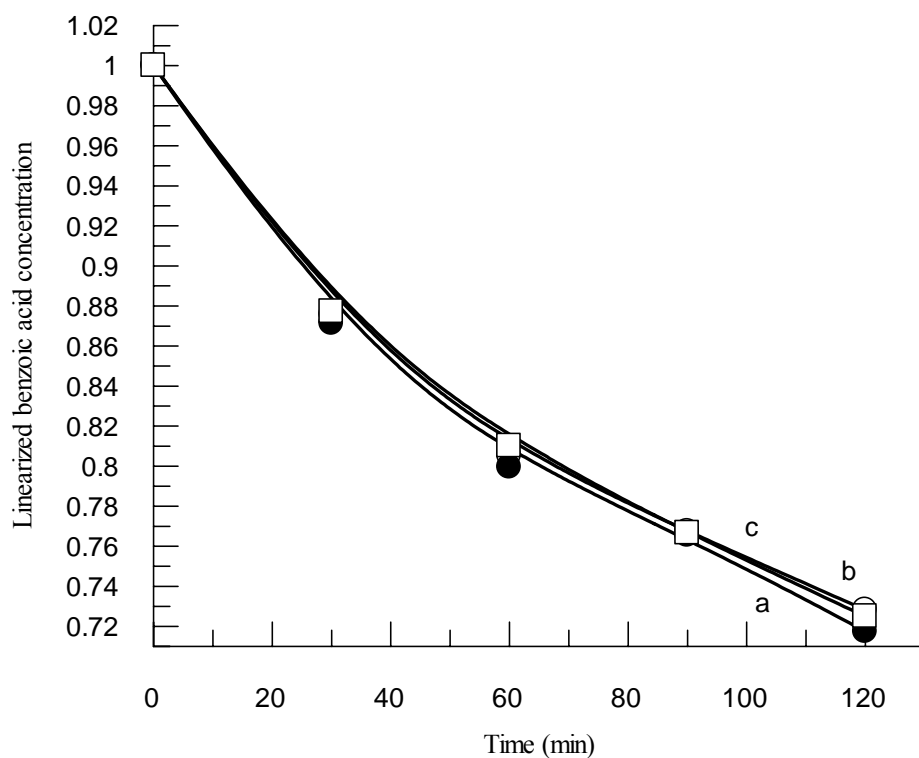


Figure (4.12): Plots of remaining benzoic acid concentration (ppm) vs. time in benzoic acid degradation experiments showing the effect of temperature, (a) 20°C, (b) 30°C, (c) 40°C. Experiments were conducted in the UV region, using AC/TiO₂/TPPHS system, AC (0.1g), TiO₂ (0.5g), TPPHS (0.006g, 1.476×10^{-5} mol), and 200 ppm benzoic acid concentration.

4.4 Discussion

4.4.1 Introduction

The concepts of sensitization and charge transfer were discussed in Chapter (3) earlier. Schemes (XII-XIV) summarize the sensitization and charge transfer concepts in degradation processes. The discussion presented there in works successfully for benzoic acid as well.

4.4.2 Effect of TPPHS dye

TiO₂ or TPPHS are not catalytically active separately in benzoic acid photo-degradation, Figure (4.3). Although TPPHS absorbs in the visible region, the TiO₂/TPPHS system was more active in the UV-region than in the visible, as shown in Figure (4.7). Turnover number values were calculated and are shown in Table (8). The Table shows that the TiO₂/TPPHS is more active than either TiO₂ or TPPHS separately. Therefore, TPPHS does not sensitize TiO₂ in the benzoic acid degradation in the visible. The TPPHS enhancement of TiO₂ activity in the UV is possibly due to charge transfer catalysis, as discussed earlier in Chapter (3). As in phenol, benzoic acid is a stable contaminant. It demands high oxidizing potential. The holes generated in the valence band of TPPHS, Scheme XIII do not have positive potential enough to oxidize benzoic acid. This is deduced from the inability of the TiO₂/TPPHS to degrade benzoic acid in the visible. Therefore, similar to phenol degradation, a sensitization mechanism should be ruled out.

The ability of TPPHS to activate TiO₂ degradation of benzoic acid in UV suggests a charge transfer catalytic process, as shown in Scheme XIV. In this case, the UV excites TiO₂ where electrons go to conduction band. The holes generated into the valence band of TiO₂ are transferred to

contaminant benzoic acid molecules in a thermodynamically allowed process. Without TPPHS, such process is slow, as observed in the absence of TPPHS. The role of TPPHS is to speed up such hole transfer in a charge transfer catalytic mechanism. Scheme XV shows that TiO_2 excitation may degrade benzoic acid, where as TPPHS with visible light should fail to do so.

Effect of activated carbon

TiO_2 /TPPHS system was supported on AC and was used to degrade benzoic acid. The AC/ TiO_2 /TPPHS system showed higher catalytic activity than the unsupported TiO_2 /TPPHS, as shown in Table (8), and Figure (4.8). Similar to earlier discussions in Chapter (3), the AC helps adsorb benzoic acid molecules. As such, the molecules are brought into close proximity to TiO_2 /TPPHS active sites. Moreover, any resulting intermediates are also adsorbed by AC and kept close to active sites which may cause complete mineralization.

In addition to TiO_2 /TPPHS catalytic activity in benzoic acid degradation, the AC is also advantageous in recovering the used catalyst. This is due to hydrophobic nature of AC, which makes filtration easier.

Effect of oxygen concentration

Parallel to phenol degradation, benzoic acid degradation demanded oxygen. With higher oxygen concentrations, the benzoic acid degradation was hindered, Figure (4.5). Therefore, the best experimental conditions were met when using an open reactor with no bubbling. These results are consistent with those observed in phenol degradation (Chapter 3) and with literature [13-14]. This adds to the practical credibility of the catalytic system, which demands no high oxygen pressures.

Effect of temperature

The temperature showed no significant effect on catalyst efficiency, with more activity observed at lower temperatures, as shown in Figure (3.11). The results are consistent with earlier literature reports, that photocatalytical oxidation rate is not much affected by changes in temperature. The degradation rate independence of temperature is reflected by the low activation energy (a few kJ/mol) compared to ordinary thermal reactions [12]. The process is technically advantageous, as it can be effectively conducted at room temperature without the costs of heating contaminated water sources.

Effect of initial contaminants concentration

Different initial benzoic acid concentrations were used. Concentrations showed slight effect on benzoic acid degradation. Two factors might be responsible for this behavior are [12]:

- The generation and migration of photo-generated electron-hole pairs and their reaction with organic compounds occur in series. Therefore, each step may become rate-determining for the overall process. At lower concentrations, the latter dominates the process and, therefore, the degradation rate should increase linearly with concentration. However, at high concentrations, the former will become the governing step, and the degradation rate increases only slowly with concentration. At a given illumination intensity, even a constant degradation rate may be observed independent of concentration.

- Intermediates generated during the photocatalytic process also affect the rate constant of their parent compounds. A higher initial concentration will yield a higher concentration of adsorbed intermediates, which may inhibit adsorption of contaminant molecules.

Effect of catalyst concentration

Effect of AC/TiO₂/TPPHS catalyst concentrations was studied. The rate of phenol degradation was independent of the catalyst concentration. This result is understandable, despite expectations. With more catalytic active sites, the reaction should be faster.

However, since we use the catalyst as suspension with the reaction mixture, many activate sites are hidden away from radiation. The total number of exposed sites is more or less constant. This means that the rate is not enhanced with increased catalyst concentration. For technical purposes, this is not advantageous. The method of AC/TiO₂/TPPHS suspension should be replaced by other methods that keep most of catalytic sites exposed to radiation.

4.4.3 Effect of MnP dye

TiO₂/MnP system was evaluated to degrade benzoic acid. The system did not function either in UV or in visible regions. This is presumably due to the holes in excited MnP having not enough power to oxidize benzoic acid in a sensitization mechanism. It also failed to behave as a charge transfer catalyst.. These results are consistent with phenol degradation.

Table (8): Values of turnover number for different catalytic systems in benzoic acid degradation

Catalyst	TiO ₂ amount g	TPPHS amount g (mol)	Turnover number*
Naked TiO ₂	0.5	0	49.4**
Dye only	0	0.006 (1.476×10 ⁻⁵)	50.4
TiO ₂ /TPPHS	0.5	0.01 (2.46×10 ⁻⁵)	307.1
	0.5	0.005 (1.23×10 ⁻⁵)	307.4
	0.5	0.004 (0.984×10 ⁻⁵)	306.2
	0.5	0.006 (1.467×10 ⁻⁵)	316.0
	0.5	0.003 (0.738×10 ⁻⁵)	307.6
AC/TiO ₂ /TPPHS	0.5	0.006 (1.476×10 ⁻⁵)	454.9
	0.5	0.012 (2.952×10 ⁻⁵)	457.2
	0.5	0.01 (2.46×10 ⁻⁵)	456.2
	0.5	0.003 (0.738×10 ⁻⁵)	454.3

*Turnover number values, (reacted PhOH moles/dye moles) were measured after 120 min reaction time.

** Turnover number value was calculated assuming presence of TPPHS (0.006 g, 1.476X10⁻⁵).

REFERENCES

- 1) R. Morrison, and R. Boyd, "Organic Chemistry", *Allyn and Bacon Inc.*, **4th edition**, (1983), 776-778.
- 2) ATSDR, Agency for Toxic Substances and Disease Registry, June 18- (2005).
- 3) D. Chatterjee, and, A. Mahata, "Photo-assisted detoxification of organic pollutants on the surface modified TiO₂ semiconductor particulate system", *Catalysis Communications*, **2**, (2001) 1-3.
- 4) D. Chatterjee, and, A. Mahata, "Photo-assisted detoxification of organic pollutants on the surface modified TiO₂ semiconductor particulate system", *Catalysis Communications*, **2**, (2001) 1-3.
- 5) A. Ajmera, S. Pangarka, and Beenakers, "Solar-assisted photo-catalytic degradation of benzoic acid using TiO₂ as a photo-catalyst", *Chemical Engineering and Technology*, **25**, (2), (2002) 180-186.
- 6) R. Single, M. Ashokkurnar and F. Grieser, "The mechanism of the sono-chemical degradation of benzoic acid in aqueous solutions", *Reserch on Chemical Intermediates*, **30**, (2004) 723-734.
- 7) V. Bresova, M. Ceppan, E. Bradstetova, M. Breza, and L. Lapcik, "Photo-catalytic hydroxylation of benzoic acid in aqueos TiO₂ suspension", *J. Photochem. Photobiol. A*, **59**, (3), (1991) 385-391.
- 8) R. Matthews, "Purification of water with near UV illuminated suspensions of titanium dioxide", *Water research*, **24** (5), (1990) 653-660.

- 9) K. Mehrotra, G. Yablonsky, and A. Ray, " Macro kinetic studies for photocatalytic degradation of benzoic acid in immobilized systems", *Chemosphere*, **60**, (2005) 1427–1436.
- 10) D. Ossi, A. Mokrini, E. Chamarro, and S. Esplugas, "Photo-degradation of benzoic acid in aqueous solutions", *Environmental Technology*, **19**, (1998) 955-960.
- 11) AOAC Official Method 979.08, copyright (1998), AOAC International.
- 12) O. Carp, C. Huisman, and A. Reller, "Photoinduced reactivity of TiO₂", *Progress in Solid State Chemistry*, **32**, (2004) 33-177.
- 13) Y. Wang, and C. Hong , " TiO₂-mediated photomineralization of 2-chlorobiphenyl: the role of O₂", *Water Research*, **34 (10)**, (2000), 2791-2797.
- 14) G. Heit, and A. Braun, "VUV-photolysis of aqueous systems: Spatial differentiation between volumes of primary and secondary reactions", *Water Sci. and Tech.*, **35 (4)**, (1997), 25-30.

CHAPTER 5

PHOTO-DEGRADATION OF TAMARON

5.1 Introduction

Tamaron (Scheme V) is a widely used insecticide, with the common name methamidophos. The CAS and IUPAC name is O,S-dimethyl phosphoramidothioate. It was first prepared by W. Lorenz for Bayer in 1965 and called Tamaron, and by P. Magee for Chevron in 1967 and called Monitor [1].

Pure methamidophos is a colourless crystalline solid with a melting point of 44.5 °C. Technical methamidophos, which is about 73% pure, is in the form of yellowish to colourless crystals. Some physical properties are given in Table (9) [2].

Table (9): Some physical properties of methamidophos (Tamaron).

Molar Mass	M.Pt. °C	B.Pt. °C	P_{vap}, (mPa) (30°C)	Sol. (H₂O) Kg/Lit	Density (g/cm⁻³), 20°C
141.1	Pure 44.5 Actual 37-39	unstable	40	2.0	1.31

Methamidophos, which is readily soluble in water (>2 kg/litre), alcohols, ketones, and aliphatic chlorinated hydrocarbons, is sparingly soluble in ether and practically insoluble in petroleum ether. This insecticide is stable at ambient temperatures. Methamidophos decomposes before its boiling point is reached (at approximately 150°C). It is effective against a broad range of insect pests (sucking, biting, and mining insects) on such crops as brassica, cotton, tobacco, sugar beet, head lettuce, and potatoes.

Methamidophos is hazardous for humans when incorrectly handled. On overexposure, typical signs and symptoms organophosphorus poisoning may occur rapidly. It is readily absorbed via skin, ingestion, and inhalation;

may cause organophosphate poisoning: weakness, headache, vomiting, excessive sweating and salivation, pinpoint pupils; in severe cases: convulsions, unconsciousness, and death due to respiratory paralysis [2].

Symptoms of poisoning: Signs and symptoms may include a feeling of exhaustion, headache, blurred vision, weakness, and confusion. Vomiting, abdominal pain, excessive sweating, and salivating may develop. The pupils are constricted. Difficulty in breathing may be experienced, due to congestion of the lungs and weakness of the respiratory muscles. Arrhythmias and cardiac failure have been reported. On severe poisoning, there will be muscle spasms, unconsciousness, and convulsion. Breathing may stop, followed by death. Although methamidophos is highly toxic, using appropriate safety precautions in exposure to it during manufacture, formulation, application and disposal, should not pose an unacceptable human health hazard.

Degradation of methamidophos in soils and natural waters is fairly rapid. The final degradation product is usually phosphoric acid. Same product has been observed when methamidophos is applied to crops [2]. Photo-electrochemical degradation using naked and/or sensitized TiO_2 was used to degrade such insecticide [3-4].

5.2 Experimental

5.2.1 Chemicals

Tamaron was purchased from Bayer, and dimethyl sulfoxide (DMSO) was obtained from Carlo, in pure forms.

Stock solution preparations

0.01M, 0.002M, and 0.001M standard solutions of Tamaron were prepared by dissolving 1.0 ml of pure Tamaron in distilled water, followed by dilution to 100 ml, 500 ml, and 1.0 L respectively. Sample solutions (100ml of 0.01M Tamaron) were also prepared.

5.2.2 Equipment

The Tamaron concentration was calculated by measuring its electronic absorption spectra on a Shimadzu UV-1601 spectrophotometer. GC-MS was also used to analyze the reaction products.

5.2.3 Photo-degradation experiments

The catalytic degradation reactor, the light source, the catalyst analysis and the photolysis experiments were discussed in Chapter 2. Tamaron degradation final product analyses are presented here.

Only one possible reaction product, from Tamaron degradation, H_3PO_4 , is reported [2], and no organic products are expected to be observed. To analyze for reaction products, the reaction mixture was taken after completion. The water was evaporated by a rotary evaporator. DMSO was used for extraction. The DMSO layer was then analyzed by GC-MS. No Tamaron was detected in the organic layer [2]. No organic products were detected either.

Same separation procedure was repeated for fresh Tamaron aqueous solutions, in a control experiment with no degradation. GC-MS results were similar to nominal Tamaron concentrations used in the control experiment. These observations indicate that Tamaron is completely degraded after enough exposure to experimental conditions.

5.2.4 Concentration measurements

The reaction progress was followed by measuring remaining Tamaron concentrations with electronic absorption spectrophotometry. A calibration curve was constructed for Tamaron using the stock solutions described earlier. The absorption spectra of standards and samples were measured on a Shimadzu UV-1601 spectrophotometer at wavelength 284nm.

5.3 Results

5.3.1 Calibration curve

A Calibration curve was performed. Figure (5.1) shows absorbance vs. Tamaron concentration. The calibration curve was used to analyze Tamaron concentrations throughout reaction course.

5.3.2 Control experiments

Control photolysis experiments were conducted with no catalyst, with no light source, or with no catalyst except AC. In these experiments, Tamaron concentrations didn't significantly change after relatively prolonged times (3h) Figure (5.2).

5.3.3 Naked TiO₂ and naked TPPHS dye

TiO₂ and TPPHS were used separately to degrade Tamaron with visible light. When TiO₂ and TPPHS were used, separately, only up to 3% loss in Tamaron concentrations occurred, Figure (5.3).

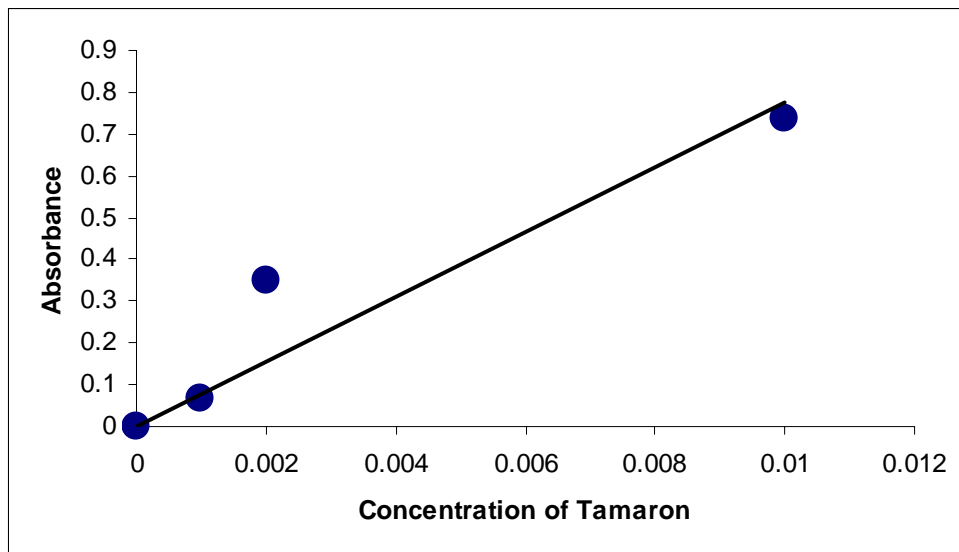


Figure (5.1): A calibration curve showing a plot of absorbance vs. Tamaron concentration (M). Measurements were conducted in aqueous media, at room temperature.

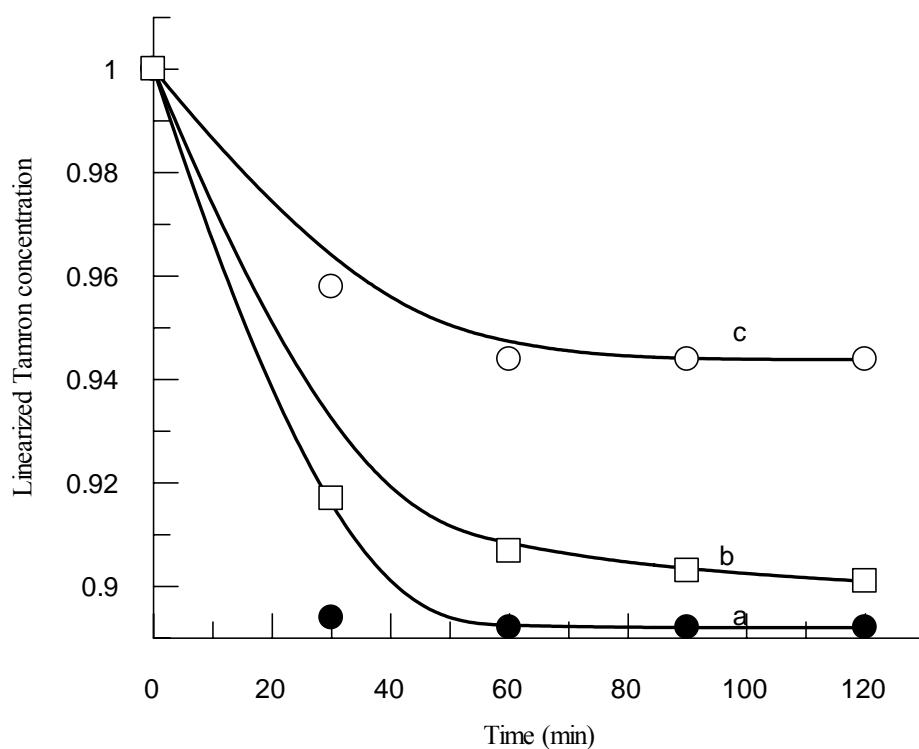


Figure (5.2): Plots of remaining Tamaron concentration (M) vs. time in Tamaron degradation control experiments. (a) visible light with no catalyst (TiO₂/TPPHS), (b) TiO₂/TPPHS catalyst with no visible light, (c) AC alone, using TiO₂ (0.5g), TPPHS (0.003g, 0.738×10^{-5} mol), AC (0.1g), and 0.01M Tamaron concentration.

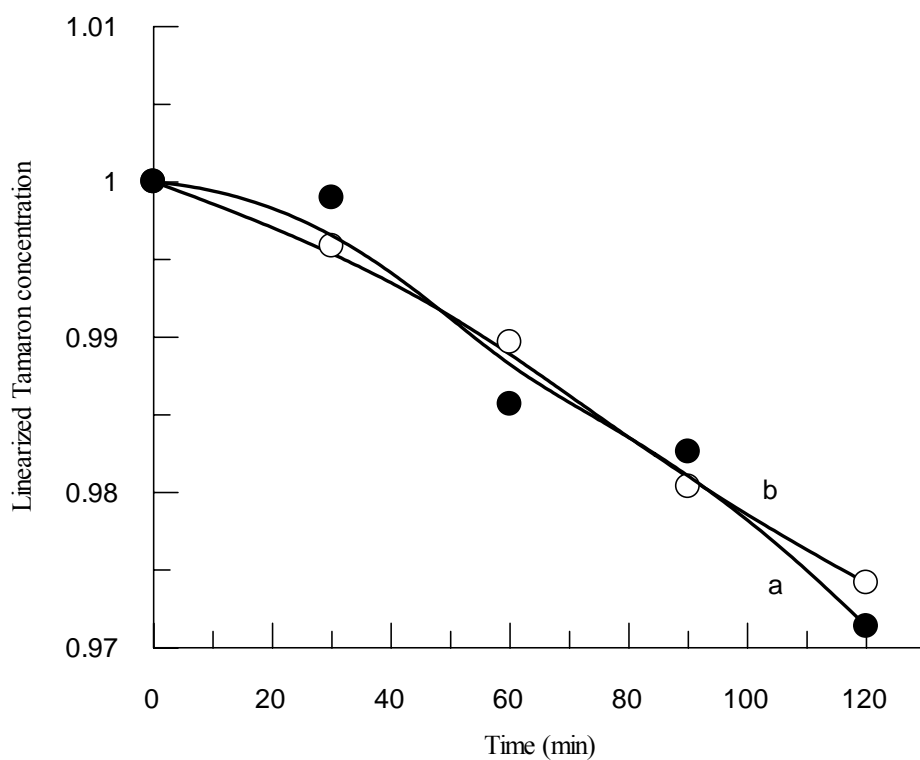


Figure (5.3): Plots of remaining Tamaron concentration (M) vs. time in Tamaron degradation experiments. (a) Naked dye (TPPHS) (b) Naked TiO₂. Experiments were conducted in the visible region at room temperature, using TiO₂ (0.5g), TPPHS (0.003g, 0.738×10^{-5} mol), and 0.01M Tamaron concentration.

5.3.4 TPPHS sensitized TiO₂ catalyst

TPPHS sensitized TiO₂ catalyst was used for Tamaron degradation with visible light. There was a noticeable change in Tamaron concentration when TiO₂/TPPHS catalyst was used in the visible and UV regions, Figure (5.4-5.5). Initial Tamaron concentration was studied and showed no effect on Tamaron degradation, Figure (5.6).

Effect of dye concentration

TPPHS sensitized TiO₂ systems were used to catalyze photodegradation of Tamaron in the visible region in an open reactor. Different dye concentrations were used. In all cases the sensitized catalyst showed sound catalytic activity, reaching up to 33% completion in 120 min., Figure (5.4). Nominal dye concentrations did not affect the rate significantly.

Effect of oxygen concentration

The effect of oxygen exposure, on Tamaron degradation was studied, in the visible. Experiments were conducted using reactors that are open to air, closed to air or bubbled with air. Figure (5.7) shows that the reaction system, which was kept open to oxygen with no bubbling, was the fastest system. The reaction was hindered by air bubbling, compared to closed systems. This indicates that oxygen is needed by the reaction but may also inhibit it when used at higher concentrations. Therefore, unless otherwise stated, all degradation experiments were conducted in an open reactor with no air bubbling.

5.3.5 AC supported TiO₂/TPPHS catalyst

TiO₂/TPPHS supported onto AC surfaces was utilized in photodegradation of Tamaron in the visible and UV regions. All Tamaron

disappeared, within 2hr, when AC/TiO₂/TPPHS catalyst was used either by UV- or visible light, Figure (5.8-5.10).

Effect of temperature

Tamaron degradation was studied using AC/TiO₂/TPPHS at different temperatures in the visible region. The rate of degradation was independent of temperature, and Tamaron disappeared in all experiments after almost the same reaction time, Figure (5.11).

Effect of catalyst concentration

Tamaron degradation was studied using AC/TiO₂/TPPHS at different concentrations in the visible region. The rate of degradation was independent of catalyst concentration when using more than 0.6g of catalyst. At lower concentrations, using catalyst amounts less than 0.6g, the rate changed with concentration, and the reaction was slower with lower catalyst amount, Figure (5.12).

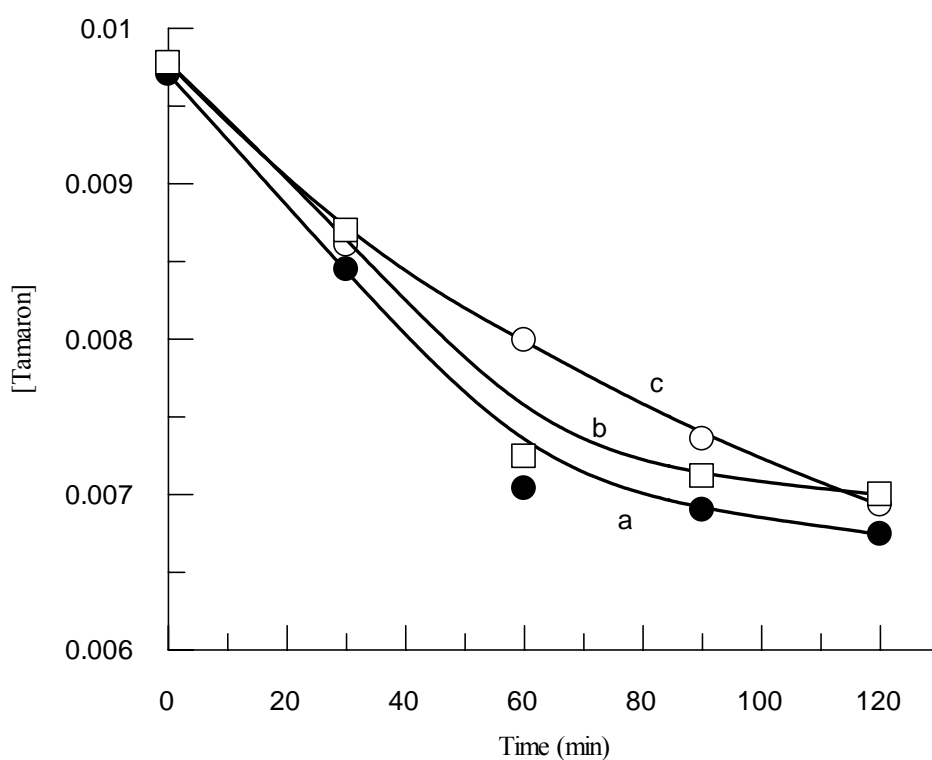


Figure (5.4): Plots of remaining Tamaron concentration (M) vs. time in Tamaron degradation experiments showing the effect of dye (TPPHS) concentration, (a) 0.005g, 1.23×10^{-5} mol, (b) 0.003g, 0.738×10^{-5} mol, (c) 0.01g, 2.46×10^{-5} mol. All experiments were conducted using visible light, at room temperature, using TiO_2 /TPPHS system TiO_2 (0.5g), and 0.01M Tamaron concentration.

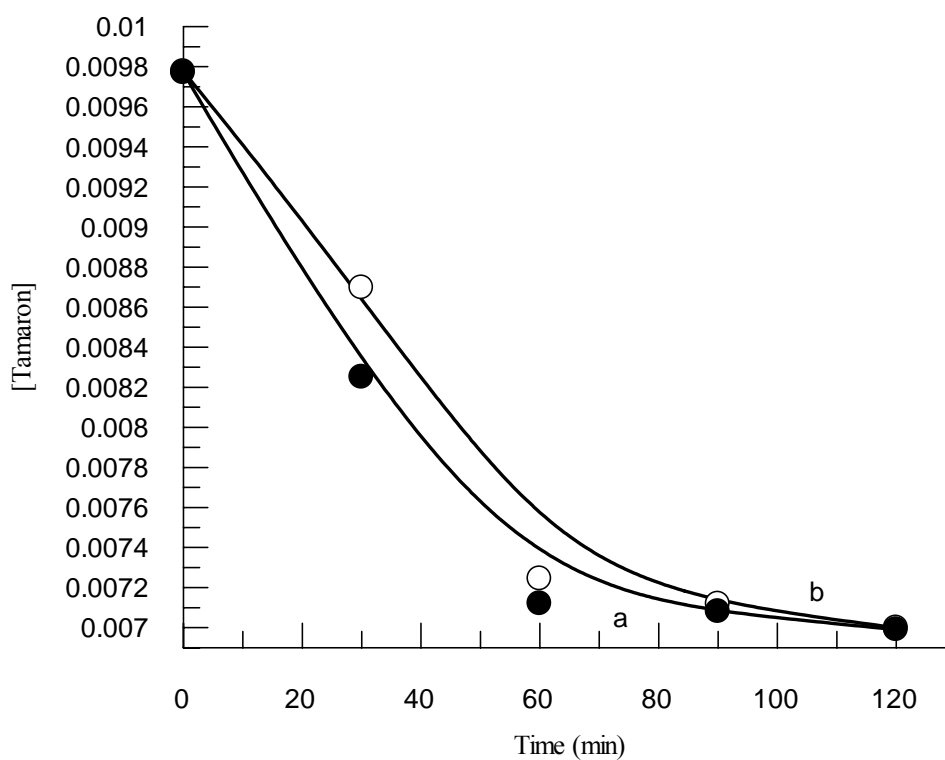


Figure (5.5): Plots of remaining Tamaron concentration (M) vs. time in Tamaron degradation experiments showing the effect of radiation, (a) UV region (b) visible region, Experiments were conducted using TiO_2 /TPPHS system TiO_2 (0.5g), TPPHS (0.003g, 0.738×10^{-5} mol), and 0.01M Tamaron concentration.

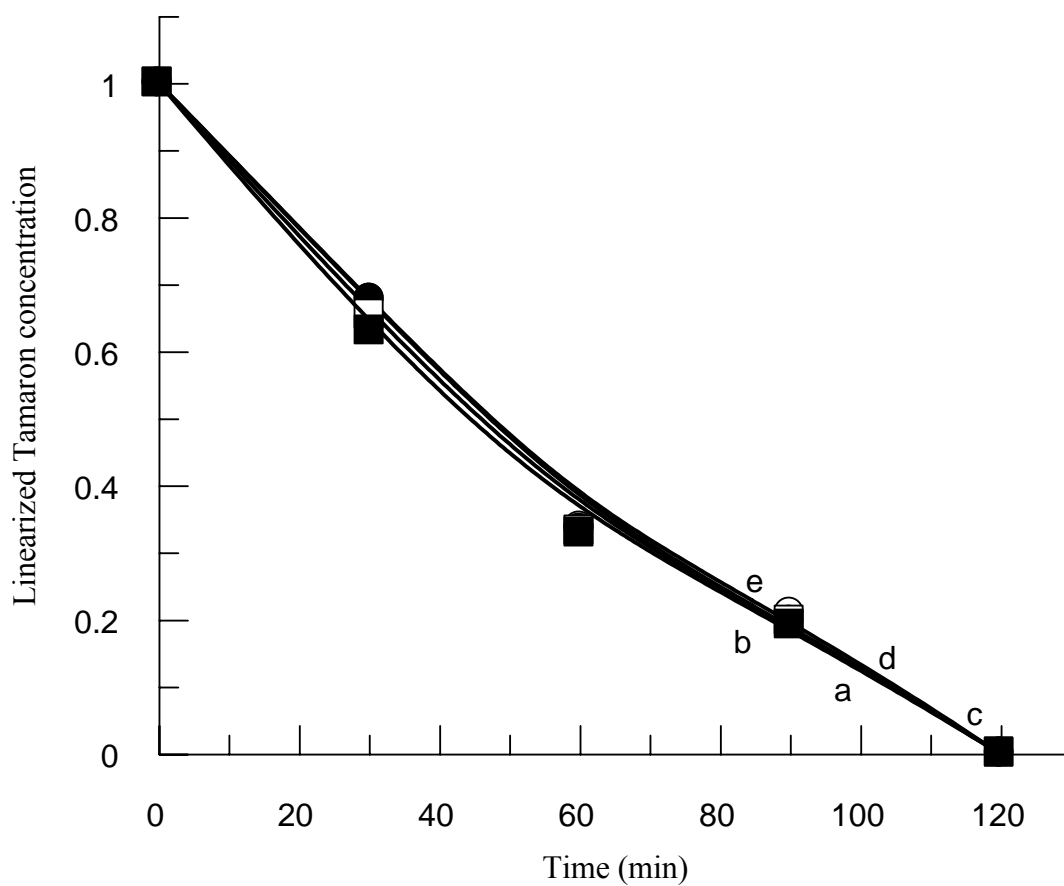


Figure (5.6): Plots of remaining Tamaron concentration (M) vs. time in Tamaron degradation experiments showing the effect of initial Tamaron concentration. (a) 0.01, (b) 0.008, (c) 0.006, (d) 0.004, (e) 0.001M. All experiments were conducted under visible at room temperature, using AC/TiO₂/TPPHS system TiO₂ (0.5g), TPPHS (0.003g, 0.738×10^{-5} mol), AC (0.1g).

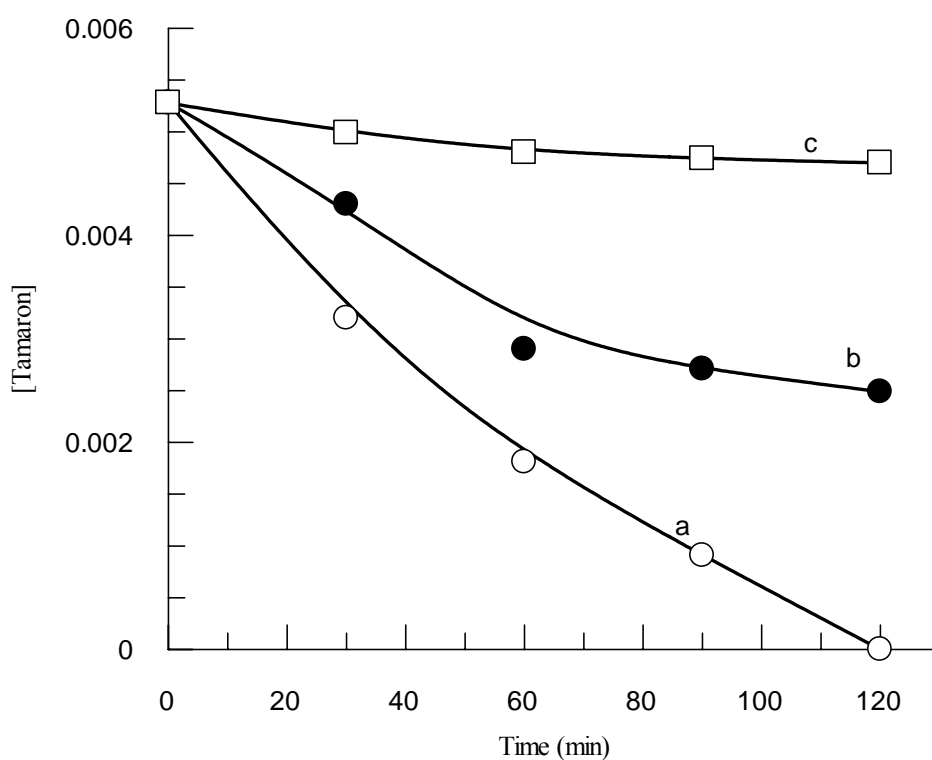


Figure (5.7): Plots of remaining Tamaron concentration (M) vs. time in Tamaron degradation experiments showing the effect of oxygen concentration, (a) open reactor, (b) closed reactor, (c) bubbles of air. Experiments were conducted in the visible region at room temperature, using AC/TiO₂/TPPHS system AC (0.1g), TiO₂ (0.5g), TPPHS (0.006g, 1.476×10^{-5} mol), and 0.01M Tamaron concentration.

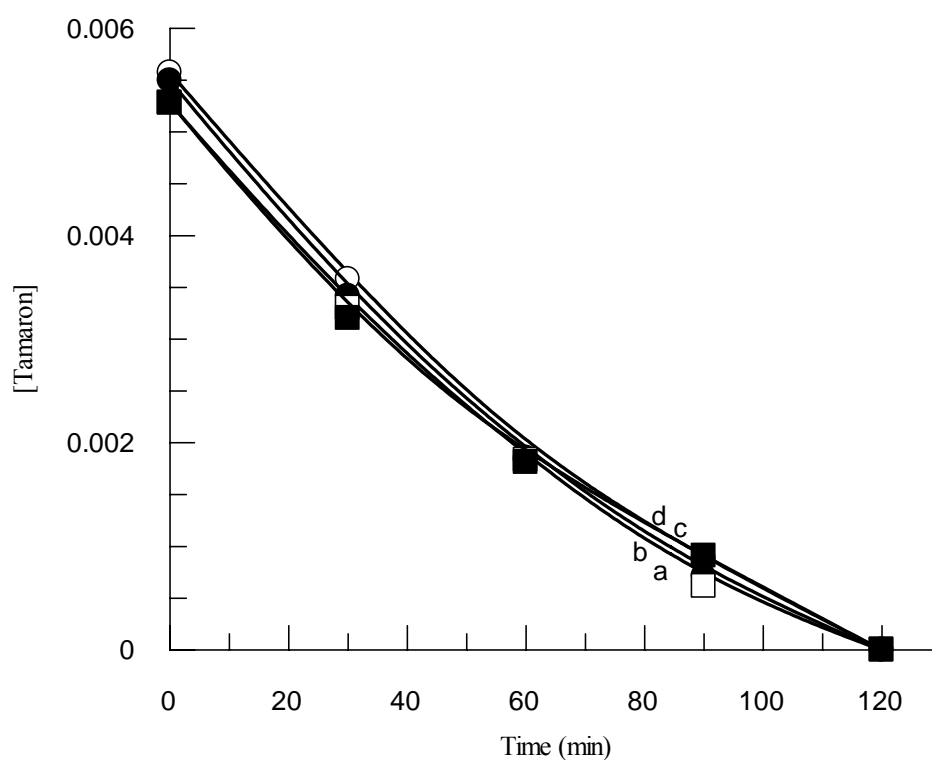


Figure (5.8): Plots of remaining Tamaron concentration (M) vs. time in Tamaron degradation experiments showing the effect of nominal dye (TPPHS) concentration, (a) 0.006g, 1.476×10^{-5} mol, (b) 0.01g, 2.46×10^{-5} mol, (c) 0.012g, 2.0952×10^{-5} mol, (d) 0.003g, 0.738×10^{-5} mol. All experiments were conducted using visible light, at room temperature, using AC/TiO₂/TPPHS system TiO₂ (0.5g), AC (0.1g), and 0.01M Tamaron concentration.

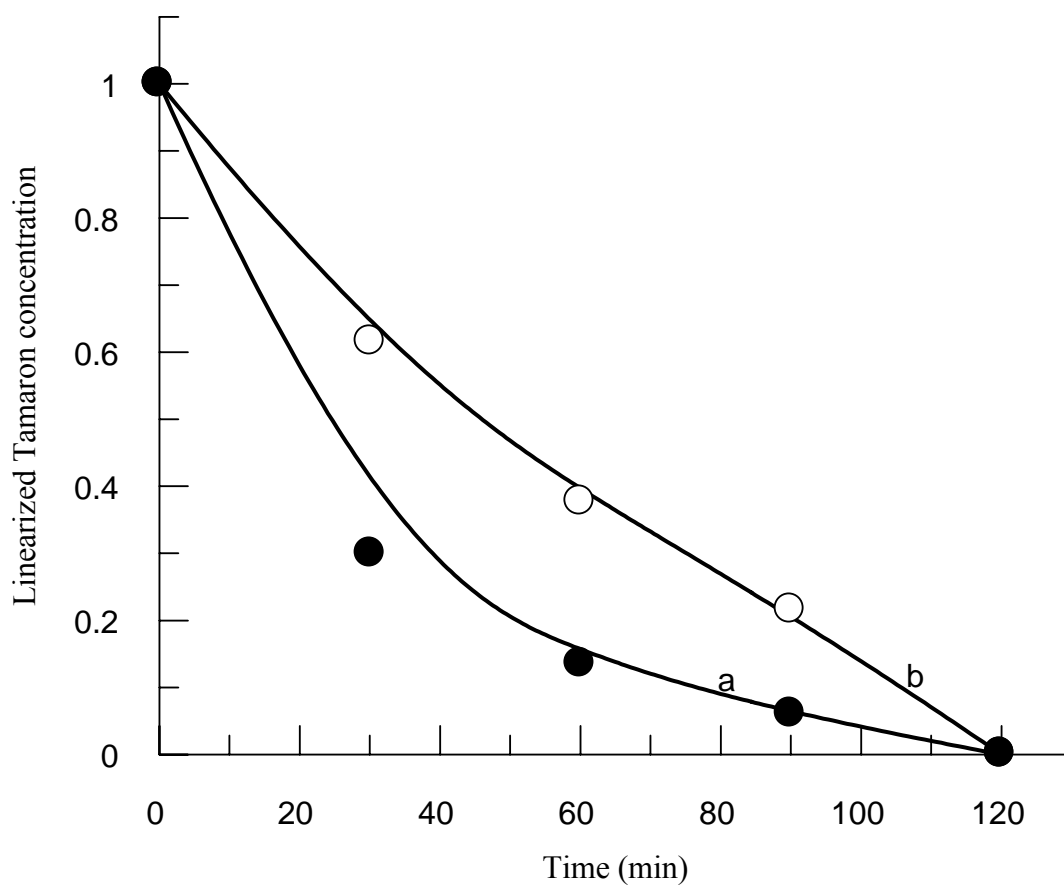


Figure (5.9): Plots of remaining Tamaron concentration (M) vs. time in Tamaron degradation experiments showing the effect of radiation, (a) UV-light, (b) visible light. All experiments were conducted at room temperature, using AC/TiO₂/TPPHS system TiO₂ (0.5g), TPPHS (0.006g, 1.476×10^{-5} mol), AC (0.1g), and 0.01M Tamaron concentration.

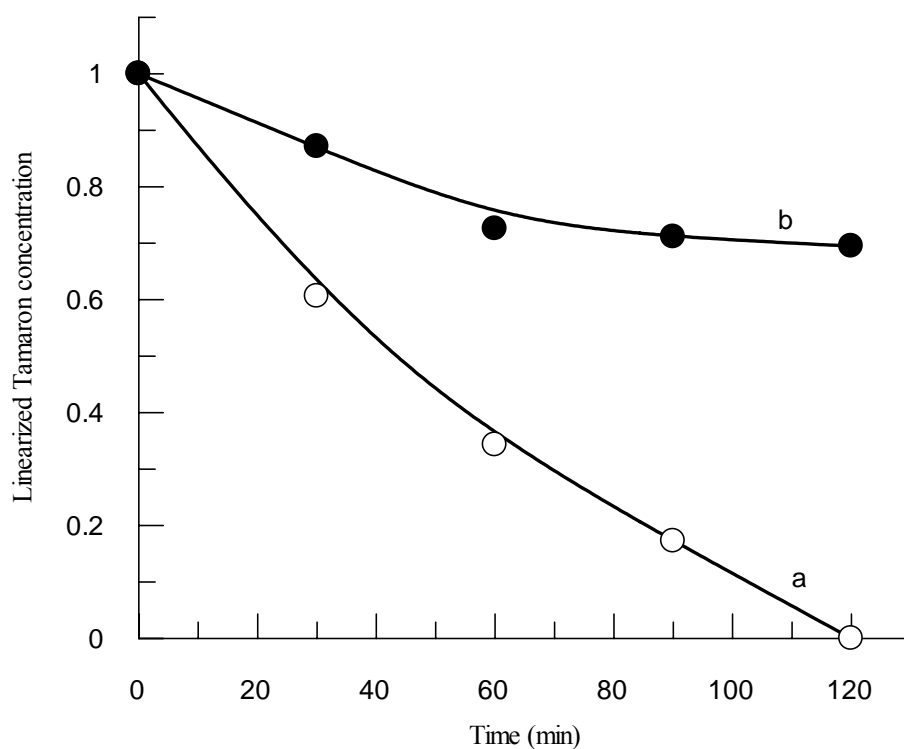


Figure (5.10): Plots of remaining Tamaron concentration (M) vs. time in Tamaron degradation experiments showing the effect of AC, (a) with AC (0.1g), (b) no AC. All experiments were conducted using visible light, at room temperature, using TiO_2 (0.5g), and TPPHS (0.006g , 1.476×10^{-5} mol), and 0.01M Tamaron concentration.

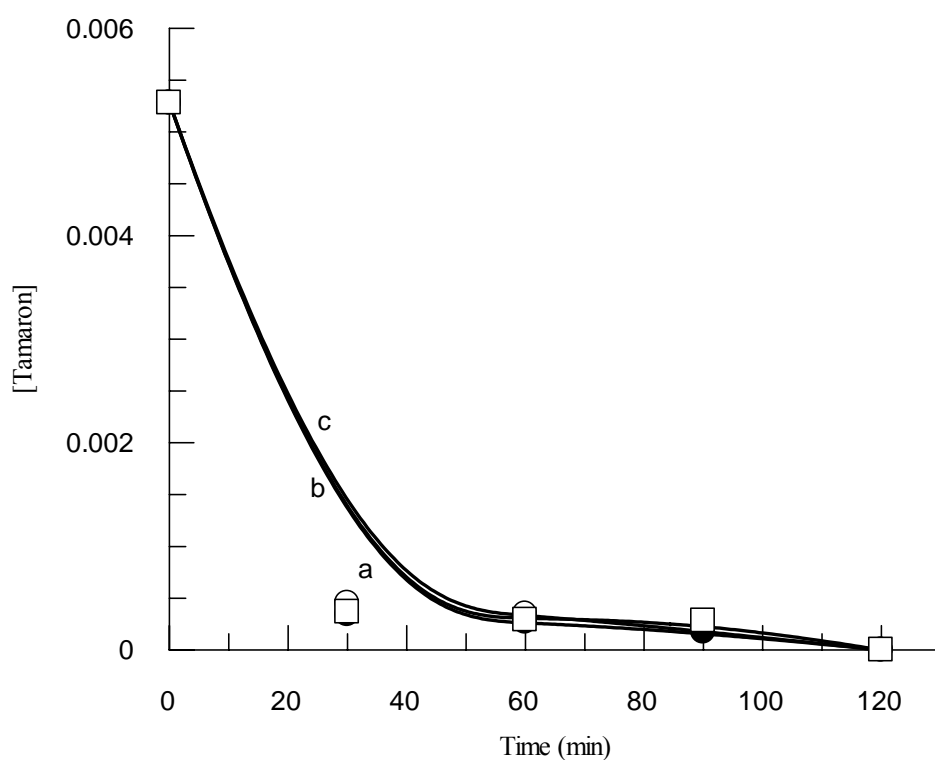


Figure (5.11): Plots of remaining Tamaron concentration (M) vs. time in Tamaron degradation experiments showing the effect of temperature, (a) 20°C, (b) 30°C, (c) 40°C. All experiments were conducted using visible light, using AC/TiO₂/TPPHS system TiO₂ (0.5g), TPPHS (0.006g, 1.476×10^{-5} mol), and AC (0.1g), and 0.01M Tamaron concentration.

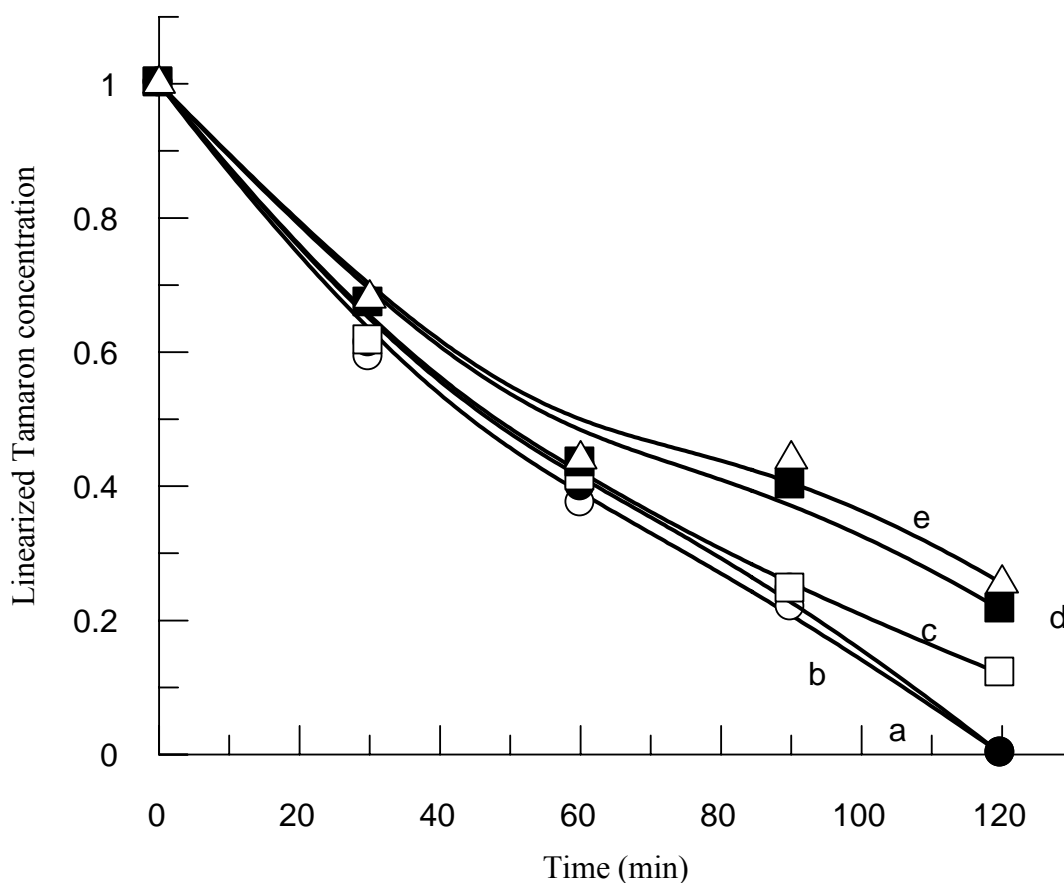


Figure (5.12): Plots of remaining Tamaron concentration (M) vs. time in Tamaron degradation experiments showing the effect of catalyst (AC/TiO₂/TPPHS) concentration. (a) 1.0g catalyst, (b) 0.6g catalyst, (c) 0.4g catalyst, (d) 0.3g catalyst, (e) 0.1g catalyst. Experiments were conducted in the visible at room temperature, using TiO₂ (0.5g), TPPHS (0.006g, 1.476×10^{-5} mol), AC (0.1g), and 0.01M Tamaron concentration.

5.3.6 Metalloporphyrin (MnP) modified TiO₂ catalyst

TiO₂ modification with 4-tetrapyridylporphyrinatomanganese(III) enhanced the catalytic activity of Tamaron degradation in both UV and visible regions. TiO₂ saturated with MnP was prepared, isolated and rinsed before use in an open reactor. Figure (5.13) shows that 20% Tamaron degradation occurred in the visible region within 120 min using TiO₂/MnP compared to only 5% degradation using naked TiO₂.

Effect of activated carbon

When TiO₂/MnP was supported onto AC, its activity was significantly enhanced. The AC/TiO₂/MnP caused complete Tamaron degradation in the visible region within 120 min., Figure (5.13).

Effect of type of radiation

The TiO₂/MnP system showed comparable catalytic activities, for Tamaron degradation, in UV and visible, as shown in Figure (5.14). The Ac/TiO₂/MnP also showed comparable activities when used in the UV and visible regions, Figure (5.15). In either case, the AC supported system showed higher catalytic activity than the unsupported one.

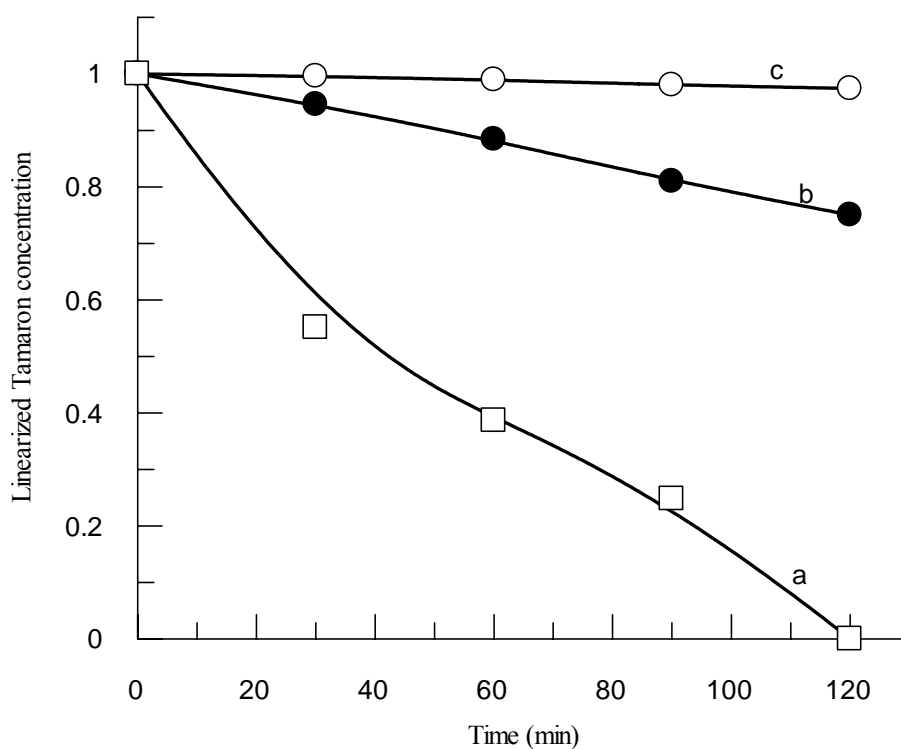


Figure (5.13): Plots of remaining Tamaron concentration (M) vs. time in Tamaron degradation experiments showing the effects of AC and MnP, (a) with AC (0.1g) (AC/TiO₂/MnP), (b) no AC (TiO₂/MnP), (c) naked TiO₂. All experiments were conducted using visible light, at room temperature, using TiO₂ (2.0g), and 0.01M Tamaron concentration.

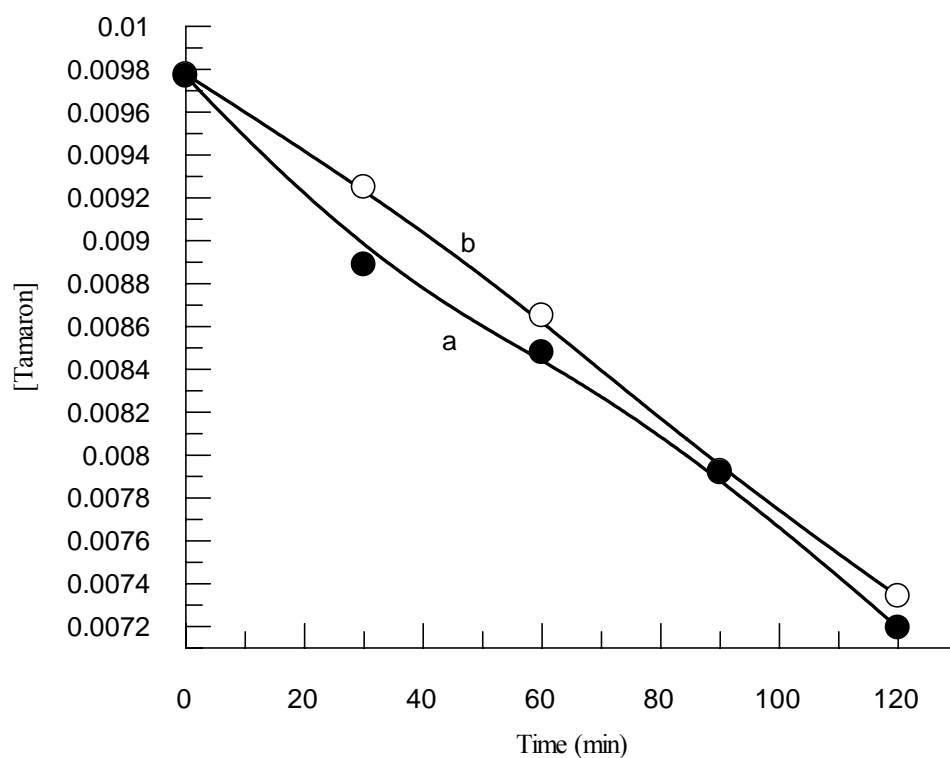


Figure (5.14): Plots of remaining Tamaron concentration (M) vs. time in Tamaron degradation experiments showing the effect of radiation, (a) UV-light (b) visible light. All experiments were conducted at room temperature, using TiO_2/MnP system TiO_2 (2.0g) presaturated with MnP, and 0.01M Tamaron concentration.

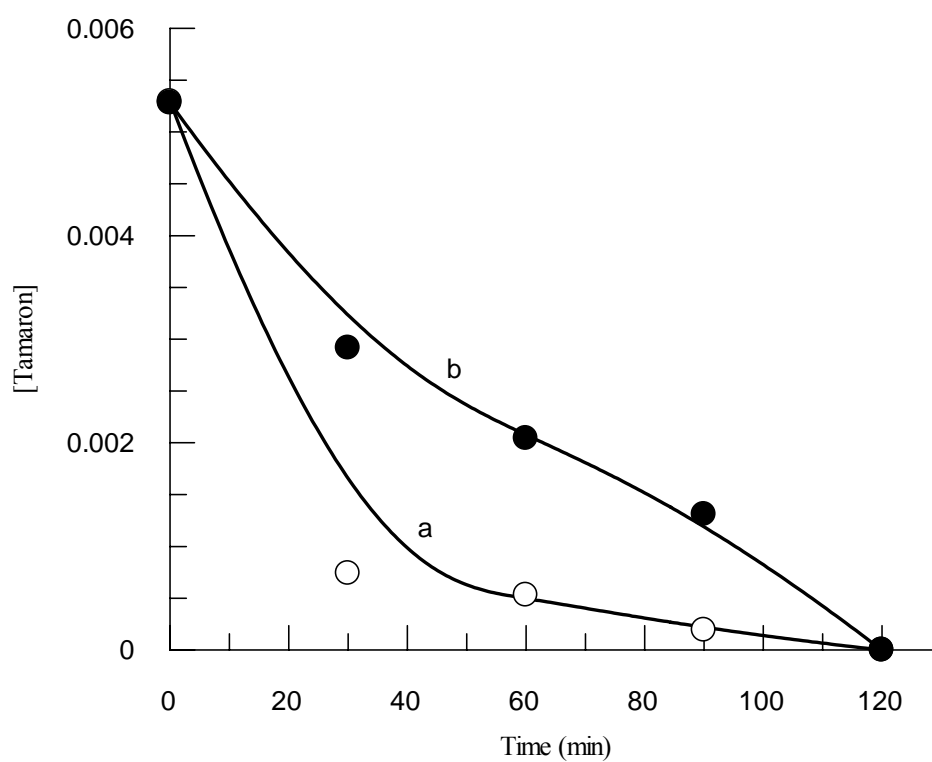


Figure (5.15): Plots of remaining Tamaron concentration (M) vs. time in Tamaron degradation experiments showing the effect of radiation, (a) UV-light, (b) visible light. All experiments were conducted at room temperature, using AC/TiO₂/MnP system AC (0.1g), TiO₂ (2.0g) presaturated with MnP, and 0.01M Tamaron concentration.

5.4 Discussion

5.4.1 Introduction

The concepts of sensitization and charge transfer are explained in Chapter (3), Schemes (XII), (XIII), and (XIV).

5.4.2 Effect of TPPHS dye

TiO₂ and TPPHS were not catalytically active when used separately in Tamaron photo-degradation, Figure (5.3). The TiO₂/TPPHS system was active in the UV (charge transfer, Schemes (XII)), and visible regions (sensitizer, Scheme (XIII)), as shown in Figure (5.5).

The sensitizing activity of TPPHS in the visible is as follows: the dye is excited by the visible light ($\lambda_{\text{max}} \sim 435$ nm, with ~ 2.8 eV), leading to formation of an electron (in the dye conduction band) and a hole (in the dye valence band). The electron, travels from the dye to the TiO₂ conduction band where it reduces oxygen molecules. The holes oxidize Tamaron molecules, by traveling from the dye valence band. The sensitization process works in Tamaron by the fact that Tamaron is easy to oxidize as it has mild oxidation potential. Scheme (XIII) summarizes the degradation process of Tamaron by TiO₂/TPPHS catalyst.

In the UV region, TPPHS behaves as a charge transfer catalyst, in a similar manner discussed earlier (p.89 and 122) for phenol and benzoic acid.

Effect of activated carbon

TiO₂/TPPHS system was supported on AC. The AC/TiO₂/TPPHS system was used to photo-degrade Tamaron, and showed higher catalytic activity than the unsupported TiO₂/TPPHS system, Table (10), and Figure

(5.10). It is assumed that AC does not affect TiO₂/TPPHS optical or electrical properties, but enhances its catalytic activity. AC adsorbs contaminant molecules, and brings them into close proximity to the TiO₂/TPPHS catalytic sites.

Effect of temperature

Temperature showed no significant effect on catalytic activity of AC/TiO₂/TPPHS in Tamaron degradation in the visible, Figure (5.11). The temperature effect, on catalytic activity of the supported system in phenol, was discussed earlier in Chapter (3). Tamaron degradation showed similar behavior to that of phenol.

Effect of oxygen concentration

Oxygen was essential for semiconductor photocatalytic degradation of Tamaron. Oxygen bubbling leads to a downturn of the reaction rate, Figure (5.7). This behavior is consistent with literature results [8-9]. The effect of oxygen concentration on catalytic activity of AC/TiO₂/TPPHS in phenol degradation was discussed earlier in Chapter 3. In this regard, Tamaron seems to show similar behavior to phenol.

Effect of initial contaminant concentration

Different initial Tamaron concentrations were investigated and showed slight increase in phenol degradation. Two factors might be responsible for this behavior: [6]

- The generation and migration of photo-generated electron-hole pairs and their reaction with organic compounds occur in series. Therefore, each step may become rate-determining for the overall process. At low concentrations, the latter dominates

the process and, therefore, the degradation rate increases linearly with concentration. However, at high concentrations, the former will become the governing step, and the degradation rate increases slowly with concentration, and for a given illumination intensity, even a constant degradation rate may be observed as a function of concentration.

- Intermediates generated during the photocatalytic process also affect the rate constant of their parent compounds. A higher initial concentration will yield a higher concentration of adsorbed intermediates, which will affect the overall rate.

Effect of catalyst concentration

Effect of catalyst concentration on degradation was studied. When using larger amounts of catalyst, more than 0.6g, the rate of Tamaron degradation was independent of the catalyst concentration. This essentially follows discussions presented earlier in Chapters 3 and 4. Since the catalyst is used as a suspension within the reaction mixture, the many active sites are hidden and not affected with increasing the catalyst concentration. It is thus reasonable that the number of efficient active sites (those exposed to light) is constant despite increasing amount of AC/TiO₂/TPPHS system. This reasoning is confirmed by the fact that the rate was affected catalyst concentrations while using amounts less than 0.6g. With lower catalyst amounts in the reaction mixture, the number of exposed active sites may increase with catalyst concentration.

5.4.3 Effect of MnP dye

The TiO₂/MnP system was prepared and used to photo-degrade Tamaron. It was active in both UV and visible regions, as shown in Figures (5.14-5.15). TiO₂/MnP system was supported on AC and used to degrade Tamaron. The AC/TiO₂/MnP system showed higher catalytic activity than the TiO₂/MnP, Figure (5.13). The AC/TiO₂/MnP system behaved in a manner similar to AC/TiO₂/TPPHS system. The effect of AC follows similar discussions.

The efficiency of MnP to sensitize TiO₂ for Tamaron degradation is understandable by the fact that it has band gap (2.68 eV, 463 nm) which is sufficient for Tamaron degradation in the visible. Table (10) shows turnover number values of MnP in Tamaron degrading.

Table (10): Values of turnover number for different catalytic systems in Tamaron degradation

Catalyst	TiO ₂ amount g	TPPHS amount (mol)	Turnover number*
Naked TiO ₂	0.5	0	16.9**
Dye only	0	0.006g (1.476×10^{-5})	19.0
TiO ₂ /TPPHS	0.5	0.01g (2.46×10^{-5})	384.3
	0.5	0.005g (1.23×10^{-5})	401.1
	0.5	0.003g (0.738×10^{-5})	376.7
AC/TiO ₂ /TPPHS	0.5	0.006g (1.476×10^{-5})	720.8
	0.5	0.012g (2.952×10^{-5})	718.4
	0.5	0.01g (2.46×10^{-5})	745.3
	0.5	0.003g (0.738×10^{-5})	714.7
TiO ₂ /MnP	2.0	0.06ml (2.4×10^{-5})	203.3
AC/TiO ₂ /MnP	2.0	0.06ml (2.4×10^{-5})	440

*Turnover number values, (reacted Tamaron moles/dye moles) were measured after 120 min reaction time

** Turnover number value was calculated assuming presence of TPPHS (0.006 g, 1.476×10^{-5}).

REFERENCES

- 1) The Merck Index, **twelfth edition**, (2000), monograph number 6014, CAS registry number 10265-92-6.
- 2) IPCS International Program on Chemical Safety, Health and Safety Guide No. 79, Methamidophos Health and Safety Guide, World Health Organization, Geneva 1993.
- 3) V. Burruel, O. Raabe, J. Overstreet, B. Wilson, and L. Wiley, "Paternal Effects from Methamidophos Administration in Mice", *Toxicology and Applied Pharmacology*, **165 (2)**, (2000) 148-157.
- 4) A. Sanjuán, G. Aguirre, M. Àlvaro, H. Gracia, and J. Scaiano, "degradation of propoxur in water using 2,4,6-triphenylpyrylium-Zeolite Y as photo-catalyst product study and laser flash photolysis", *Appl. Cat. B: Environmental*, **25**, (2000) 257-265.
- 5) D. Dionysiou, A. Khodadoust, A. Kern, M. Suidan I. Baudin, and J. Laïne, "Continuous-mode photocatalytic degradation of chlorinated phenols and pesticides in water using a bench-scale TiO₂ rotating disc reactor", *Applied Catalysis B: Environmental*, **24**, (2000) 139-155.
- 6) O. Carp, C. Huisman, and A. Reller, "Photoinduced reactivity of TiO₂", *Progress in Solid State Chemistry*, **32**, (2004) 33-177.
- 7) A. Sanjuàn, G. Aguirre, M. Alvaro, And H. García, "2,4,6-Triphenylpyrylium ion encapsulated within y zeolite as photocatalyst for the degradation of methyl parathion", *Wat. Res.*, **34 (1)**, (2000) 320-326.

- 8) G. Geit, and A. Braun, "VUV-photolysis of aqueous systems: Spatial differentiation between volumes of primary and secondary reactions", *Water Sci. and Tech.*, **35 (4)**, (1997) 25-30.

CHAPTER 6

**CONCLUSIONS AND SUGGESTIONS FOR
FURTHER WORK**

6.1 CONCLUSIONS

6.1.1 Phenol degradation

- 1) TiO_2 or TPPHS were catalytically inactive, when used separately, in phenol photo-degradation with UV or visible. The combined TiO_2 /TPPHS did not catalyze the reaction in the visible region, but in UV region, the modified catalyst was catalytically active.
- 2) In the TiO_2 /TPPHS, the role of the dye is attributed to a charge transfer catalytic effect. The TPPHS may thus activate the catalytic system in the UV by behaving as a catalyst to transfer the holes between the TiO_2 valence band and the phenol molecules.
- 3) AC/ TiO_2 /TPPHS system showed higher catalytic activity than the TiO_2 /TPPHS in the UV region. This was attributed to the ability of AC to preferentially adsorb phenol molecules.
- 4) No significant temperature effect, on catalyst efficiency in phenol photo-degradation, was observed.
- 5) Oxygen is essential for semiconductor photocatalytic degradation of phenol, but higher oxygen concentrations lead to a downturn in the reaction rate.
- 6) TiO_2 /MnP did not effectively activate the phenol photo-degradation, in UV or in visible regions.
- 7) The recovered AC/ TiO_2 /TPPHS catalyst failed to be reused.

6.1.2 Benzoic acid degradation

- 1) Neither TiO_2 nor TPPHS were catalytically active, when used separately, in benzoic acid photo-degradation. The combined TiO_2 /TPPHS did not catalyze the reaction in the visible region, but in UV region, the modified catalyst was catalytically active.
- 2) The TiO_2 /TPPHS role is attributed to a charge transfer catalytic effect. The TPPHS may thus activate the catalytic system in the UV by behaving as a catalyst to transfer the holes between the TiO_2 valence band and the benzoic acid molecules.
- 3) AC/ TiO_2 /TPPHS system showed higher catalytic activity than the TiO_2 /TPPHS in benzoic acid photo-degradation in the UV region. This is presumably due to AC activity to adsorb benzoic acid molecules.
- 4) No significant temperature effect, on catalyst efficiency in benzoic acid photo-degradation, was observed.
- 5) Oxygen is essential for semiconductor photocatalytic degradation of benzoic acid, but higher oxygen concentrations lead to a downturn of the reaction rate.
- 6) TiO_2 /MnP did not activate the benzoic acid photo-degradation, in UV or in visible regions.

6.1.3 Tamaron degradation

- 1) TiO_2 and TPPHS were not catalytically active separately in Tamaron photo-degradation. The combined TiO_2 /TPPHS system was active in both the UV and visible regions. In the visible region, TPPHS works

as sensitizer for Tamaron photo-degradation, and in the UV region it behaves as a charge transfer catalyst.

- 2) AC/TiO₂/TPPHS system showed higher catalytic activity than the TiO₂/TPPHS in Tamaron degradation in both UV and visible regions. This is attributed to the ability of AC to adsorb Tamaron.
- 3) There was no significant temperature effect on catalyst efficiency in Tamaron photo-degradation.
- 4) Oxygen is essential for semiconductor photocatalytic degradation of benzoic acid, but higher oxygen concentrations lead to a downturn of the reaction rate.
- 5) TiO₂/MnP system was catalytically active for Tamaron degradation in both UV and visible regions. AC/TiO₂/MnP system showed higher catalytic activity than the unsupported TiO₂/MnP.

6.2 SUGGESTIONS FOR FURTHER WORK

- 1) Using other semiconductors, such as ZnO, in water purification processes.
- 2) Using other dyes, such as 8-hydroxyquinoline.
- 3) Find suitable ways to reuse the supported catalyst. Thin films of TiO₂ could be prepared onto AC surfaces. This would enlarge TiO₂ surface areas. AC particle size effect may also be investigated in a future work.
- 4) Support TiO₂/TPPHS and other systems onto other insoluble materials, such as sand, glass, clay and zeolites.

- 5) Degrade other wide-spread water contaminants, such as drug formulations, fertilizers, chlorinated hydrocarbons, and other insecticides and pesticides, onto TiO_2 /TPPHS and other systems.

- 6) Replace the magnetic stirring method by other non-destructive methods. Continuous flow reactors, using fixed-bed catalyst technique, may be examined. AC/ TiO_2 /dye systems may be stabilized onto reaction internal walls as thin films to maximize exposure to radiation.

List of Abbreviations

Symbol	Abbreviation
SLJSC	Solid Liquid Junction/ Space Charge
E_c	Conduction band
E_v	Valence band
E_{bg}	Band gap energy
eV	electron-volts
E_f	Fermi level
RED	Redox
OX	Oxidant
CMP	Chemical-Mechanical Polishing
AFM	Atomic Force Microscope
SEI	Semiconductor Electrode Interface
UV	Ultra Violet Light
MnP	Tripyridylporhyrinatomanganese(III)
TPPHS	Triphenylpyrilium hydrogen sulfate
AC	Activated Carbon
DMSO	Dimethyl Sulfoxide

Symbol	Abbreviation
TCE	Trichloroethylene
HOQ	8-hydroxyquinoline

APPENDIX

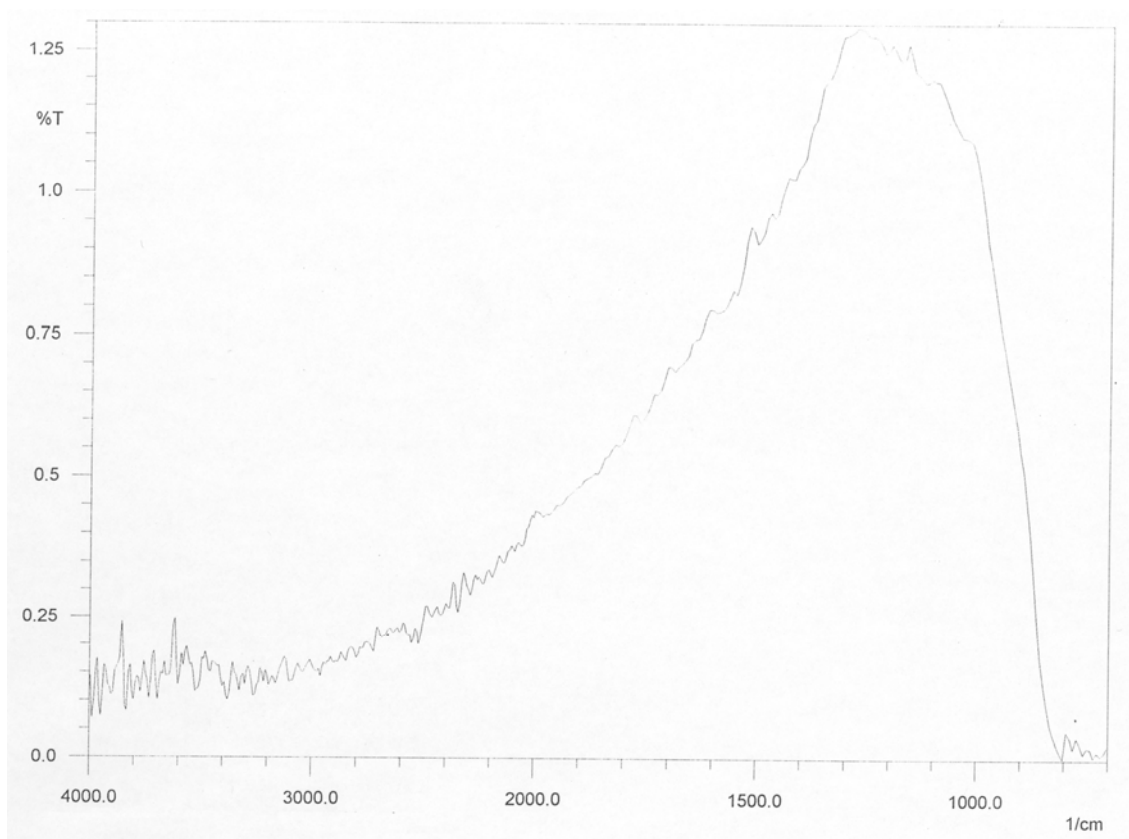


Figure (A): Solid state IR spectrum for fresh AC/TiO₂/TPPHS sample.

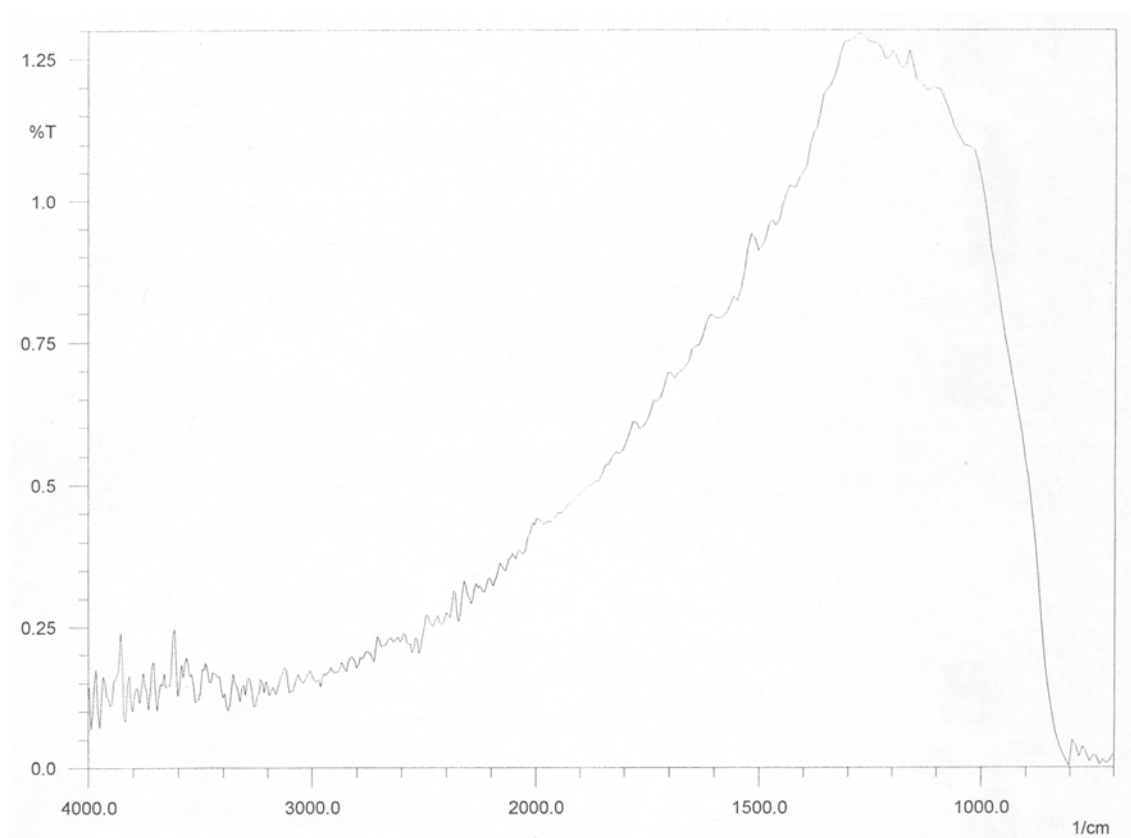


Figure (B): Solid state IR spectrum for AC/TiO₂/TPPHS sample recovered from photo-catalytic experiments of phenol with UV.

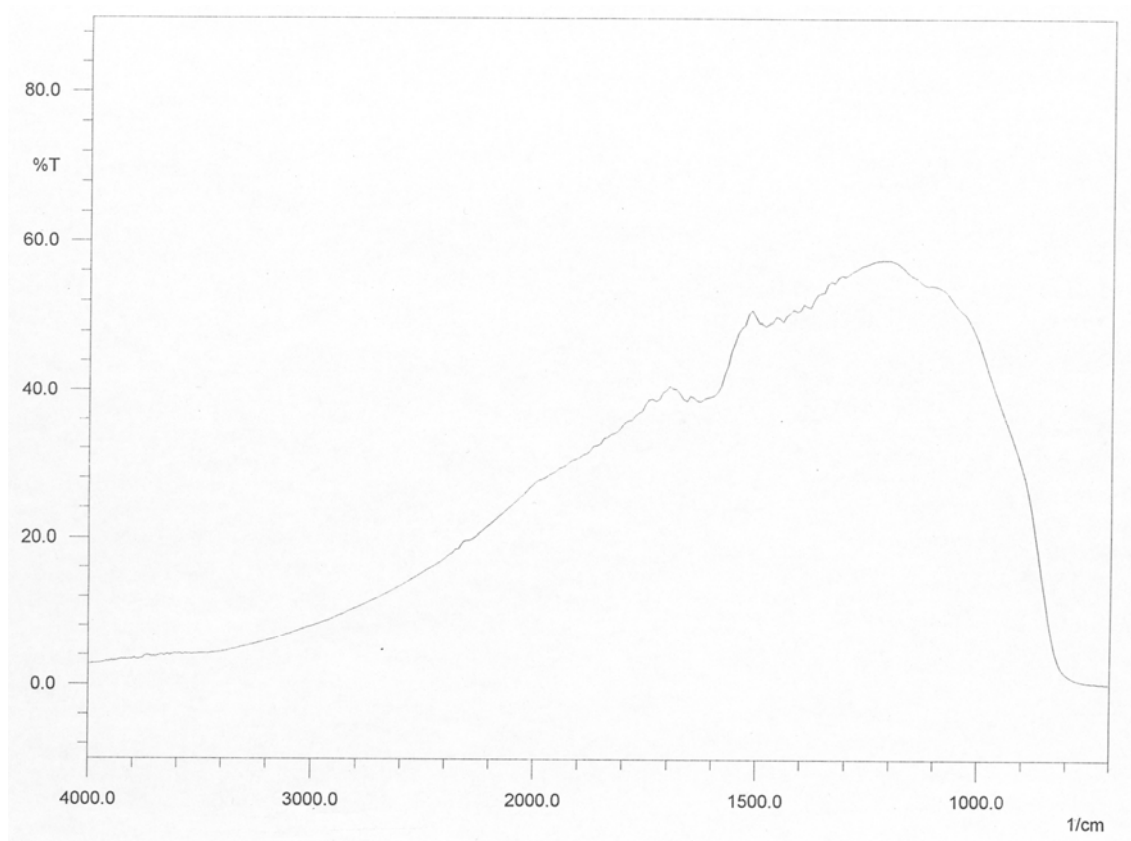


Figure (C): Solid state IR spectrum for fresh TiO₂ sample.

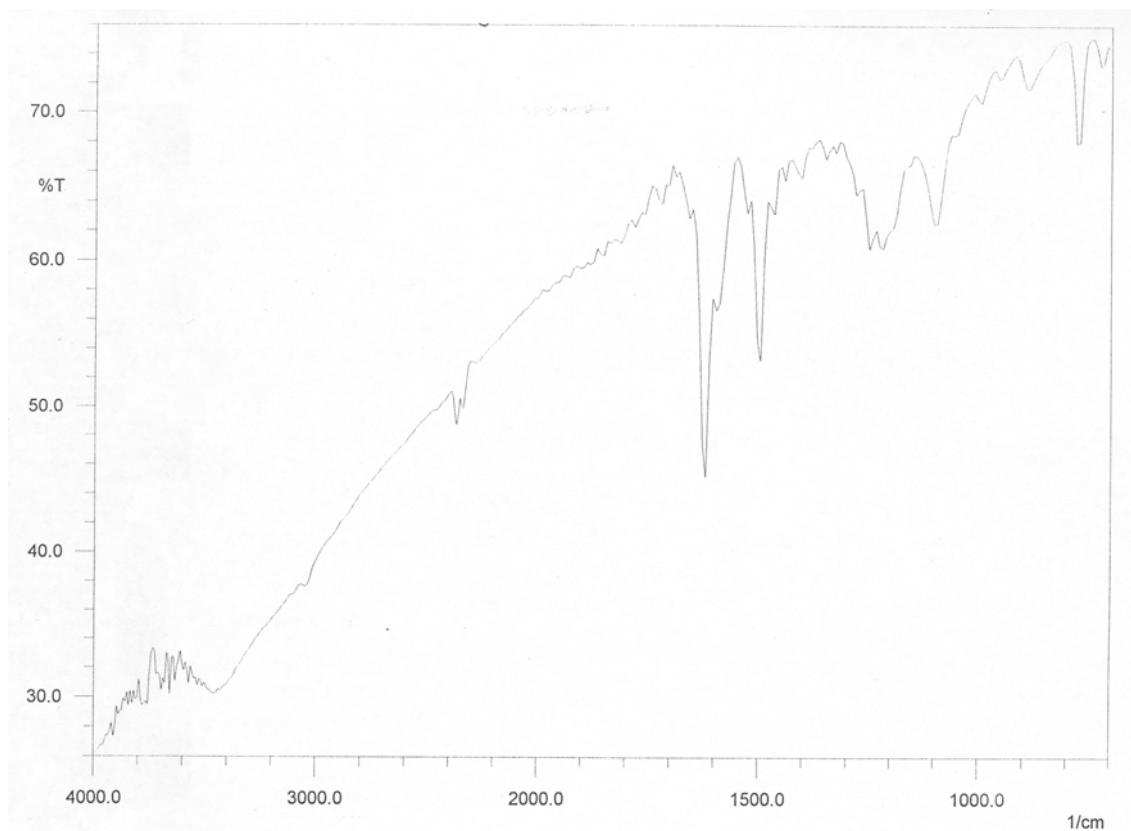


Figure (D): Solid state IR spectrum for fresh TPPHS sample.

TiO₂

..

.

الرسالة استكمالاً لمتطلبات درجة الدكتوراة في الكيمياء بكلية الدراسات العليا في جامعة
النجاح الوطنية في نابلس، فلسطين

2005

ب
TiO₂

..

.

TiO₂
()

(من) TiO₂

(MnP TPPHS)

AC/TiO₂/MnP AC/TiO₂/TPPHS
TPPHS

TiO₂

()

MnP TPPHS

٤

TiO₂

TiO₂

AC/TiO₂/MnP AC/TiO₂/TPPHS